Evaluating Spatial Normalization Methods for the Human Brain

Veronica Susanne Smith

A thesis submitted in partial fulfillment
of the requirements for the degree of

Master of Science in Electrical Engineering

University of Washington

2005

Program Authorized to Offer Degree:
Department of Electrical Engineering

Abstract

Evaluating Spatial Normalization Methods for the Human Brain

Veronica Susanne Smith

Chair of the Supervisory Committee:
Professor Linda S. Shapiro
Department of Electrical Engineering
Department of Computer Science

Cortical stimulation mapping (CSM) studies have shown cortical locations for language function are highly variable from one subject to the next. Because no two cortical surfaces are alike and language is a higher order cognitive function, observed variability is attributable to a combination of functional and anatomical variation. If individual variation can be normalized, patterns of language organization may emerge that were heretofore hidden. In order to discover whether or not such patterns exist, computer-aided spatial normalization is required. Because CSM data has been collected on the cortical surface, we believe that a surface-based normalization method will provide more accurate results than will a volume-based method. To investigate this hypothesis, we evaluate a surface-based (Caret) and volume-based method (SPM2). For our application, the "ideal" method would i) minimize variation as measured by spread reduction between cortical language sites across subjects while also ii) preserving anatomical localization of sites.
Evaluation technique: Eleven MR image volumes and corresponding CSM site coordinates were selected. Images were segmented to create left hemisphere surface reconstruction for each patient. Individual surfaces were registered to the colin27 human brain atlas using each method. Deformation parameters from each method were applied to CSM coordinates to obtain post-normalization coordinates in 2D space and 3D ICBM152 space. Accuracy metrics were calculated i) as mean distance between language sites across subjects in both 2D and 3D space and ii) by visual inspection of post-normalization site locations on a 2D map. **Results:** Globally, we found no statistically significant difference between CARET (surface-based method) and SPM2 (volume-based method) as measured by both spread reduction and anatomical localization. Local analysis showed that more than twenty percent of total mapping errors were mapped incorrectly by both methods. There was a statistically significant difference between Caret and SPM2 mapping of type 2 errors.

TABLE OF CONTENTS

LIST OF FIGURES

LIST OF FIGURES continued

LIST OF TABLES

ACKNOWLEDGMENTS

Thank you to Donna Hanlon and David Van Essen for their invaluable collaboration. A special thank you to Richard Martin for being a great mentor and key contributor. To Dr. George Ojemann, I offer sincere appreciation for your years of work in neuroscience and suggesting this thesis topic. Thanks to Anthony Rossini and Thomas Lumley for biostatistics consulting. Many thanks to Linda Shapiro, Jim Brinkley, David Corina and the University of Washington Structural Informatics Group and Foundational Model of Anatomy colleagues for your ongoing encouragement, feedback and support.

I am forever grateful for the encouragement, support and guidance I received from Amy Feldman-Bawarshi and Frankye Jones from my beginning efforts to the attainment of this degree. To Jennifer Girard, Ron Howell and Craig Duncan, I offer thanks for putting your support into words and believing that I could change tracks successfully. Hank Hayes and Abigail Van Slyck were also supportive mentors long before as well as during this effort—thank you.

To Korin and Lois Haight, I offer my gratitude for being my most precious chosen family. Chris Galvin was there, especially during the tough times, to help keep perspective and light the way when I couldn't see where I was going. To my mother, I offer my thanks for being more than a survivor and showing me that I could make my own way in the world. To my father, I offer my sincere appreciation for helping me excel academically. To Natalie, I offer my deepest gratitude for making this opportunity possible and for your unwavering love and support throughout this journey.

DEDICATION

In honor of Frederick D. Hamrick III and Carolyn McGee Hamrick.

Section 1: Introduction

1.1 Registration of Medical Images

Within medical research and especially in neuroscience, medical images are used to investigate, diagnose and treat disease processes as well as understand normal development. In neuroscience research studies, it is often desirable to compare functional and structural images obtained from the brains of patient cohorts. In addition, the amount of data produced using ever-improving technology for generating medical images, increases exponentially with each successive generation of imaging systems. It is essential, therefore, to have reliable, efficient, and accurate methods for comparing and combining structural and functional brain images across subjects. While the problem of comparing the brains of different individuals is an old one, the development of computer-aided alignment, referred to as 'intersubject registration' or 'spatial normalization' has been substantial in the last decade.

We use the term 'registration' to mean determining the spatial alignment between images of the same or different subjects, acquired with the same or different modalities, and also the registration of images with a given coordinate system. The term 'normalization' is usually restricted to the intersubject registration situation and is the term we will use in this paper. Spatial normalization accuracy is a critical step to accurate quantitative analysis of the human cortex and is the focus of this research.

Normalization is a form of alignment that involves two parts:

1) Positional normalization transformation: determination of a transformation that relates the position of features in one image or coordinate space to the position of the corresponding feature in another image or coordinate space. The symbol **T** will represent this type of transformation.
2) Intensity normalization transformation: determination of a transformation that both relates the position of corresponding features and enables us to compare the intensity values at those positions. The symbol *T* will represent this type of transformation. Using the language of geometry, we refer to the normalization transformation as a 'mapping' (Hill et al, 2000). The problem of accurately mapping data across subjects is confounded by two factors: anatomical variation and functional variation.

1.2 Anatomical Variation

Notorious for the irregularity in depth and patterning of cerebral cortex convolutions, the human brain structure varies notably from one person to the next. The human brain is an organ that is exponentially more complex than other organs in the body. For example, the human lung has a single primary function: respiration. On the other hand, brain function includes regulating all bodily functions, language, the five senses and conscious thought, among others. When looking at structural features like shape, surface and borders of the lung versus the brain, we again are reminded of the brain's complexity. In ***Gray's Anatomy***, it requires four times the amount of visual and spatial description to characterize gross brain anatomy compared to that of the lung.

The cerebral cortex in particular reveals the brain's structural complexity. The sulci (concavities) and gyri (convexities) as viewed on the cortical surface serve as key landmarks to neuroscientists. The ***Atlas of Cerebral Sulci*** by Ono *et al.* is a reference book documenting anatomical variation of the cerebral sulci as a step toward describing and categorizing the highly varied structural patterns of the cortical surface. Ono compared sulcal patterns of 25 autopsy human specimen brains examined for anatomical variation and consistency in location, shape, size, dimensions and relationship to parenchymal structures (Ono *et al.,* 1990). Ono analyzed a total of 28 sulci: 15 large main sulci, six short main sulci and seven others. Six of the large main sulci are key landmarks. They include central sulcus, lateral fissure (AKA Sylvan fissure), collateral sulcus, callosal sulcus, calcarine sulcus and parieto-occipital sulcus. These sulci tend to have more stable sulci patterns compared to other landmarks.

The central sulcus, located on the lateral surface of the frontal lobe is the most important and constant landmark on the convexity of the brain. However, even this sulcus has notable variation upon visual inspection of the shape of its inferior end. Ono found three different types of shapes in the specimen brains. In the right hemisphere, 52% of the inferior ends were straight, 28% had a Y and 20% had a T shape. In the left hemisphere, it was found that 80% of the inferior ends were straight and 20% were T-shaped as outlined in table 1.

Table 1. Incidence rates of inferior end of central sulcus patterns as determined by Ono et al.

INFERIOR END SHAPE	LEFT HEMISPHERE	RIGHT HEMISPHERE
Straight	80 %	52 %
Y-shape	20 %	28 %
T-shape	0 %	20 %

Table 2. Incidence rates of superior temporal sulcus patterns found in 25 human autopsy specimen brains.

PATTERN	LEFT HEMISPHERE	RIGHT HEMISPHERE
Continuous	28 %	36 %
Interrupted w/ 2 segments	32 %	48 %
Interrupted w/ 3 segments	16 %	16 %
Interrupted w/ 4 segments	24 %	0 %

Greater variability was found on the lateral surface in the superior temporal sulcus. In table 2, there are four patterns and the occurrence rate of those patterns. Notice how the patterns in this case are much less predictable than the shape of the inferior end of the central sulcus.

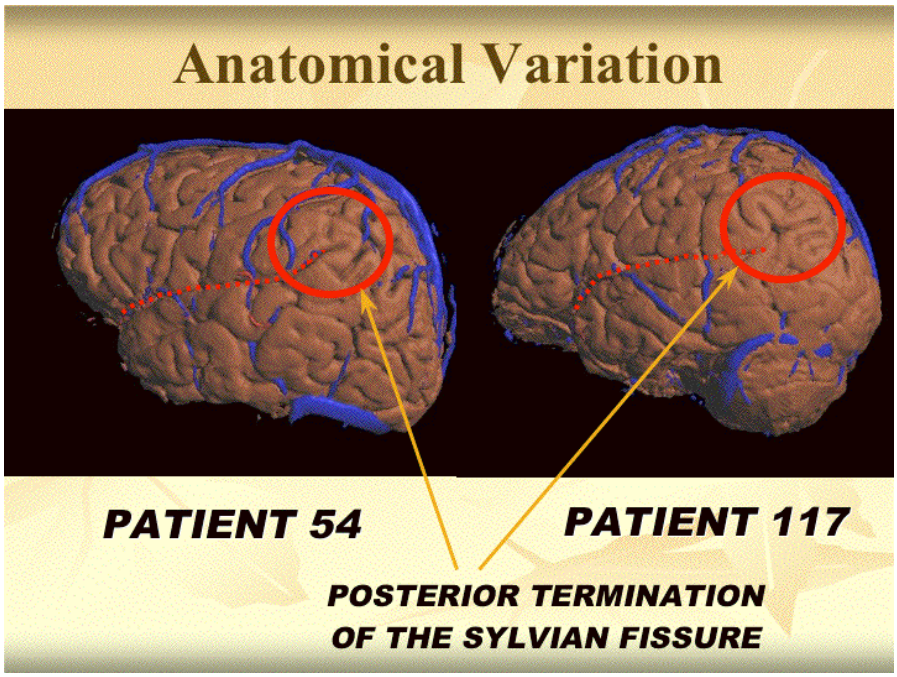

Figure 1. Left hemisphere of two different subject's volume reconstructions. Red dashed line traces the lateral fissure. Notice how the posterior end of this landmark, circled in red, differs across brains.

Ono's study provides a broad analysis of cortical folding patterns. A localized example of variation is demonstrated in figure 1. In this figure there are two volume reconstructions created from Magnetic Resonance Images (MRI), using SKANDHA, a 3-D visualization software tool (Prothero, 1995). The posterior tip of the lateral fissure is circled in red. The difference between individual cortical folding patterns within the circled region is clear even to an untrained observer. This degree of gross cortical structural variation between any two individuals makes it difficult to accurately compare cohorts.

1.3 Functional Variation

The anatomy of the brain houses sensory, motor and cognitive functions. While language-related functions were the first to be ascribed to a specific location in the human brain (Broca, 1861), there is much more validation of and consensus around the anatomical location for sensory and motor functions. A "classical model" of language organization, based on data from aphasic patients with brain lesions, was popularized during the late 19th century and remains in common use (Binder et al., 1997). In its most general form, this model defines a frontal, "expressive" area for planning and executing speech and writing movements, named after Broca, and a posterior, "receptive" area for analysis and identification of linguistic sensory stimuli, named after Wernicke (Wernicke, 1874). Although many researchers generally accept this basic scheme, there

is not universal agreement on many of the details as well as whether or not Broca and Wernicke's areas are truly canonical (Binder *et al*., 1997). Ojemann *et al.* found in their electrical stimulation mapping investigation of 117 epilepsy patients that the generally accepted model of language localization in the cortex needed revision. The combination of discrete localization in individual patients and substantial individual variability between patients found in the study demonstrated that language cannot be reliably localized based on anatomic criteria alone. (Ojemann *et al.,* 1989)

Adding to the complexity of language function is that key findings in neuroscience and cognitive science have shown that learning experiences change the physical microstructure of the brain, which alter its functional organization. According to Bransford, "New synapses (junctions through which information passes from one neuron to another) are added that would never have existed without learning, and the wiring diagram of the brain continues to be reorganized throughout one's life."(Bransford *et al.,* 1999)

An example of experience determining how parcels of the brain are used can be found in the brains of deaf people where some cortical areas typically used to process auditory information in hearing people become organized to process visual information. There are also demonstrable differences found across the brains of deaf people who use sign language and those who do not. These structural and functional differences are presumably due to differing language experiences.

Another example of plasticity akin to the deaf reorganizing temporal cortex for visual processing is blind subjects' visual cortex reorganizing for language processing. Blind subjects asked to generate verbs in response to heard nouns showed changes, as measured by fMRI, in the visual cortex. Responses were greater and broader in early blind subjects than in late blind subjects (Burton, 2003).

The functional data used in our research is cortical stimulation mapping for language localization (described in Section 1.5). Figure 2 shows cortical stimulation sites identified as statistically significant for naming errors are located in different areas of subjects' left hemispheres. This example of the same function being located in clearly different parts of the brain demonstrates the marked individual functional variability in cortical locations essential for language production.

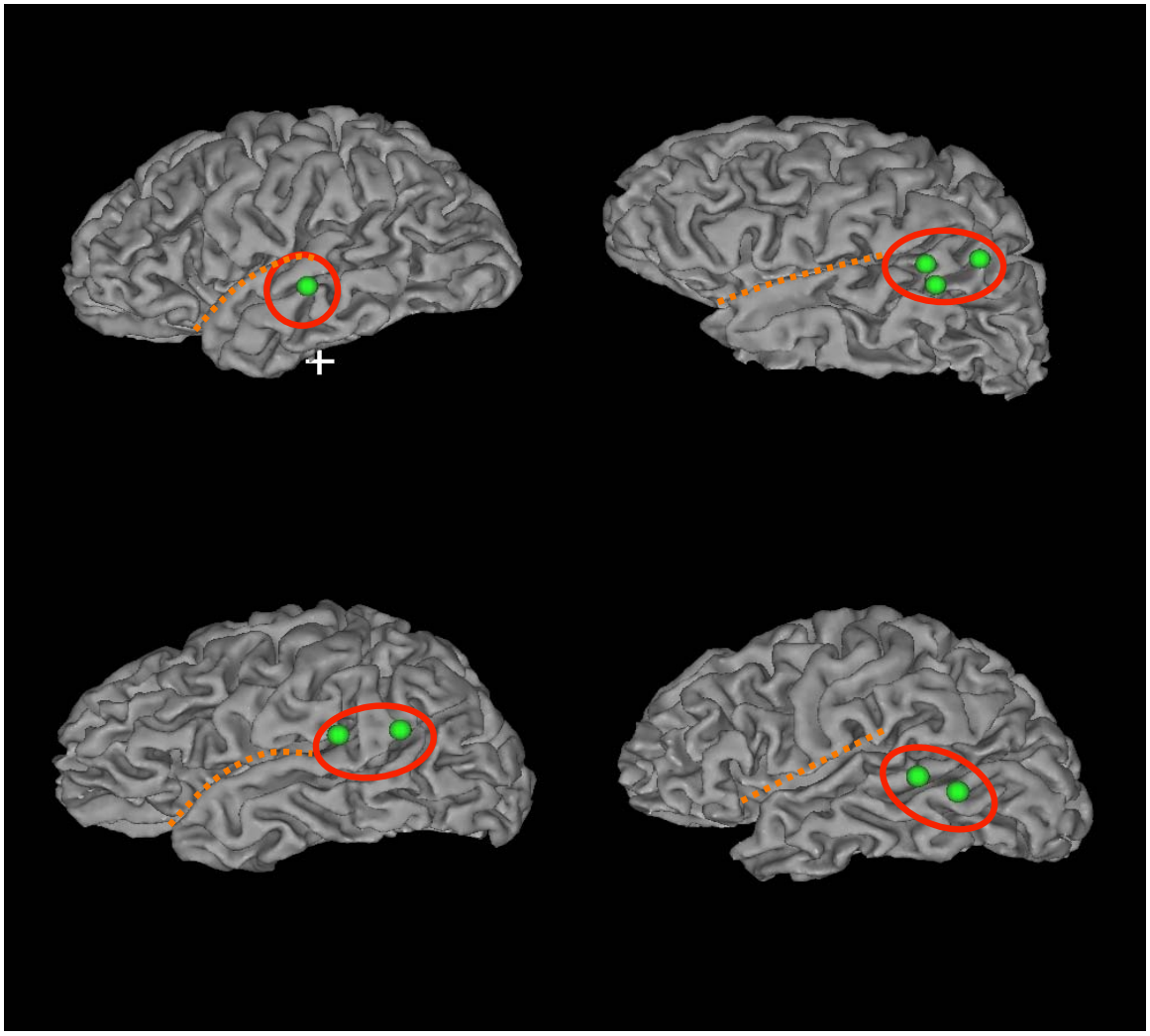

Figure 2. Functional Variation: surface reconstructions of four subject's left hemispheres. The green spheres represent sites that interrupted language production when electrically stimulated during awake neurosurgery. Note how sites responsible for the same function appear on different areas of the cortex depending on the subject.

1.4 Survey of Spatial Normalization Methods

Computer-aided spatial normalization is a widely used solution for relating the anatomy and functionality of multiple brains in neuroscience and is a critical step in quantitative analysis of the human brain cortex. It is not practical, nor desirable, to completely normalize the function and structure of one brain to another. Rather, the goal of most researchers is to bring an individual's functional and structural data into a common visualization substrate with a set of common coordinates. Having registered cortical structures, one can perform group or individual analyses of structure and function to assess normal group differences in terms of age, gender, genetic background, handedness, etc. (Ashburner *et al.*, 2003; Davatzikos and Bryan, 2002; Mangin *et al.,* 2003; Thompson *et al*., 2001b). We can also better define disease-specific signatures and detect individual cortical atrophy based on computational anatomy methods (May *et al.,* 1999; Thompson *et al.,* 2001a; Toga and Thompson, 2003). Other applications for spatial normalization methods include automatic cortical structural labeling and visualization (Le Goualher *et al.,* 1999), functional brain mapping (Toga and Mazziotta, 2000), and neurosurgical planning (Kikinis *et al.,* 1991). Given the wide array of intersubject registration applications, many image analysis methodologies have been developed to address this need.

We define **T** as the spatial transformation (mapping) from source image to target image. We define *T* as the transformation that maps both position and intensity. The first category of spatial normalization methodology employs feature-based matching techniques. Normalization algorithms that make use of geometrical features in images such as points, lines and/or surfaces, determine the mapping of **T** (positional normalization transformation) by identifying features such as sets of image points that correspond to the same physical entity visible in both images, and calculating **T** for these features. Such algorithms iteratively determine **T**, and then infer *T* (intensity normalization transformation) from **T** when the algorithm has converged. For the purposes of this paper, we will refer to methods that use this type of algorithm as 'surface-based.'

The second category employs volumetric transformations involving intensity values. These normalization algorithms iteratively determine the image transformation *T* that optimizes a voxel similarity measure. We will refer to such methods as 'volume-based' (Hill *et al.*, 2000).

Both surface-based and volume-based normalization methods may employ a 'rigid body transformation', in other words there are six degrees of freedom (DOF) in the transformation: three translations and three rotations. The key characteristic of a rigid body transformation is that all distances are preserved. Rigid body transformations ignore tissue deformation and are widely used in medical applications where the structures of interest are either bone or enclosed with bone and are commonly used to register head and brain images. In the case of intersubject registration, however, rigid body normalization does not provide enough DOF for adequate intersubject registration. Some registration algorithms increase the DOF by allowing for anisotropic scaling, giving nine DOF, and skews, giving 12 DOF. This type of transformation is referred to as affine and can be described in matrix form. Also, an affine transformation preserves parallel lines. A rigid-body transformation can be considered a special case of the affine, in which scaling values are unity and skews equal zero (Hill *et al.,* 2000).

While Hellier *et al.* did not find significant differences between an affine, a rigid and three non-affine normalization methods when evaluating local measures based on matching of cortical sulci; they did find that for global measures the quality of the registration is directly related to the transformation's DOF (Hellier *et al.,* 2003). Collins and Evans compared rigid and non-affine normalization methods. In this study, the rigid method revealed problems in maintaining accurate global head shape and shape of internal structures like the ventricles as well as an error rate more than 50% higher than the non-affine method (Collins and Evans, 1997).

Crivello's comparison of one simple affine and three non-affine normalization methods including i) fifth order polynomial warp, ii) discrete cosine basis functions and iii) a movement model based on full multi-grid approaches support Hellier's findings. When Crivello *et al.* used the four methods to normalize 20 subjects' MRIs and PET volumes to the Human Brain Atlas (HBA), they found the full multi-grid approach, due to the large number of DOF, provided enhanced alignment accuracy as compared to the other three methods. The fifth order polynomial warp and discrete cosine basis function approaches exhibited similar performances for both gray and white matter tissues and the affine approach had the lowest registration accuracy (Crivello *et al.,* 2002).

Many authors refer to affine transformations as linear. This is not strictly true, as a linear map is a special map $\boldsymbol{L}$ that satisfies: $L(\alpha x + \beta x') = \alpha L(x) + \beta L(x')$ where $\forall x, x' \ni \Re$ and $x =$ any point in a mapping. The translational part of an affine transformation violates this. Thus, an affine map is more correctly defined as the composition of linear transformations with translations (Hill *et al*., 2000).

Grachev's anatomically based assessment of the Talairach stereotaxic transformation (Talairach and Tourneaux, 1988), a piece-wise affine algorithm, and a fifth-order polynomial transformation (Woods *et al.,* 1998) revealed that both methods located about 70% of anatomical landmarks with an error of 3 mm or less. For landmark accuracy less than or equal to 1 mm, the Woods method located about 40% of differences versus 23% for Talairach, again demonstrating the superior accuracy of non-affine over affine spatial normalization methods (Grachev *et al.,* 1998).

Davatzikos *et al.* compared two non-linear methods: SPM (Statistical Parametric Mapping), the most widely used method for analysis of functional activation images, and STAR (Spatial Transformation Algorithm for Registration). They found that STAR resulted in relatively better registration (Davitzikos *et al*., 2001). SPM employs a volume-based approach that minimizes the sum of the squared differences between the source image and target image while maximizing the prior probability of the transformation. The maximum a posteriori solution is found iteratively: the algorithm starts with an initial parameter estimate and searches from there. The SPM algorithm stops when the weighted sum of square differences no longer decreases or after a finite number of iterations (Salmond *et al*., 2002). The STAR algorithm differs from the SPM approach in that it employs an elastic instead of a parametric transformation, thus it has thousands of DOF compared to the relatively low DOF allowed for by SPM. Additionally, STAR applies surface-based curvature matching along the cortex, thus incorporating shape information in the matching mechanism. These differences were attributed to STAR's improved registration (Davitzikos *et al*., 2001).

SPM is one of many volume-based non-linear spatial normalization methods that have been developed and used over the years. Others include deformable templates using large deformation kinematics (Christenson *et al*., 1996), elastic deformation algorithm (Gee *et al.,* 1993), intersubject averaging and change-distribution analysis (Fox *et al*., 1988), unified framework for

boundary finding in a Bayesian formulation (Wang *et al*., 2000), statistical and geometric image matching (Gee *et al*., 1994), automated image registration (AIR) (Woods *et al*., 1998), octree spatial normalization (OSN) (Kochunuv *et al*., 1999), automatic non-linear image matching and anatomical labeling (ANIMAL) (Collins and Evans, 1997), analysis for functional neuro images (AFNI) (Cox, 1996) and maximization of mutual information (MMI) (Rueckert *et al*, 2001; D'Agostino *et al*., 2002).

Surface-based non-linear spatial normalization methods include STAR, hybrid surface models (Thompson and Toga, 1996), deformable surface algorithm (Davatzikos and Bryan, 1996), generalized Dirichlet solution for mapping brain manifolds (Joshi *et al.,* 1995), thin-plate splines (Bookstein, 1989), unified non-rigid feature registration (Chui *et al.,* 2003), computerized anatomical reconstruction and editing tool kit (Caret) (Van Essen *et al.,* 2001), Freesurfer (Fischl *et al*., 1999), BrainVoyager (Kiebel, Goebel and Friston, 1999) iconic features (PASHA) (Cachier *et al*., 2002) and active ribbons (Bizais, 1997).

There are also spatial normalization methods that incorporate aspects of both volumetric transformations and surface-based matching. They include hybrid volumetric and surface warping (Liu *et al*., 2004) and hierarchical attribute matching mechanism for elastic registration (HAMMER) (Shen and Davatzikos, 2002), diffusing models (Thirion, 1998) and robust multi-grid elastic registration (ROMEO) (Hellier and Barillot, 2003).

Researchers want to know, "What are reasonable expectations for each registration method?" Crum has observed that there is a problem in the neuroimaging community in that we do not usually know the quality of non-linear registration methods. We lack the necessary framework to explicitly estimate and localize error for non-linear registration tools. He argues that as research studies become more sophisticated, it is increasingly important to understand and measure the degree, regional variation and confidence in the correspondences established by any given registration. The solution lies in measuring quality at all stages of a non-linear registration task. We must prescribe success criterion, quantify i) technical image quality, ii) relationship quality between underlying biology and imaged features, and iii) registration quality (Crum *et al.,* 2003). Hill concurs that it is desirable to determine both the expected accuracy of a technique and also the degree of accuracy obtained for any given set of data (Hill *et al.,* 2001).

Like Hellier and Crivello, we wanted to evaluate the differences between spatial normalization procedures by testing them on a given neuroimaging data set to determine which method should be chosen for analysis (Hellier *et al*., 2003; Crivello *et al*., 2002). Other studies comparing normalization methods in the literature include (Fischl *et al*., 1997; Gee *et al*., 1997; Grachev *et al.,* 1999; Minoshima *et al*., 1994; Roland *et al*., 1997; Senda *et al*., 1998; Sugiura *et al.,* 1999). Currently, the Neuroimaging Visualization and Data Analysis lab (NeuroVia) at the University of Minnesota is conducting an evaluation of several spatial normalization methods including AIR, SPM, ANIMAL, HAMMER, PASHA, ROMEO and DEMONS (http://www.neurovia.umn.edu/neurovia.html). These studies used a variety of evaluation metrics including the dispersion metric of selected landmarks, differential characteristics, tissue classification, spatial homogeneity of selected anatomical features such as major sulci, overlap percentage of restricted volume of interest, cross-comparison of 3D probability maps and visual assessment.

Given the data set collected from cortical stimulation mapping for language localization, we wanted to know what would be the best spatial normalization method to use for intersubject registration to a canonical brain atlas. Friston states that goodness of a spatial transformation can be framed in terms of face validity (established by demonstrating the transformation does what it is supposed to), construct validity (established by comparison of techniques), reliability and computational efficiency. In this evaluation study, conducted as part of the University of Washington Human Brain Project, we address construct validity by comparing a surface-based and volume-based normalization method and establishing an expected accuracy measure for the given data set. We also address face validity by visual assessment of functional transformation to anatomical substrate. Computational efficiency, reliability and overall cost-benefit analysis are also discussed.

1.5 Cortical Stimulation Mapping and the Visual Comparison Approach

Since language function has been shown to vary significantly across patients, the technique of intraoperative stimulation mapping is used in order to plan for treatment of temporal tumor or intractable epilepsy at the University of Washington. Devised by Penfield and Roberts, stimulation mapping was based on the observation that applying a current to some cortical sites blocked ongoing object naming, although no effect of stimulating these sites was reported by the quiet patient. Based on this work, stimulation mapping for language localization became an accepted part of resective surgical technique for epilepsy. Stimulation mapping is used for localizing language function within a hemisphere after lateralization has been determined preoperatively by the intracarotid amobarbital perfusion test. Our data set consists of 11 patients who underwent surgery on the left, dominant hemisphere. In order to insure that cortical surface sites without evoked naming errors could be resected with a low risk of postoperative language deficit, stimulation mapping must indicate both where language function is located and where it is not. The extent of the craniotomy is determined in part by this consideration, covering both the areas of the proposed resection and also the likely language locations (Ojemann *et al*., 1989).

The patient is put under general anesthesia for the craniotomy. Prior to mapping, rolandic cortex is identified by stimulation and the threshold for after discharge in the electrocorticogram (ECoG) is established for the area of association cortex to be sampled with language mapping. Language mapping is conducted with the largest current that does not evoke after discharges. Typically this current is in the 1.5 to 10 mA range, measured between peaks of biphasic square-wave pulses with a total duration of 2.5 msec (1.25 msec for each phase). This current is delivered from a constant-current stimulator in four second trains at 60 Hz across 1-mm bipolar electrodes separated by 5 mm. Sites for stimulation mapping are randomly selected to cover the exposed cortical surface, including areas where language function is likely located as well as proposed resection. Typically there are 10-20 stimulation sites per subject that are identified with sterile numbered tags and recorded with a digital intraoperative photo (Ojemann *et al*., 1989).

Once the craniotomy is complete, local anesthesia is applied to the dura and scalp and the patient is brought to an awakened state in preparation for stimulation mapping, typically three to four hours after the operation has begun. The awakened patient is shown slides of line drawings of familiar objects like planes, boats, trees, etc. The slides are projected at four-second intervals, with the patient trained to name each one as it appears. This is an easy task, and there are frequently no naming errors on slides presented in absence of stimulation. Out of the 117 subjects included in the Ojemann study, the highest error rate without stimulation was 22%. While the patient names the slides, sites identified by numbered tags are successively stimulated, with the current applied as the slide appears and continuing until the appearance of the next slide. At least one slide without stimulation separates each stimulation and no site is stimulated twice in succession. Usually several slides intervene between each stimulation, and all sites are stimulated once before any site is stimulated a second time. Three samples of stimulation effect are usually obtained. Intraoperative manual scoring of errors and their relations to stimulation provides immediate feedback to the neurosurgeon (Ojemann *et al*., 1989). If the stimulation of a site results in a naming error at least two of the three times, the site is determined to be essential for language function. These sites are considered essential for language function because i) resecting tissue close to such areas usually results in postoperative aphasis ii) avoiding them by 1.5 to 2 cm avoids such language deficits and iii) all aphasic syndromes include anomia (Modayur *et al*., 1997). In addition, the patient's responses and markers indicating when and where stimulation occurred is recorded on audio tape and used to later check the results to determine if the sites that were identified as essential for language function are statistically significant for naming errors as determined by the subject's responses with and without stimulation.

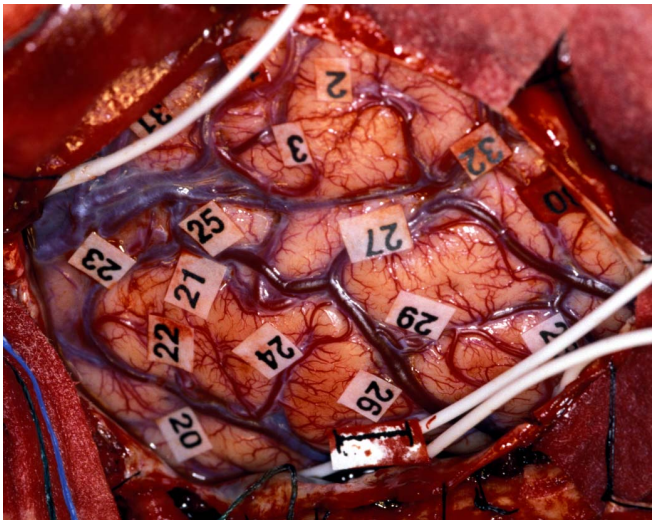

Figure 3. Surgical photograph taken during preparation for a left hemisphere temporal lobe resection. The numbered tags identify sites that have been electrically stimulated, referred to as cortical stimulation sites.

A visual comparison approach is used to transpose the location of the numbered tags as seen in figure 3 to a 3D volume reconstruction of the cortical surface including veins and arteries. The interactive mapping process is facilitated by the Skandha4 software package. As shown in figure 4, the language mapping module graphic user interface (GUI) includes the intraoperative photo, the MR volume data, a 3D rendered image of the brain and a palette of numbers. The neuroanatomist expert determining the localization of the sites is blind to whether or not sites had naming errors associated with them. All localization endeavors were given a confidence rating on a scale from 1 to 5, where 1 is "not at all confident" and 5 is "very confident." The ratings were determined by amount and quality of images and descriptions. Using the blood vessels and anatomical structure in the rendering as landmarks, the expert drags and drops the number that corresponds to the number in the photo onto the rendered image. Once the site has been dropped, a 'pick'operation is performed in order to determine the closest surface facet to the site. The site is assigned a 3D coordinate in MR 'magnet space' in which the center of the MR magnet is the origin. This data is stored in a cortical stimulation mapping (CSM) database.

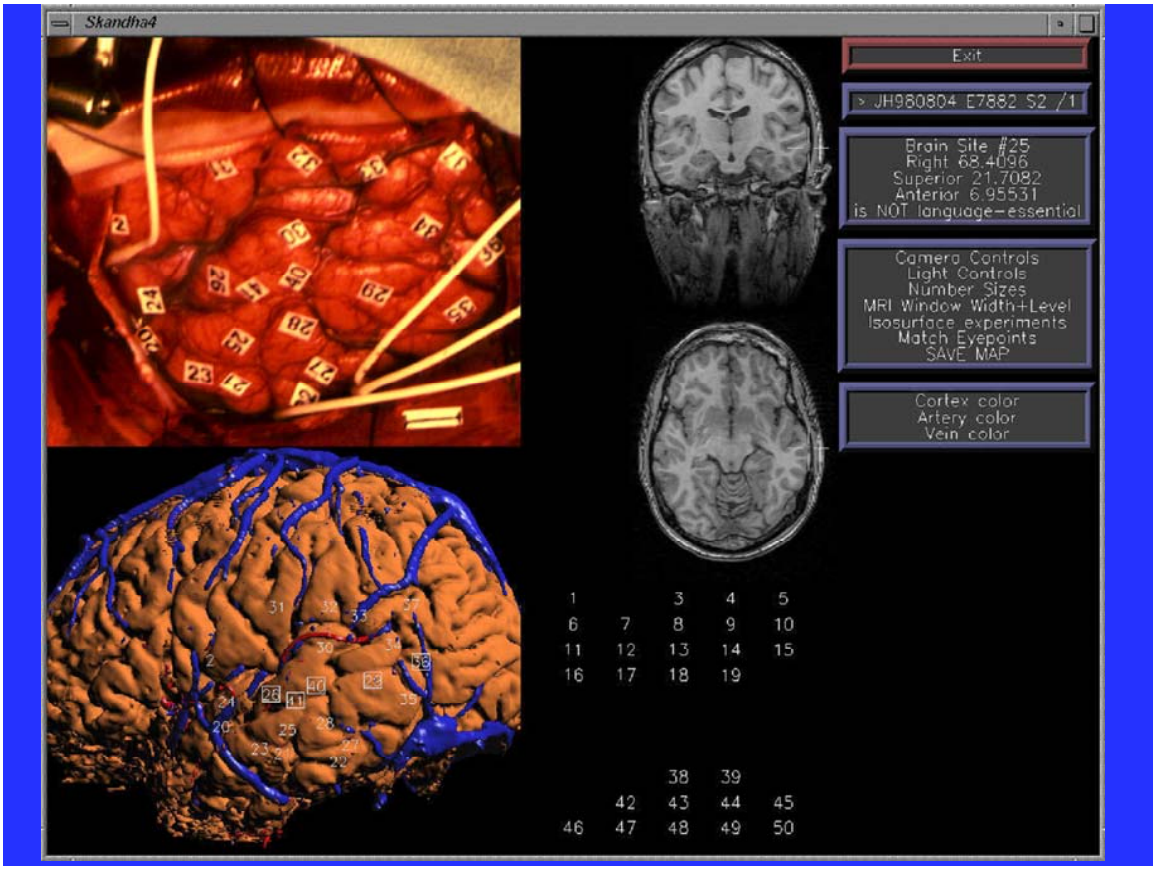

Figure 4. Skandha4 GUI used in the visual comparison approach

According to repeatability studies, any given mapping will typically fall within a distance of 5.1 mm of the true site location as measured by the mean of all the mappings (6 mappings included in the study). Since the language site locations mapped during surgery are accurate to 1 cm, the accuracy achieved using the visual comparison approach was deemed satisfactory (Modayur *et al*., 1997). We found in a comparison of three independent mappings of two subject's CSM sites (n = 41 sites) that any given mapping could vary by an average of 7.5 mm, still within the 1 cm margin of error for site location mapped during surgery.

1.6 Hypothesis

In this case study, we expected that reducing variation would better reveal functional patterns of language production that exist in CSM language sites, which have been identified as statistically significant for naming errors during neurosurgery. We believed that the problem of analyzing CSM functional data across subjects can be solved using computer-aided spatial normalization. As a result, we asked this key question: "What is the best spatial normalization method for registering two or more brains such that the observed variation in the functional areas after registration, as measured by cortical stimulation mapping (CSM), is the smallest?"

Because the data we used in our case study was collected on the cortical surface, we expected that a surface-based normalization method, which relies on selected cortical surface landmarks, would result in less variation between CSM language sites as compared to a volume-based normalization method. For the same reason, we expected that the surface-based normalization method would result in more accurate anatomical localization of CSM site locations.

Section 2: Survey of Evaluation Tools

Developing and implementing an evaluation technique for spatial normalization methods required that we explicitly select tools for surface reconstruction, surface flattening, a target atlas and spatial normalization.

2.1 Surface reconstruction tools

There have been many efforts to develop automated and semi-automated methods for reconstructing the convolutions of the cerebral cortex. The tools surveyed are available outside the laboratories in which they were developed.

Surface Reconstruction by Filtering and Intensity Transformations, called SureFit, was designed at the Washington University Van Essen lab and is based on an underlying physical model of cerebral cortex and its appearance in structural MRI. The cerebral neocortex consists of a slab-like sheet of gray matter, with approximately uniform thickness, folded into outward folds, called *gyri*, and inward folds, called *sulci.* The transition from gray matter to the underlying white matter is called the inner boundary. The cortical surface, called pial, is where the gray matter meets the cerebrospinal fluid (CSF) and defines the outer boundary (Van Essen *et al.,* 2001).

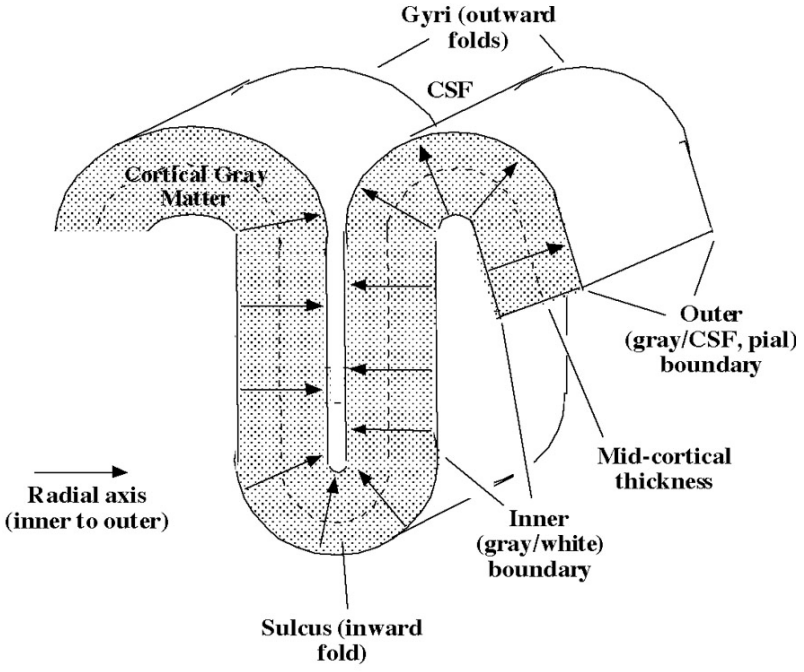

Figure 5. A schematic model showing a patch of folding cortex

SureFit generates a set of probabilistic maps for the location of gray matter, white matter, the inner(gray-white) boundary, and the outer (pial) boundary as substrates for the segmentation process using Gaussian intensity transformations (Van Essen *et al.,* 2001). This generation requires a complex set of filtering operations, intensity transformations, and other volumetric operations applied to the image intensity data.

All filtering operations are applied to the 3D image volume. Inner and outer boundary maps are particularly important, because they are combined to form a position map along the radial axis, which runs from the inner to the outer boundary. The result is a position map along the radial axis that is thresholded. The thresholding generates an initial cortical segmentation with a boundary running approximately midway through the cortical sheet. The initial segmentation is used as the substrate for generating an explicit surface reconstruction (Lorenson, 1987). SureFit currently involves five major processing stages for segmentation as shown in figure 6.

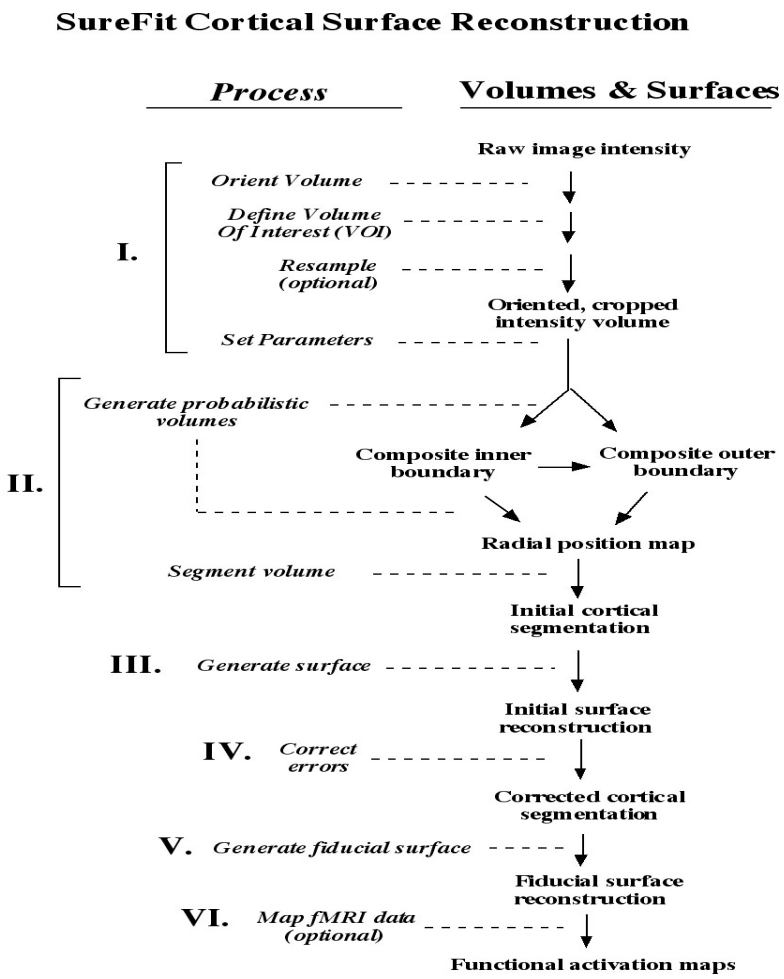

Figure 6. Five steps for creating a surface reconstruction using SureFit. We completed the first five steps for each subject's left hemisphere. Instead of mapping fMRI data as the sixth step, we mapped CSM data.

Other tools considered include Freesurfer (Dale *et al.,*1999), mrGray-2.0 (Teo *et al.,* 1998) and BrainVoyager (Goebel *et al.,* 1997). We selected SureFit primarily due to our past experience with the tool and the desire to collaborate with the Van Essen Lab.

2.2 Surface flattening tools

The complex geometry of the human brain contains many folds and fissures making it impossible to view the entire surface at once. Since most of the cortical activity occurs on these folds, it is desirable to view the entire surface of the brain in a single view. This can be achieved using flat maps of the cortical surface, which are essentially unwrapped cortical surfaces in a 2D plane (Van Essen *et al.,* 2001). Cortical flat maps also make it easier to see the depths and complete shape of the sulci. Algorithms for creating flat maps do require cutting, compression and stretching of the surface, causing some distortion. All cortical flattening methods aim to minimize geometric distortion. We considered the following tools for creating cortical flat maps in this case study:

- Computerized Anatomical Reconstruction and Editing Tool Kit (CARET) (http://brainmap.wustl.edu/caret)
- mrUnfold-5.0 (http://white.stanford.edu/~brian/mri/segmentUnfold.htm)
- BrainVoyager (http://www.brainvoyager.de)
- FreeSurfer (http://surfer.nmr.mgh.harvard.edu)

We selected Caret to flatten surfaces for two reasons. First, SureFit was selected for image segmentation and is distributed and supported by the same lab as Caret. Thus, SureFit is designed to interface seamlessly. In fact, work is underway to incorporate SureFit into the Caret software suite. Secondly, since we selected Caret as one of the spatial normalization methods, using the same software suite for flattening made for a streamlined evaluation protocol.

2.3 Target Atlases

Ideally a target atlas will not bias the final solution. An ideal template would consist of the average of a large number of MR images that have been registered to within the accuracy of the spatial normalization technique (Ashburner and Friston, 2000).

Talairach

Jean Talairach and Pierre Tournoux created the now famous book, **Co-Planar Stereotaxic Atlas of the Human Brain,** in 1988. Talairach and Tournoux dissected and photographed a post mortem brain of a 60 year-old female subject, creating a proportional coordinate system often referred to as “Talairach space” for neurosurgical studies. This atlas was widely used in international brain imaging studies and continues today to be the most widely used human brain

atlas. Talairach space consists of 12 rectangular regions of the target brain that are piecewise affine transformed to corresponding regions in the template brain. Using this transformation, a point in the target brain can be expressed in Talairach space coordinates, which allows for comparison to similarly transformed points from other brains (Brinkley and Ross, 2002).

Today there is a database and data retrieval system named Talairach Daemon developed at the University of Texas, San Antonio that performs the registration of target brains to the Talairach template brain (http://ric.uthscsa.edu/projects/talairachdaemon.html). This system returns anatomical labels using Brodmann area names for the cerebral cortex and other traditional, feature-based terms when queried with a stereotaxic coordinate from an individual subject's brain. Thus, the Talairach Atlas provides a symbolic representation (textual) of the brain.

The entire Talairach brain has been anatomically labeled using a five-level, volume-based, terminological hierarchy. Level One ("hemisphere") has six components: left and right cerebrum; left and right cerebellum; left and right brainstem. Level Two ("lobe") divides each hemisphere into lobes or lobe equivalents. In cerebrum and cerebellum, lobes are as traditionally defined. In brainstem, three lobe-equivalents are defined: midbrain, pons and medulla. In both cerebrum and cerebellum, brain areas lying deep in traditionally defined lobes are termed sub-lobar. Level Three ("gyrus") divides each lobe into gyri or gyral equivalents. Nuclear groups, such as thalamus or striatum, are gyral equivalents. Level Four of the hierarchy is tissue type. Each gyrus or gyral equivalent is segmented into grey matter, white matter and CSF. Level Five of the hierarchy is cell population. Cerebral cortex is labeled by Brodmann area. Nuclear groups are labeled by subnuclei. Cytoarchitectonic labels for cerebellar cortex and tract labels for white matter are being developed but are not yet available.

The Talairach Daemon's labels are stored as a volume array (1 mm isometric voxels) spanning the extent of the brain in the Talairach 1988 atlas. This corresponds to approximately 500,000 voxels. Each voxel in this array contains a pointer to voxel-specific brain information. This information is called a relation record and is managed as a linked list. A relation record can store any information that is recorded using Talairach coordinates. To eliminate the need for storing

duplicate information in relation records, each record contains pointers to the information rather than the information. This scheme offers the potential for extremely high speed access to information within the relation records (Lancaster *et al.,* 1997).

MNI305 and ICBM152

The Montreal Neurological Institute (MNI) wanted to define a template brain that was more representative of the human population than the single brain used by Talairach and Tournoux. They created a new template that was approximately matched to the Talairach brain via a two-step process. First, they used 241 normal MRI scans, and manually defined various landmarks and the edges of the brain. Each brain was scaled to match the landmarks to equivalent positions on the Talairach atlas. Second, a sample set of 305 normal MRI scans from right-handed male (239) and female (66) individuals were normalized to the average template of the first 241 brains using an automated 9 parameter affine transform. From this, MNI generated an average of the 305 brain scans. This atlas is known as the MNI305 atlas and was the first template created at MNI. The current standard MNI template is named the ICBM152 because the International Consortium for Brain Mapping adopted this atlas as their standard template. The ICBM152 atlas was created from an average of 152 normal MRI scans that were normalized to the MNI305 using a 9 parameter affine transform (Brett, 2003).

colin27 Atlas

A MNI lab member, Colin Holmes, underwent 27 MR brain scans. These scans were then coregistered (registered to each other) and averaged to create a detailed MRI dataset of one brain. The average of the 27 scans was then registered to the ICBM152 space to create what is called "colin27," also known as the Colin atlas. This template is used as a standard template in the MNI brainweb simulator.

ICBM Probabilistic Atlases

Arthur Toga, Laboratory of Neuro Imaging (LONI) Director, and John Mazziotta, UCLA Brain Mapping Center Director and principal investigator of ICBM, lead a team of researchers who have created a variety of probabilistic atlases as they work to achieve the team's ultimate goal of a four-dimensional atlas and reference system that includes both macroscopic and microscopic information on structure and function of the human brain in 7,000 persons between the ages of 18 and 90 years. As discussed, the fact that no single, unique physical representation for the human brain is representative of the entire species, the variance must be encapsulated in an appropriate framework.

Mazziotta and Toga have chosen a probabilistic framework in which intersubject variability is captured as a multidimensional distribution. Accessing data from a probabilistic atlas will produce a probability estimate of structures and function based on the distribution of samples obtained. This frameworks also differ from frameworks like the ICBM152, which is an average brain space. The average brain framework is created using a density-based approach. An atlas using the density-based approach is an average space constructed from the average position, orientation, scale and shear from all the individual subjects. It is, therefore, both an average of intensities and of spatial positioning. Probabilistic atlases, like the ICBM Tissue Probabilistic Atlas and Lobular Probabilistic Atlas proceed as follows:

- Classify the desired components (tissue type or lobe type in these cases)
- Average the separate components across the subjects to create probability fields for each component that represent the likelihood of finding each component at a specified position for an individual brain that has been linearly aligned to the atlas space (Toga and Mazziotta, 2000).

PALS-B12 Atlas

The Population-Average Landmark- and Surface-based atlas (PALS-B12) is a new electronic atlas developed at the Washington University Van Essen Lab. Designed for brain-mapping analysis, it is derived from the MRI volumes of 12 normal young adults and includes both volume-based (MRI) and surface-based representations of the cortical shape. The population average and individual subject representations were created using Caret, a surface-based method of spatial normalization discussed in Section 2.4. The atlas includes sulcal depth maps as a standard shape representation and depth-difference maps can be used to view differences between individuals and across populations. The atlas also includes probabilistic representations of the population average surface and volume (Van Essen, 2005).

This atlas was designed specifically to avoid the inevitable bias introduced when using a single brain atlas as a target. A 'multi-fiducial mapping' method is introduced that maps volume-averaged group functional data (e.g. fMRI) onto all 24 individual hemispheres in the atlas, followed by spatial averaging across the individual maps, yielding a population-average surface representation that shows the most likely regions of activation and the maximal extent of plausible activation.

We selected the colin27 for primarily two reasons relating to the type of metrics we wished to use. First, we wanted to measure pre-normalization and post-normalization distances between language sites across brains both in 2D and 3D space. If we were to use an average brain atlas (like ICBM152), the blurring that occurs from averaging multiple brains would distort the flat map distances significantly after normalization, because the sulci would become significantly shallower due to averaging as compared to the sulci in the individual flat maps. Second, evaluation of anatomical localization using CPS required visualization of the data on a single brain so as to determine if a site is indeed in the correct parcel. The blurring of sulci and gyri that is a result of averaging individual MR images would make the evaluation very difficult if not impossible. Given these constraints, we selected the colin27 atlas that we received from the Laboratory of Neurological Imaging (LONI) at UCLA and registered it to MNI152 space using SPM2.

2.4 Spatial normalization methods

We considered five spatial normalization software tools that are commonly used within and outside the labs in which the tool was created. Other tools are discussed in Section 1.4. In Section 6 we discuss possible future work of evaluating other methods to provide further insight into how each method impacts results as well as the expected accuracy, efficiency and distinct benefits of each method. We selected a method from each of the two categories discussed in Section 1 as representative samples of each approach.

2.4.1 Surface-based anatomical normalization methods

Caret (http://brainmap.wustl.edu/caret)

Caret is a software tool developed by David Van Essen, Heather Drury and John Harwell at Washington University. Options for surface-based transformation allow for the source to be deformed to the target while constrained by explicitly designated landmarks, called 'Core6' landmarks. Core6 includes the fundi of the calcarine sulcus, central sulcus and lateral fissure; the anterior half of the superior temporal gyrus (STG); and the medial wall cortical margin (split into dorsal and ventral portions). These landmarks were selected on the basis of their consistency in location and extent. Caret deforms flat maps or spherical maps. The spherical registration is more accurate and uses an algorithm developed by Bakirciogli *et al.* (Van Essen *et al.,* 2001). The basic strategy is to draw landmarks as prescribed by the Core6 guidelines on the source map, then the landmark contours are resampled to establish corresponding numbers of landmark points on each source and target landmark contour. The landmarks are then used as constraints for the deformation algorithm. The deformation entails using Laplacian differential operators constrained to the tangent space of the sphere and basis functions that are expressed as spherical harmonics.

FreeSurfer (http://surfer.nmr.mgh.harvard.edu)

FreeSurfer is a software suite developed by Anders Dale and Bruce Fischl at Massachusetts General Hospital's Martinos Center for Biomedical Imaging and CorTechs Lab, Inc. Freesurfer employs a spherical transformation to establish a uniform surface-based coordinate system. Using this coordinate system, points on any of the surface representations for a given subject can be indexed. Freesurfer employs a procedure that aligns a cortical hemisphere with an average surface, based on an average convexity measure. By maximizing the correlation of the convexity measure between the individual and the average, the procedure computes an optimal mapping to a

canonical target (Fischl *et al.,* 1998). The FreeSurfer algorithm is very similar to Caret, except that FreeSurfer normalization uses all sulci in maximizing correlation instead of a selected set of landmarks, as is the case for the Caret algorithm. There is some evidence that the limited landmark method may be superior, but more evidence is needed to exhaustively compare these registration methods (Desai, 2004).

BrainVoyager (http://brainvoyager.de)

BrainVoyager software was developed by Rainier Goebel, Maastricht University, originally introduced as a tool for analysis and visualization of functional and structural imaging data in 1998. It is now a commercial software package featuring cortex-based inter-subject normalization based on gyral/sulcal patterns of individual brains as well as other functions listed previously (Goebel, 2000).

2.4.2 Volume-based anatomical normalization methods

Analysis of Functional NeuroImages (AFNI)
(http://afni.nimh.nih.gov/afni/about/descripadfaad)

AFNI is a software environment for processing and displaying functional MRI data on an anatomical substrate. It was designed and written at the Medical College of Wisconsin, primarily by Robert Cox, now director of scientific and statistical computing core at the National Institute of Mental Health. It is a free software package that uses a base unit of data storage called the '3D dataset,' which consists of one or more 3D arrays of voxel values with some control information stored in a header file. AFNI's spatial normalization feature requires the user to select various markers first to align the anterior commisure and posterior commisure and a second set of markers to define the bounding box of the subject's brain. Then a 12 sub-volume piecewise linear transformation to Talairach coordinates is performed for both anatomical and functional volumes (Cox, 1996).

SPM2 (http://www.fil.ion.bpmf.ac.uk/spm/)

Karl Friston originally developed the software and associated theory for routine statistical analysis of functional neuroimaging data. SPM*classic* was the first version of the software suite released in 1991 with the intent of promoting collaboration and a common analysis scheme across

laboratories. SPM has had five major revision releases since 1991. In this study, we consider the most recent release, SPM2 ,released in 2003.

Spatial normalization using SPM2 is achieved by registering the individual MR images to the same target image, by minimizing the residual sum of squared differences between them. The first step in spatially normalizing each image involves matching the image by estimating the optimum 12-parameter affine transformation (Ashburner et al., 1997). A Bayesian framework is used, whereby the maximum a posteriori estimate of the spatial transformation is made using prior knowledge of the normal variability of brain size. This step has been made more robust in SPM2. Affine registering image A to match image B should now produce a result that is much closer to the inverse of the affine transformation that matches image B to image A. A regularization (a procedure for increasing stability) of the affine transformation has also changed. The penalty for unlikely warps is now based on the matrix log of the affine transform matrix being multivariate and normal.

The second step accounts for global nonlinear shape differences, which are modeled by a linear combination of smooth spatial basis functions (Ashburner and Friston, 1999). The nonlinear registration involves estimating the coefficients of the basis functions that minimize the residual squared difference between the image and the template, while simultaneously maximizing the smoothness of the deformations. This step has been improved in that the bending of energy of the warps is used to regularize the procedure, rather than membrane energy. This model seems to produce more realistic looking distortions. It is worth noting that this method of spatial normalization corrects for global brain shape differences, but does not attempt to match other cortical features (Ashburner and Friston, 2000).

Section 3: Methods

Subjects

The subjects were 11 patients (5 female, 6 male, age range 23-52 years) undergoing resection treatment at the University of Washington Medical Center for chronic epilepsy (n = 11). Seven patients were right handed. All cortical stimulation occurred in the subject's left hemisphere, which was identified as the subject's language-dominant hemisphere in all subjects determined by pre-surgery WADA testing (Corina *et al*., 2005). Subject demographics are summarized in table 3.

Table 3. Subjects' gender, age, handedness and verbal IQ (VIQ)

			Handed	
BrainID	**Gender**	**Age**	**ness**	**VIQ**
54	M	25	R	107
55	M	30	R	83
58	M	23	-	86
60	M	38	-	72
61	F	35	R	91
62	F	24	-	92
63	M	42	R	125
117	F	41	-	97
164	M	42	R	94
170	F	52	R	75
176	F	41	R	82

Evaluation technique protocol

To test our hypothesis we developed a six-step evaluation protocol:

1: select MRI volumes

2: create surface reconstruction

3: create flat map

4: assign coordinates, function and cortical parcellation to each CSM site

5: apply spatial normalization to anatomical and functional data

6: evaluate methods using spread reduction and anatomical localization measures

Step 1: Select MRI volumes

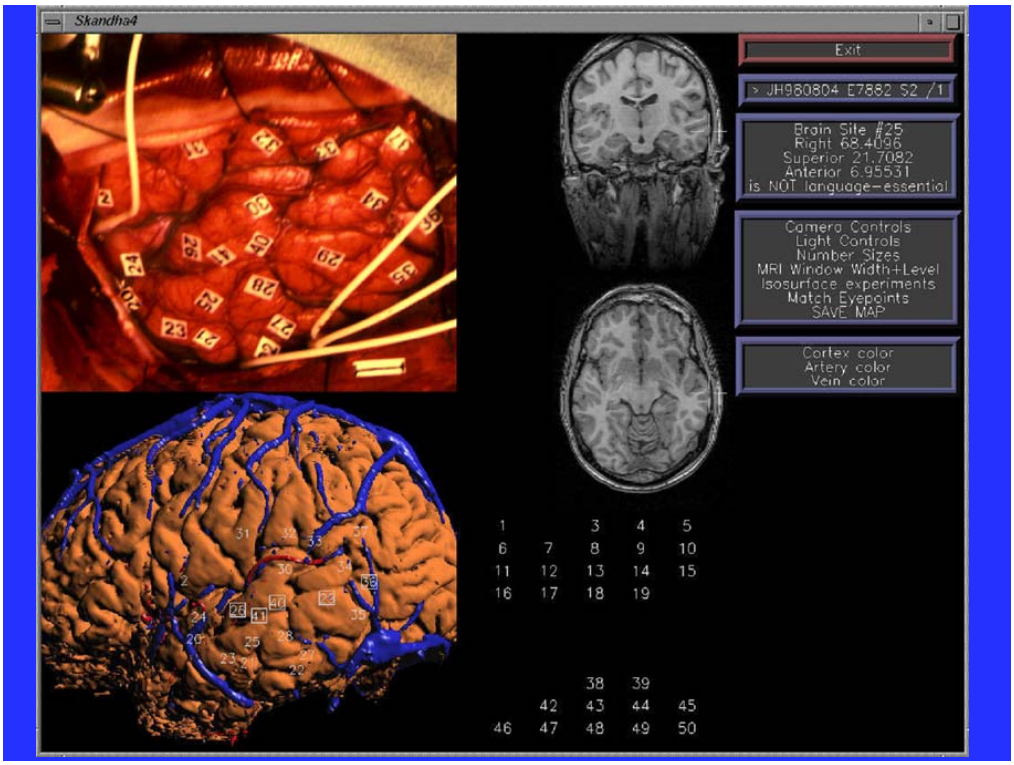

Figure 7. Visual Brain Mapper screen shot. Upper left is a neurosurgery photo of the left temporal lobe with sterilized labels identifying various cortical sites. To the right are coronal and axial slices from the patient's MRI taken prior to surgery. At lower left is the lateral left hemisphere view of a 3D brain model including arteries and veins created from the patient's MRI, venogram and arteriogram.

We selected 11 MR images from a University of Washington Structural Informatics Group database of over 90 patients (CSM database). We screened the database images for left hemisphere surgery, quality and lesions.

The first level of screening eliminated patients whose surgery was conducted on the right hemisphere. By including only left hemispheres in this case study, we limit our scope to focus on one major structural element of the brain. While left hemisphere surgeries are more common than right hemisphere surgeries, future work would need to include analysis of the right hemisphere as well as the left.

Image quality was the next level of screening. We determined quality by uniformity of voxel intensity values, gray-white contrast within the image and artifacts, especially in the left temporal

lobe, our primary region of interest. Working with a SureFit expert, we were able to screen out images that would require substantial manual error correction due to poor image quality. In one instance (P62), non-uniformity of intensity was an issue. Using FSL's fast algorithm (http://www.fmrib.ox.ac.uk/fsl/fast) significantly improved the quality of the image, making it possible to include the image in the data set. The final level of screening eliminated subjects with large lesions.

Step 2: Create Surface Reconstruction

As discussed in Section 2.1, we selected SureFit to create surface reconstructions of the fourth cortical layer of the left hemisphere of each subject's brain. Figure 8 contains three of the 11 surface reconstructions segmented for this study and the surface reconstruction of the target atlas, colin27.

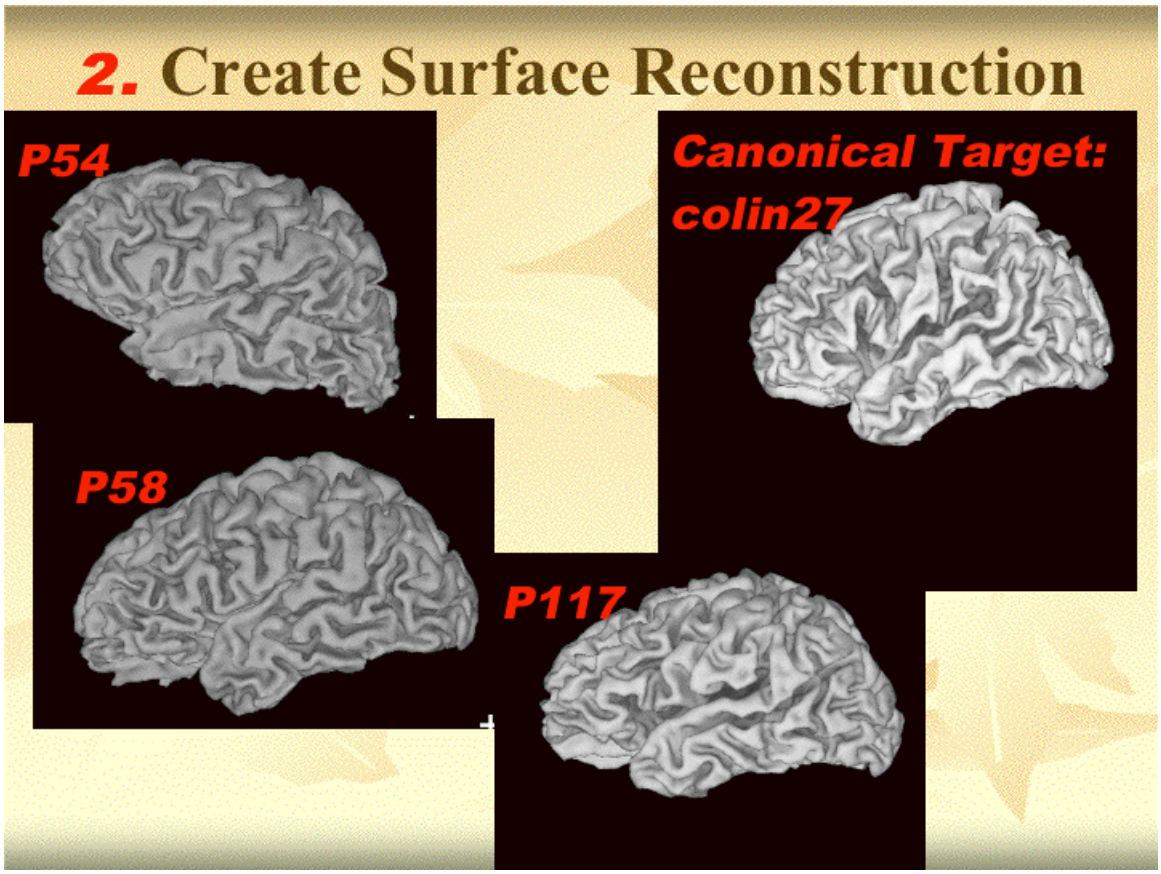

Figure 8. Surface reconstructions of four left hemispheres created using SureFit

Prior to launching the automated segmentation process, the MRI volume was resampled to 1 mm cubic voxels and cropped to included only the left hemisphere. The segmentation generated a cortical surface reconstruction in approximately 1- 2 hours using a Dell Dimension dual 450Mhz processor running Debian Linux.

Error detection and correction involved automatic correction and interactive editing. Topological errors, called 'handles,' in the initial segmentation are typically attributable to noise, large blood vessels, or regional inhomogeneities in the structural MRI volume, or a combination of these. Errors were localized by inflating the initial surface reconstruction to a highly smoothed ellipsoidal shape and using the orientation of surface normals to identify regions, called 'crossovers,' where the surface is folded over itself. Clusters of surface nodes associated with crossovers were mapped from the surface reconstruction into corresponding voxel clusters in the volume. The automated error correction process tested for different types of handles in the vicinity of each location determined to have an error.

The localized patches used for these tests conformed to the shape of temporary segmentations that are based on different threshold levels for the radial position map. If the trial patch reduced the number of topological handles in the segmentation, as determined by an Euler count applied to the volume (LeeT-C *et al.,* 1994), it was accepted as a permanent correction and the process moved on to the next error patch. (Van Essen, *et al*., 2001)

The automated error correction process sometimes failed, especially for handles that were notably large or irregular. Such errors were corrected using interactive editing. For each handle that remained after automatic error correction, the analyst used the object limits and 3D viewer to identify the vicinity of each remaining handle. Voxels were then added or removed one at a time or in small clusters using dilation and erosion steps within small masked regions. Error correction was completed when no visible handles remained on the cortical surface reconstruction. The quality of the SureFit-generated cortical segmentations was evaluated by visual inspection of segmentation boundaries and of surface contours overlaid on the anatomical volume. This assessment suggested that surfaces are generally accurate to within about 1 mm of their desired trajectory (Van Essen, 2005).

Step 3: Create Flat Map

To aid in method evaluation, we created cortical flat maps using Caret as outlined in Section 2.2. The SureFit specification file for the individual surface reconstruction was loaded into Caret. The 'Flatten Surface' functionality was selected. Then the six default cuts outlined on the medial surface of the left hemisphere were inspected. The calcarine cut and medial wall cut were always redrawn to match the specific structure of the individual surface. The remaining cuts (cingulate cut, frontal cut, Sylvian cut, temporal cut) were redrawn, as needed, using the 'Draw Border' functionality. These cut lines were used to determine where the inflated surface was split in order to achieve a cortical flat map. Figure 9 shows the template cut lines on the surface reconstruction, and figure 10 shows how the surface reconstruction and flat map correlate.

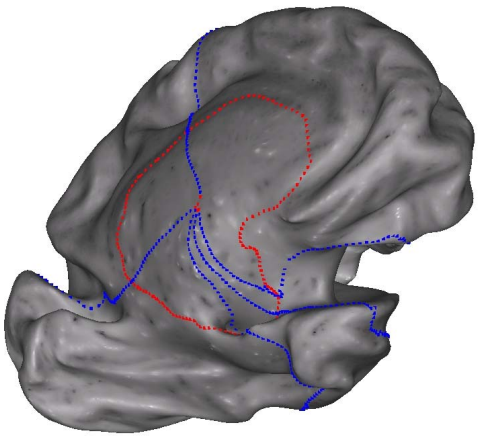

Figure 9. Template cuts for flattening. The red dashed line traces the medial wall cut. Five other cuts include calcarine, cingulate, frontal, lateral and temporal drawn in blue.

Once the cut lines were set, the automatic flattening took place. Flattening took 30-60 minutes on a Dell Dimension 450 with dual processors running Debian Linux.

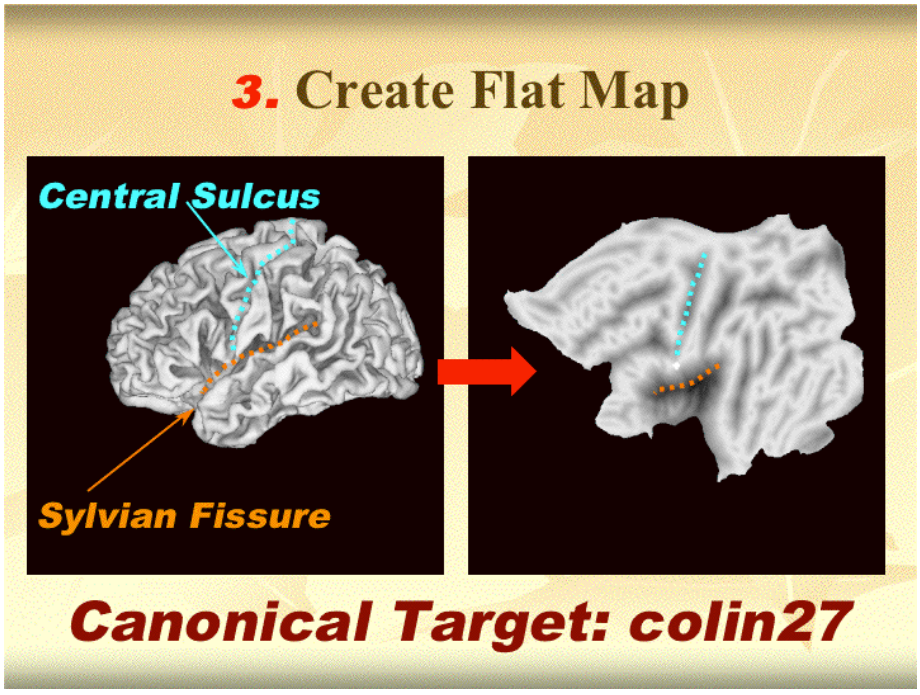

Figure 10. Relationship of 3D surface reconstruction to 2D flat map

Step 4: Assignment of Coordinates, Function and Cortical Parcellation to Sites

In Section 1.5 we described how cortical stimulation data was collected during neurosurgery and mapped to a coordinate system using the visual comparison approach. Additionally, the neuroanatomist expert assigned an anatomical location to each site based on a cortical parcellation system (CPS), designed as a scheme for examining the neural substrate through intelligent computer querying of the CSM database (Corina *et al.,* 2005). This system divides the lateral surface of the cortex into 37 subdivisions, labeled using the Foundational Model of Anatomy (FMA) expansion of NeuroNames terminology and is shown in figure 11.

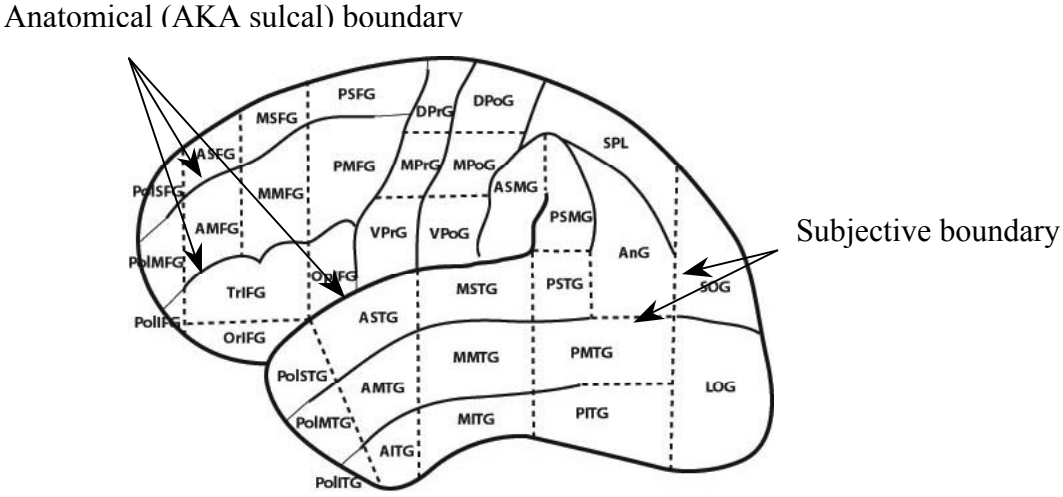

Figure 11. Cortical Parcellation System for lateral cortical surface

The data retrieved from the CSM database included the 3D coordinates and CPS anatomical localization for each of the 198 sites recorded for the 11 subjects. The coordinate file was then input into both the surface-based and volume-based methods and transformed accordingly. In Caret, a spherical registration algorithm used landmark borders to create a deformation map. SPM2 spatially normalized the individual volume image to the avg152T1 Minc file to create a deformation file, which was aligned to ICBM152 space. The deformation for each method was applied to the individual coordinate file in magnet space

coordinates, resulting in a normalized coordinate file. The result was a set of coordinate files registered to the same reference space: ICBM152 space. These normalized coordinate files were used to evaluate accuracy of each method based on spread reduction between sites and preservation of anatomical localization (Step 6).

Of the 198 CSM sites, we were especially interested in the 21 sites identified as statistically significant for naming errors (see table 4). Such sites have been found within and outside areas classically considered language function regions. We believe that a hidden pattern of language production exists that could be revealed with the help of spatial normalization. Statistical significance was derived by analysis of the patients' responses. Analysis included comparing the patient's pre-surgery test responses to the intraoperative test responses. To determine whether naming disruption at a site determined by the neurosurgeon was an effect of stimulation or attributable to the baseline naming error rate of the subject, a within-subject analysis of naming errors was carried out. Fischer's exact test ($p < 0.05$) was used to compare each subject's baseline performance, derived from the naming error rate in each control trial associated with the site, regardless of target, and performance under stimulation at that site. This definition of baseline, restricted to the controls associated with a certain site, was established to eliminate variation in performance due to fatigue, inattention, and other physical factors experienced by the subject during the procedure. The p value represents the reliability that an error was observed under stimulation relative to the unstimulated baseline for each individual site (Corina *et al*., 2005).

Table 4. Summary of statistically significant language site anatomical localization

ID	CSM #	Location		ID	CSM #	Location
P54	20	PSTG		P61	30	PSMG/AnG
P54	30	PSTG		P62	33	OpIFG
P54	35	PSTG		P62	35	TrIFG
P54	36	PSMG		P63	25	MSTG
P55	41	MSTG		P117	21	ASMG
P58	32	PMTG		P117	33	PSMG
P60	29	MSTG		P164	35	VPRG
P60	31	PMTG		P164	40	ASMG
P61	25	MSTG		P170	26	MSTG
P61	28	PMTG		P176	28	MSTG
P61	29	PMTG				

Generating pre-normalization coordinates that could be compared across subjects required shifting the individual volume images into a common grid (i.e. standard voxel size, origin and orientation). Without a common grid, we could not reasonably establish baseline distances between language sites across subjects, which is necessary in order to measure spread reduction after normalization (Step 6). Each subject's volume has its own magnet center, and in some cases the chin may be rotated up or down or slightly to the side. For pre-normalization coordinates, we aligned the anterior commissure (AC) and posterior commissure (PC) using the AFNI software package. This process resampled the volume to cubic 1 mm voxels and applied a rigid registration to align the volumes to a common origin: the intersection of the superior edge and posterior margin of the AC. AFNI also rotated the volume as needed so that its Y axis runs from the inferior edge of the PC to the AC origin. Using AFNI, the AC superior edge and posterior margin, the inferior edge of the PC and two mid-sagittal points were selected. AFNI then computed transformation information that it stores in the volume .HEAD files. Then, the AFNI command line utility, Vecwarp, was called to apply the transform to the individual coordinates, resulting in pre-normalization AC-PC aligned coordinate files. These coordinate values were used to calculate the pre-normalization distances (Euclidean distance) between language sites across subjects (measure described in step 6).

Step 5: Spatial Normalization

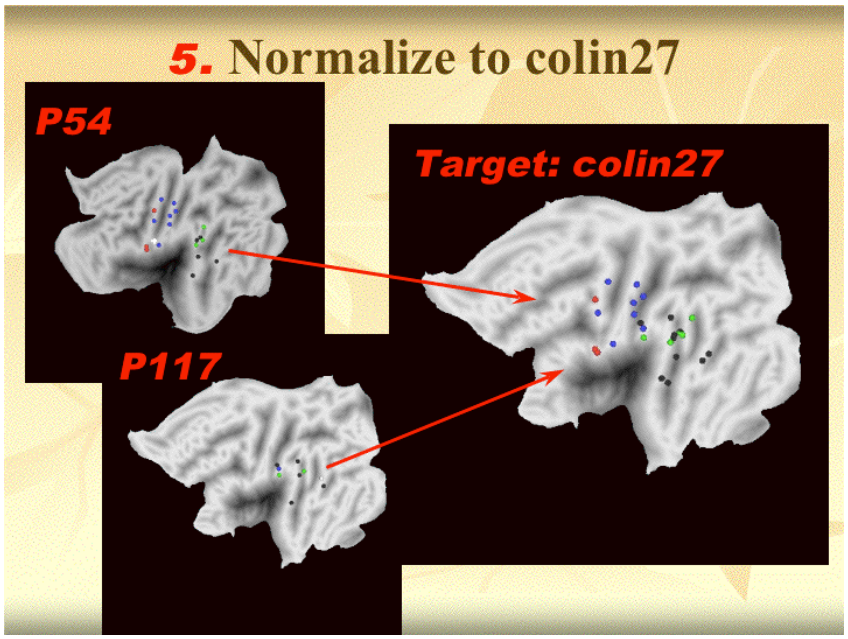

Figure 12. Visualization of the normalization process

Surface-based normalization

To normalize the individual surface (source) to the colin27 atlas (target), we first need to select the Core6 landmarks required to constrain the registration as discussed in Section 2.4.1. To delineate landmarks traces along the sulci fundi, inflated surfaces of the individual hemisphere and the corresponding colin27 atlas hemisphere were viewed side by side. Endpoints for each landmark trace were drawn as prescribed by the Core6 protocol. Complete landmark traces were then drawn between the endpoints on the flat map using the visualization of cortical folding to determine the trajectory of the fundus (see figures 13 and 14). Landmark contours were projected onto the surface and saved as a 'border projection file' in a 'barycentric' format. The file was then mapped to the spherical standard surface that was used for registration. Spherical registration was started using the 'Deform Spherical Map' function with the deformation selection 'Deform Individual to Atlas and Deform Atlas to Individual.' Drawing landmarks for one subject took 15-30 minutes. The automatic normalization process took approximately 15 minutes per subject on a Dell Dimension dual 450Mhz processor running Debian Linux.

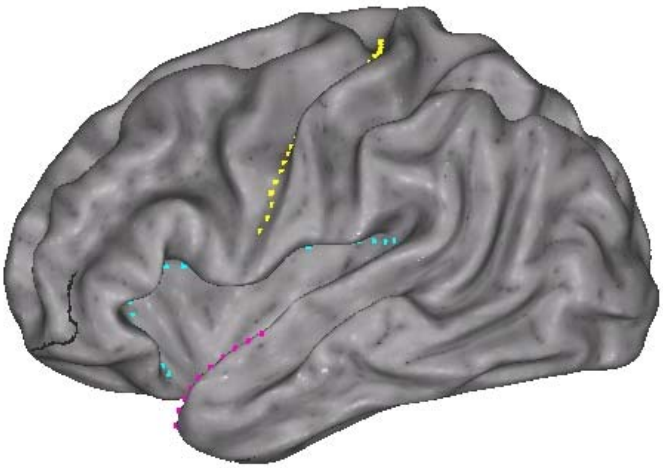

Figure 13. Inflated left hemisphere surface reconstruction with three of the Core6 landmark traces. The yellow trace is along the fundus of the central sulcus, turquoise trace is along the lateral fissure fundus and pink trace is along the tip of the superior temporal gyrus.

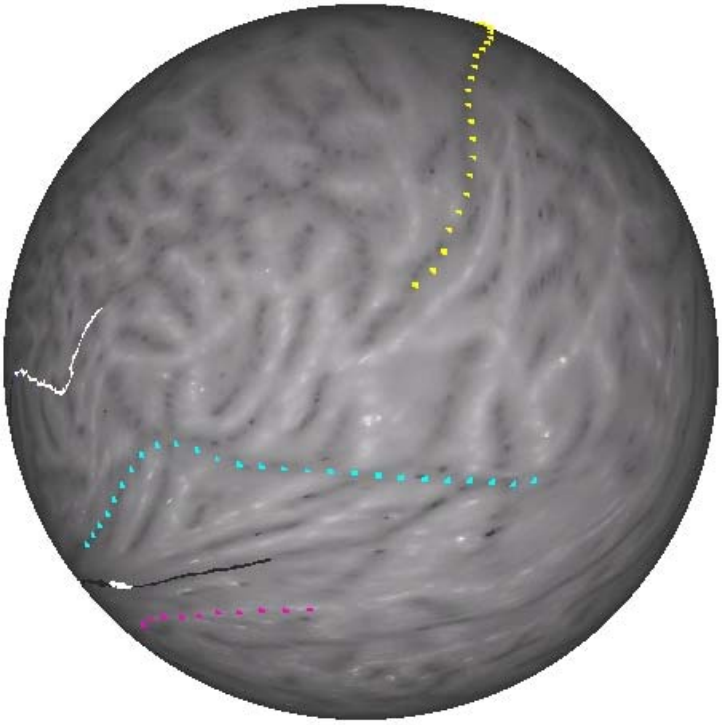

Figure 14. Spherical surface used for registration to atlas. Note the landmark traces that correspond to the inflated surface traces in Figure 13.

Volume-based normalization

To normalize the source to the target using SPM2 we input the subject's MR image in the form of a Minc file with X increasing from patient left to right. No flipping was done during normalization. With the exception of using the template bounding box and cubic 1 mm voxel dimensions, the default spatial normalization settings were used. The selected template image was a T1 Minc average volume of the MNI152 discussed in Section 2.3. Header and image warp files were automatically written. Then, the 'Deformation' function, which writes header and image deformation files using the normalized .mat file as input, was called. Next, the 'Invert Deformation' function, which writes header and image inverse deformation files based on input of the individual's Minc volume, was called. The interactive normalization process took 15-20 minutes per subject on a Dell Dimension dual 450 Mhz processor running Debian Linux.

Step 6: Evaluation

Language Site Spread Reduction

In order to measure the change in distances between language sites across subjects prior to and after applying selected spatial normalization methods; we needed to first measure these distances. The following equations show how we measured distances between any two subjects. We expanded these calculations for each of the 11 subjects and calculated $\left\{\overline{B_p B_2}, \overline{B_p B_3}, ..., \overline{B_p B_{10}}\right\}$. For subject p, the average distance between language sites in subject p and subject p' prior to normalization: $\overline{B_p B_{p'}} = \frac{1}{n * m} \sum_{i=1}^{n} \sum_{j=1}^{m} D(x_{pi}, x_{p'j})$. The average distance between language sites in subject p and subject p' post-normalization:

$$\overline{B_p B_{p'}} = \frac{1}{n * m} \sum_{i=1}^{n} \sum_{j=1}^{m} D(y_{pi}, y_{p'j})$$

where B = individual left hemisphere; n = number of language sites identified for subject p; m = number of language sites identified for subject p'; D = Euclidian distance between points. X is a variable representing site coordinates prior to normalization. Y is a variable representing site coordinates after normalization. Euclidian distance between points was measured according to this equation: $D(a, b) = \sqrt{\sum_{k=1}^{d} (a_k - b_k)^2}$

where d = 2 or 3 depending on whether the coordinates are 2D or 3D.

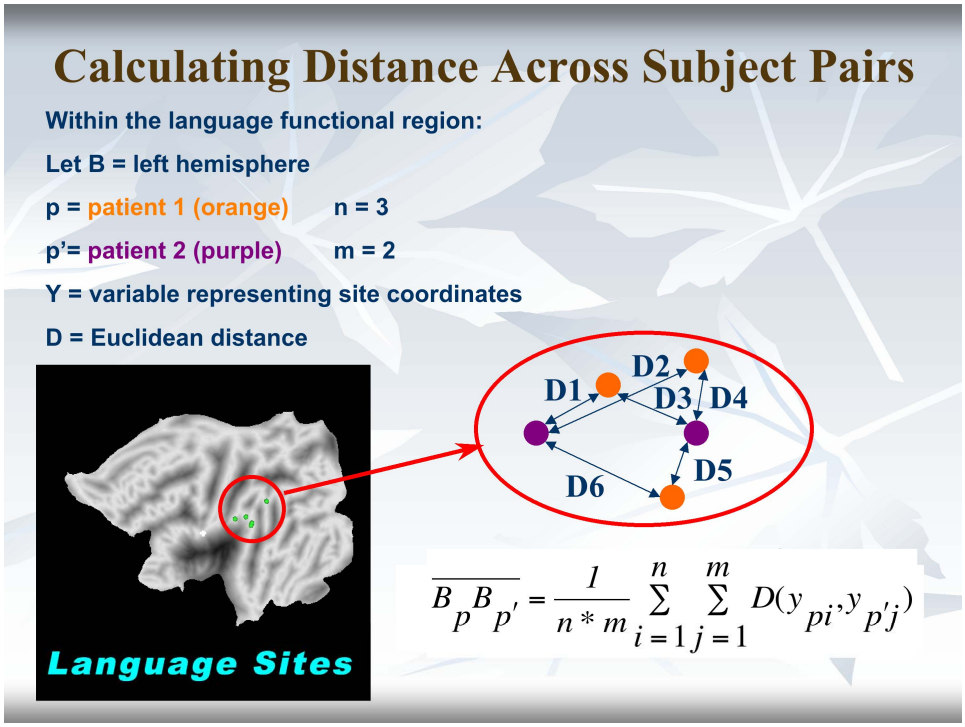

Figure 15. Calculating average distance between language sites across two subjects, represented by the orange and purple sites respectively

Figure 15 illustrates the distance calculation using three language sites of one subject (orange) and two language sites from another subject (purple). Our distance measure used only the distances between the orange and the purple sites.

We believe that the combination of anatomical and functional variation increases the distance between language sites across patients. It follows, then, if anatomical variation is reduced, the distance between language sites across brains will be reduced. Therefore, we expect that the distance between language sites across patients, what we will refer to as 'spread,' will get smaller after spatial normalization. The optimal method will maximize spread reduction. This hypothesis assumes that the volume and surface areas of the source and target hemispheres are the same. As we can see in Table 5, the mean surface and volume areas of the 11 subjects are less than the target's surface and volume areas.. To accommodate for this difference, we calculated the ratio of the mean subject volume and surface area to the corresponding colin27 volume and surface area.

Table 5. Surface and volume areas of the 11 subjects' an atlas' left hemispheres

ID	Gender	Left Hem Surface mm^2	Left Hem Volume mm^3
54	M	86914	559616
55	M	89032	512958
58	M	99459	606962
60	M	79299	466446
61	F	85156	510960
62	F	77723	448175
63	M	75418	465153
117	F	81613	498930
164	M	88962	554765
170	F	71963	423512
176	F	67072	409783
average	**-**	**82055**	**496115**
colin27	**M**	**107368**	**714773**

Given the difference between the volume and surface areas of our source and target hemispheres, we calculated an expected change in post-normalization distances. We used the following values to estimate the expected post-normalization distance (EPoD):

PrD = average pre-normalization, AC-PC aligned distance between 21 language sites

CSA = colin27 surface area

CVA = colin27 volume area

ASA = average surface area of 11 subjects

AVA = average volume area of 11 subjects

CVA/AVA = 1.4407

CSA/ASA = 1.3085

In order to accurately estimate EPoD, we considered that linear distances do not increase linearly with the increase of volume or surface areas. A linear dimension will increase by the square root of M as the surface increases by M times. In the case of a volume, a linear dimension will increase by the cubed root of N as the volume increases by N times. We used the following equations to calculate EPoD in 2D and 3D space:

2D space: $EPoD = \sqrt{CSA / ASA} \times \Pr D$

3D space: $EPoD = \sqrt[3]{CVA / AVA} \times \Pr D$

Having normalized for the increase in surface and volume area of the target atlas, we were prepared to compare the actual post-normalization distances to the expected values. We calculated average distance between language sites in both 2D space and 3D space. Thus, we used two different coordinate systems: For 2D space we used the Caret coordinate space which sets the ventral tip of the central sulcus as the origin (white cross in Figure 16 and Figure 17 on the flat maps) and for 3D space, we used the ICBM152 coordinate space.

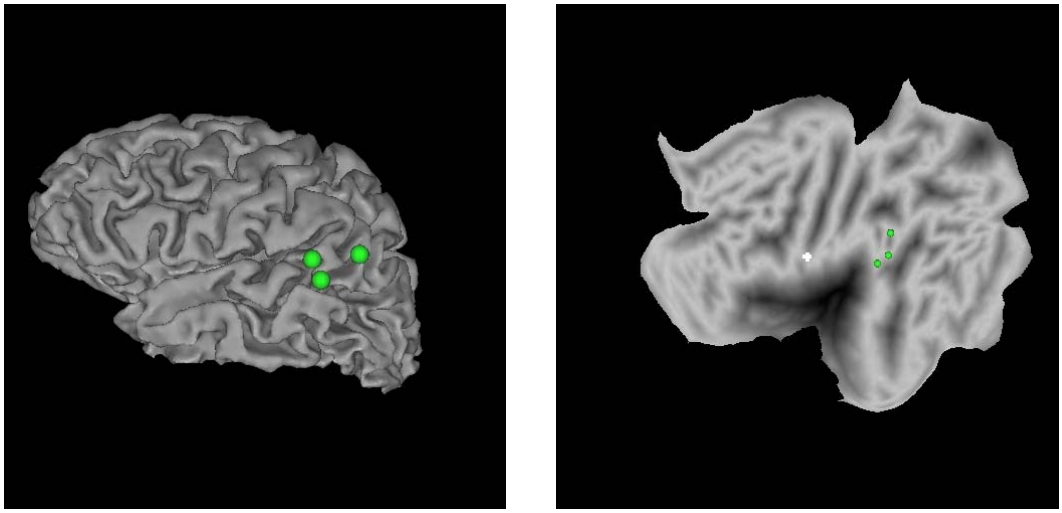

Figure 16. P54 language sites mapped in 3D(left) and 2D(right) space

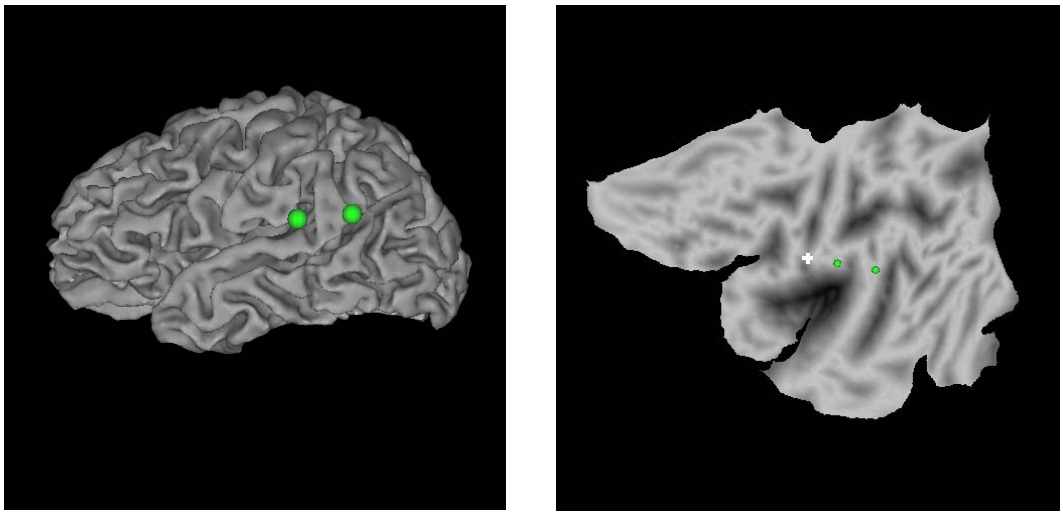

Figure 17. P117 with language sites mapped in 3D and 2D space

Anatomical Localization

To measure how well anatomical normalization methods preserve anatomical location, we used CPS as outlined in step 4. Following normalization using both methods, the neuroanatomist expert viewed cortical flat maps including sulcal depth patterns and cortical sites via the Caret GUI. The SPM2 normalization was viewed on the left side of the screen and the Caret data on the right side of the screen. Each site number was identified via a mouse click. The neuroanatomist identified the normalized location of each mapped site based on CPS. The author recorded the post-normalization parcellations and compared them to the pre-normalization parcellations, assigning a score and/or error type. A correct mapping received a score of 1. Error types and scores were assigned as follows:

- Type 1 Error: The site is located in an incorrect parcel across a subjective boundary and receives a score of -0.25. Figure 18 illustrates this error type.
- Type 2 Error: The site is located in the sulcus adjacent to the correct parcel and receives a score of -0.5. Figure 19 illustrates this error type.
- Type 3 Error: The site is located in the incorrect parcel across a sulcal boundary and receives a score of -1. Figure 20 illustrates this error type.

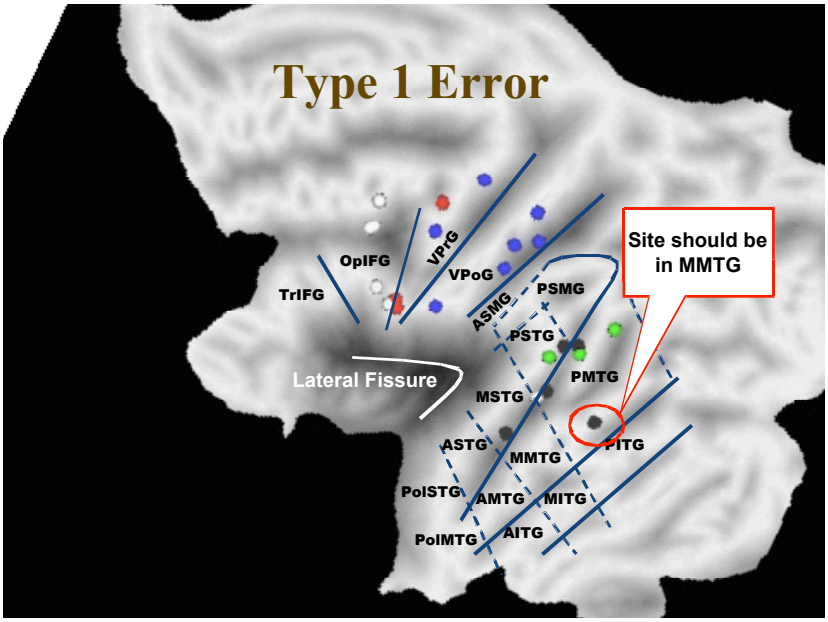

Figure 18. Example of Type 1 Error: Site is mis-mapped to a parcel across an subjective boundary as delineated by a dashed line.

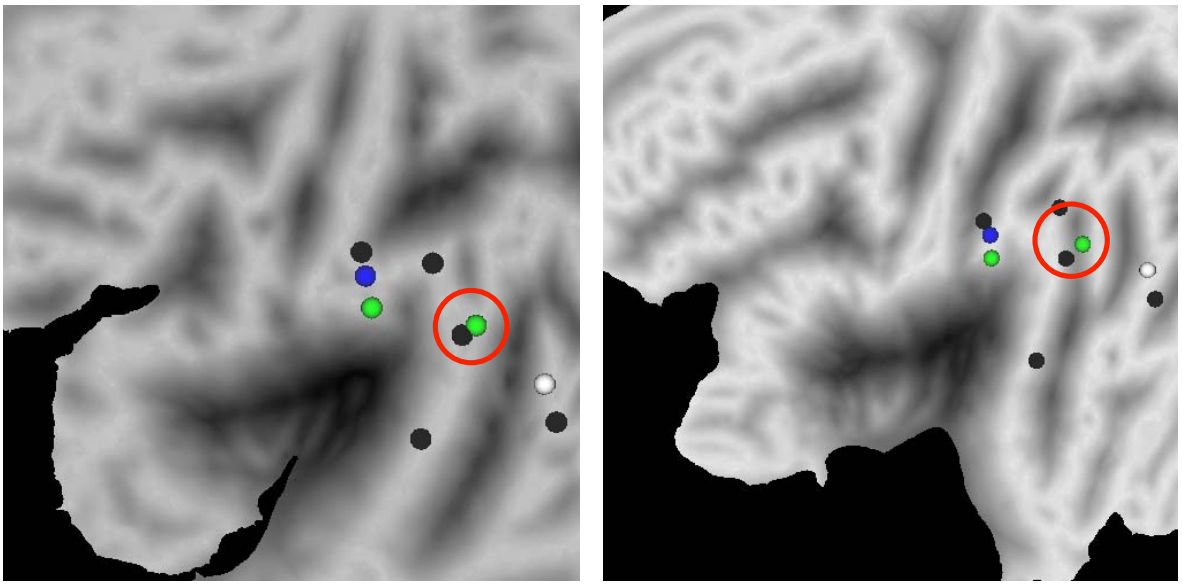

Figure 19. Example of Type 2 Error: P117 Pre-norm sulcal depth flat map with cortical sites on the left. Post-norm flat map with normalized cortical sites on colin27 on the right. The language site (green) has dropped into the sulcus

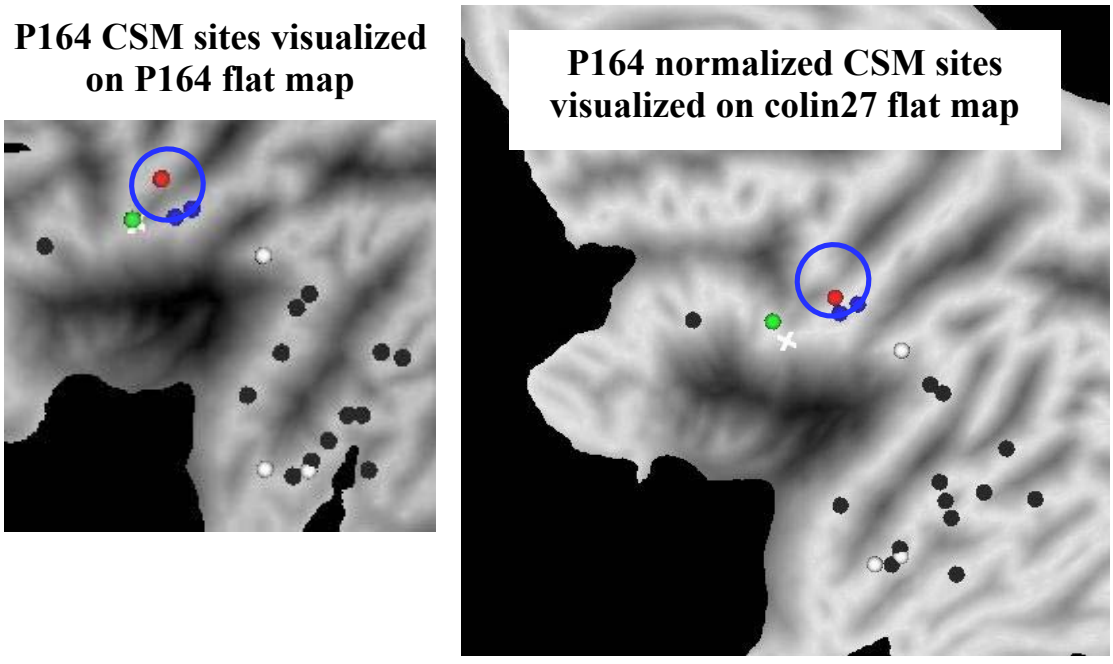

Figure 20. Example of Type 3 Error: P164 pre-normalized location of motor site (red) circled in blue is mapped incorrectly as seen on the right. The post-normalization location has been moved across a sulcus from VPrG to VPoG.

Section 4: Results

To determine which spatial normalization method would best transform cortical stimulation mapping data to a target atlas, we measured both spread between statistically significant language sites across subjects and preservation of anatomical localization as described in Section 3. Table 6 summarizes the results of the analysis for both measures. In 2D space, Caret reduced the average distance between language sites across subjects 3 mm more than SPM2. Caret reduced the average 3D distance between language sites across subjects .6 mm more than SPM2. Using the jackknife estimate of variance, we did not show a statistically significant difference between the surface-based and volume-based methods (Efron and Tibshirani, 1993).

Table 6. Summary of Results

	2D Spread Reduction	3D Spread Reduction	Localization Accuracy Rate
Caret	6.9 mm	2.8 mm	79.6%
SPM2	3.9 mm	2.2 mm	78.0%

Anatomical localization accuracy rates as analyzed using a paired t test revealed a statistically insignificant difference in overall accuracy between the surface-based method, resulting in 63 errors, and the volume-based method's 62 errors when mapping a total of 198 sites. Qualitative analysis of the error types provides more insight into some common and unique problems of spatial normalization in this case study. Most notably, of the 125 total errors, 38 sites, 60% of total errors, were incorrectly mapped by both methods. Also, a paired t test showed a statistically significant difference in the type 2 errors mapped by both methods. While SPM2 normalization resulted in only one type 2 error, Caret normalization resulted in 18 such errors.

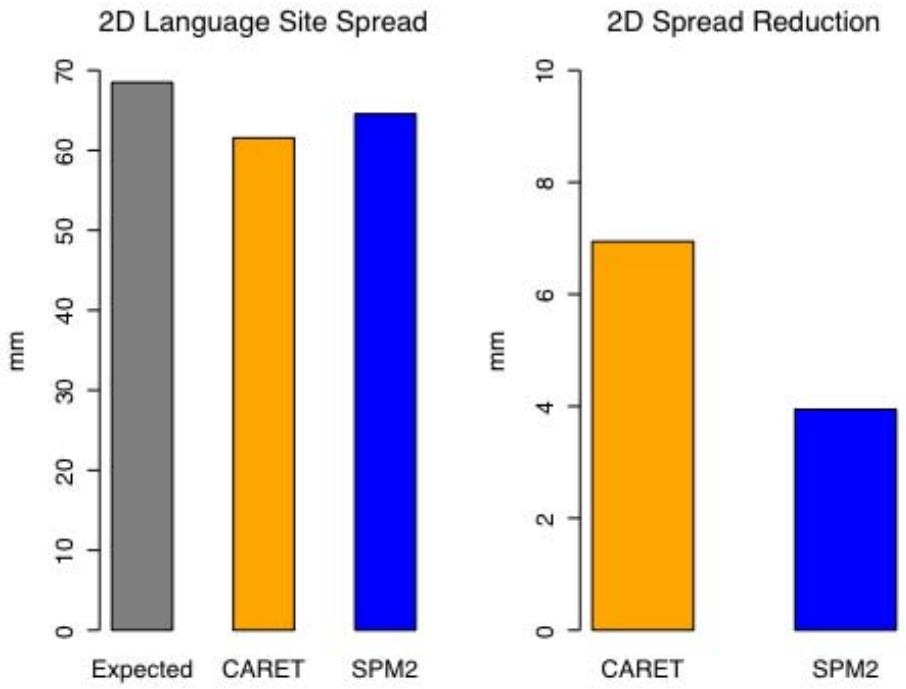

Figure 21. 2D analysis of mean distance between 21 language sites across 11 subjects

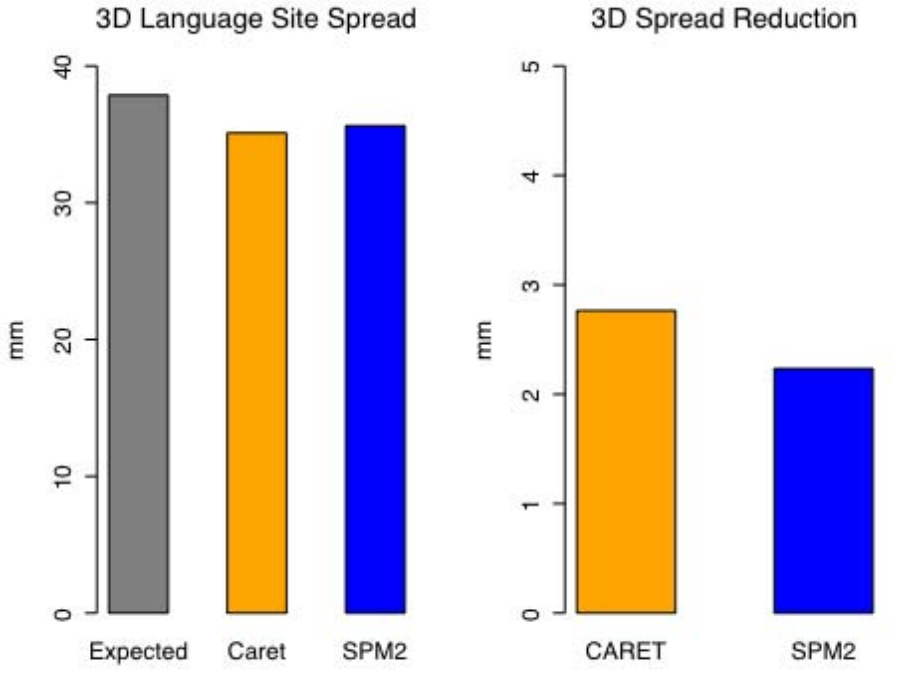

Figure 22. 3D analysis of mean distance between 21 language sites across 11 subjects

Table 7. Caret Error Type Summary

ID	Type 1 Error	Type 2 Error	Type 3 Error	Total Error
54	0	4	3	7
55	2	2	4	8
58	1	1	2	4
60	1	2	5	8
61	4	2	1	7
62	1	1	2	4
63	2	1	7	10
117	0	2	1	3
164	0	1	2	3
170	4	2	0	6
176	3	0	0	3
Totals	**18**	**18**	**27**	**63**

Table 8. SPM2 Error Type Summary

ID	Type 1 Error	Type 2 Error	Type 3 Error	Total Error
54	0	0	5	5
55	1	0	8	9
58	1	0	4	5
60	2	1	5	8
61	3	0	3	6
62	3	0	2	5
63	6	0	2	8
117	0	0	0	0
164	2	0	5	7
170	3	0	2	5
176	3	0	1	4
Totals	**24**	**1**	**37**	**62**

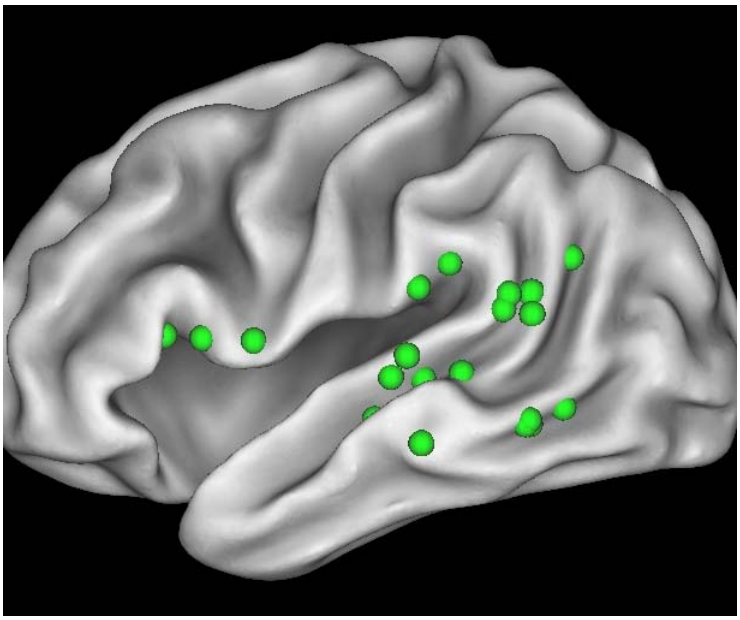

Figure 23. Caret mapping of 21 language sites viewed on colin27 inflated surface reconstruction

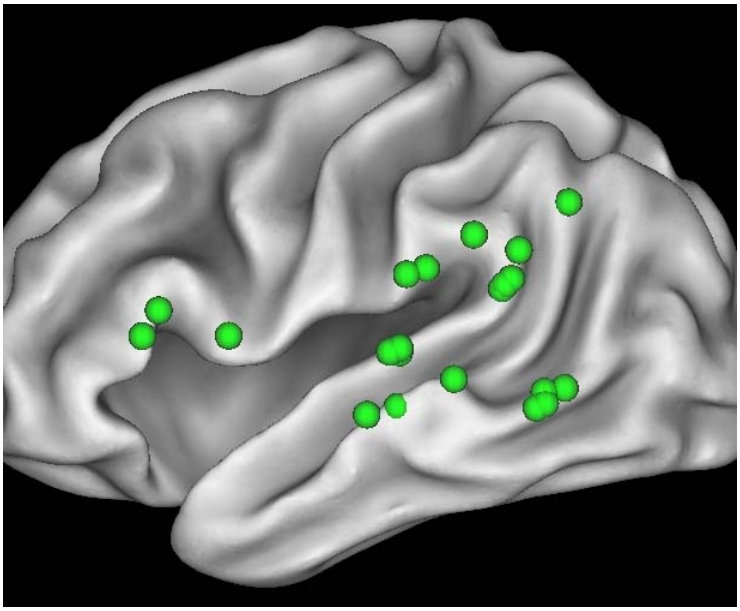

Figure 24. SPM2 mapping of 21 language sites viewed on colin27 inflated surface reconstruction

Error Rate Analysis by CPS Parcel

The middle part of the superior temporal gyrus (MSTG) had the most assigned CSM sites accounting for over 12% (24 of 198 sites) of all CSM sites mapped. The average error rate in this parcel, as measured by averaging the sum of the Caret error rate and the SPM2 error rate, was also high. 54.2% of MSTG sites were incorrectly mapped. Other parcels with 7 or more assigned sites having an error rate of 50% or more were the posterior part of the supramarginal gyrus (PSMG) and the ventral part of the precentral gyrus (VPrG).

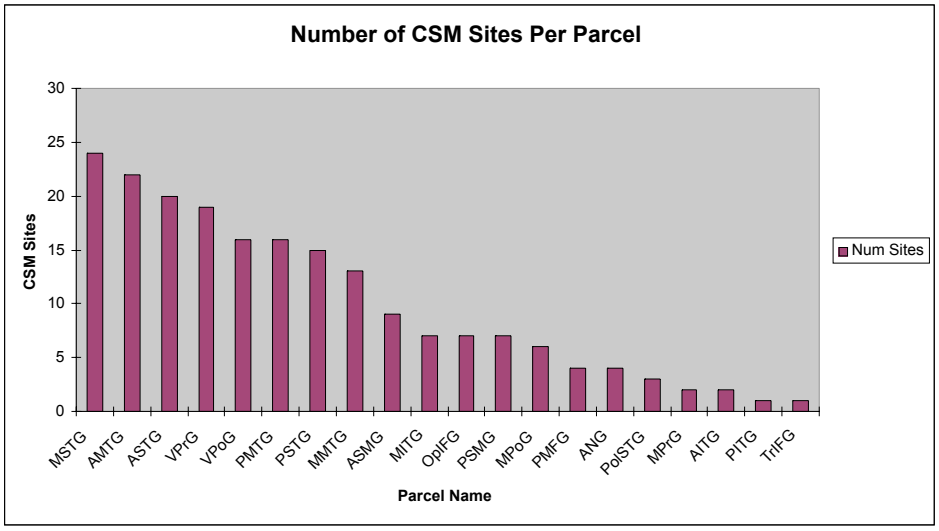

Figure 25. Summary of 198 CSM sites included in this study broken down by CPS parcel.

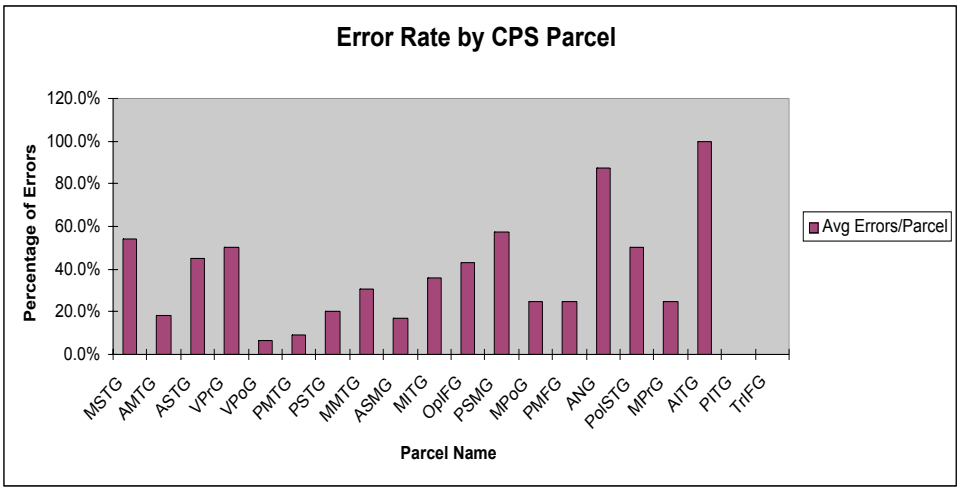

Figure 26. Summary of error rate by CPS parcel, descending left to right, from the parcel with the most sites (MSTG) to the parcel with the least sites (TrIFG).

Error Type Analysis

A paired t test of all error types showed that the methods differed on average by less than a tenth of an error per subject. The confidence interval (-1.2, 1.4) revealed that either method could be better than the other by more than one error per subject.

Analysis of type 3 errors revealed the average difference for this error type was less than one error per subject, Caret normalization could result in as much as two errors less per subject than SPM2, while a SPM2 normalization could result in not more than 1 error less per subject than Caret.

Type 2 error differences were statistically significant ($p < .01$). The confidence interval showed that a SPM2 normalization could result in more than 2 errors less per subject than Caret, while a Caret normalization could result in not more than 1 error less per subject than SPM2. Type 2 errors are discussed in Section 5.

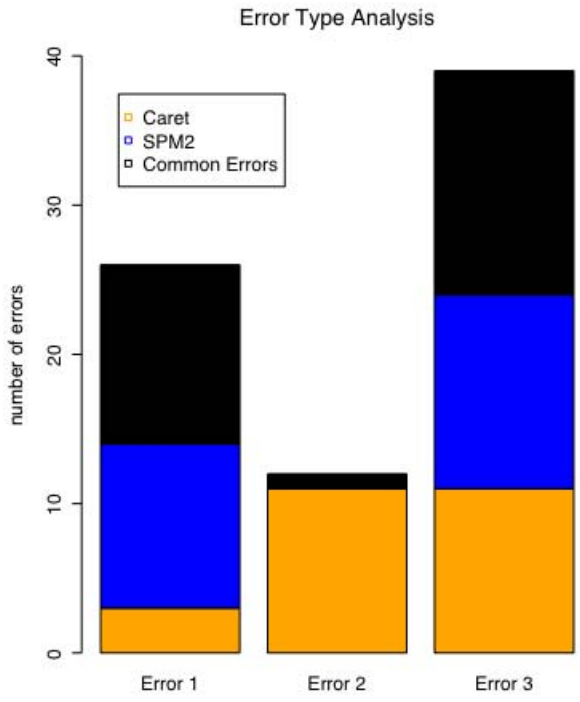

Figure 27. Break down of same-type and unique mapping errors. Orange bar indicates errors unique to Caret. Blue bar indicates errors unique to SPM2. Black bar indicates errors shared by both methods.

Same-Error-Type Mappings

Figure 27 breaks down errors by type and whether the error was unique to one method or common to both for a given site mapping. This analysis includes 105, or 84% of the 125 total errors. Of the 38 common errors, 28 (20.7% of all errors) site mappings for both methods were assigned the same error type (table 9). The remaining ten common errors were assigned different error types, depending on the method. If the 28 same-error-type mappings had been correctly mapped, 12 of the sites would have been located on the superior temporal gyrus (STG), four on the angular gyrus (AnG) and four on the precentral gyrus (PrG), accounting for more than 71% of the same error type mappings.

Table 9. Same-Error-Type Mappings: CSM sites mapped incorrectly by both methods and assigned the same error types. Language sites are in bold with green background.

			CARET			SPM2		
ID	CSM #	Location	Score	Error	Correct Gyrus?	Score	Error	Correct Gyrus?
P54	42	MSTG	-1	3	no/MMTG	-1	3	no/MMTG
P54	37	PMFG	-1	3	no/VPrG	-1	3	no/VPrG
P55	25	AMTG	-0.25	1	MMTG	-0.25	1	MMTG
P55	33	AnG	-1	3	no/PSMG	-1	3	no/PSMG
P55	41	MSTG	-1	3	no/MMTG	-1	3	no/MMTG
P55	34	PSTG	-1	3	no/PMTG	1	3	no/PMTG
P58	9	VPrG	-1	3	no/VPoG	-1	3	no/VPoG
P60	34	AnG	-1	3	no/PMTG	-1	3	no/PSTG
P60	25	MITG	-0.5	2	sulcus	-0.5	2	sulcus
P60	26	MSTG	-1	3	no/MMTG	-1	3	no/MMTG
P60	29	MSTG	-1	3	no/MMTG	-1	3	no/MMTG
P60	11	VPrG	-0.25	1	no/VPoG	-0.25	1	no/VPoG
P61	31	AnG	-0.25	1	PMTG	-0.25	1	PMTG
P61	21	ASTG	-1	3	no/AMTG	-1	3	no/AMTG
P61	26	MMTG	-0.25	1	PMTG	-0.25	1	PMTG
P61	30	PSMG/AnG	-0.25	1	PSMG	-0.25	1	PSMG
P62	28	MSTG	-1	3	no/MMTG	-1	3	no/MMTG
P62	34	OpIFG	-0.25	1	VPrG	-0.25	1	VPrG
P62	3	VPrG	-1	3	no/VPoG	-1	3	no/VPoG
P63	23	ASTG	-1	3	no/MMTG	-1	3	no/MMTG
P63	32	OpIFG	-0.25	1	VPrG	-0.25	1	VPrG
P63	3	VPrG	-0.25	1	VPoG	-0.25	1	VPoG
P164	23	ASTG	-1	3	no/AMTG	-1	3	no/AMTG
P164	21	PolSTG	-1	3	no/AMTG	-1	3	no/AMTG
P170	21	AMTG	-0.25	1	MMTG	-0.25	1	MMTG
P170	23	ASTG	-0.25	1	PolSTG	-0.25	1	PolSTG
P176	24	MMTG	-0.25	1	AMTG	-0.25	1	AMTG
P176	27	MSTG	-0.25	1	ASTG	-0.25	1	ASTG

The same-error-type mappings, if scored using the protocol outlined in Section 3 (step 6), represent a total deduction of 18.5 points. If these deductions were credited to the actual scores for both methods, the resulting accuracy rate for both methods would increase by more than 9% resulting in 88.89% accuracy for Caret and 87.37% accuracy for SPM2. Discussion on how to improve mapping accuracy follows in Section 5.

Unique-Error-Type Mappings

Unique Caret errors (16) accounted for 25% of all Caret errors. Analysis of these errors reveals that 31% of the errors should have been mapped to the middle part of the superior temporal gyrus (MSTG). The other two parcels with the most common errors were the posterior part of the superior temporal gyrus (PSTG), with 19% of errors, and the middle part of the middle temporal gyrus (MMTG), with 13% of errors. Type 2 errors accounted for 56% of unique Caret errors. Type 3 errors accounted for 38% of these errors, and there was a single type 1 error (6%).

Table 10. Summary of errors unique to the Caret spatial normalization method.

	CARET				
ID	CSM #	Location	Score	Error	Correct Gyrus?
P54	21	MSTG	-0.5	2	sulcus
P54	43	MSTG	-0.5	2	sulcus
P54	20	PSTG	-0.5	2	sulcus
P54	30	PSTG	-1	3	NO/PMTG
P55	20	ASTG	-1	3	no/AMTG
P58	25	ASTG	1	3	no/AMTG
P60	32	PMTG	-0.5	2	sulcus
P60	10	VPoG	-1	3	no/ASTG
P60	40	PSTG	-1	3	no/PMTG
P61	34	MPrG	-0.25	1	VPrG
P61	22	ASTG	-0.5	2	sulcus
P62	27	ASTG	-0.5	2	sulcus
P63	25	MSTG	-0.5	2	sulcus
P63	20	ASTG	-1	3	no/AMTG
P63	41	AMTG	-1	3	no/MITG
P63	22	MSTG	-1	3	no/MMTG
P63	26	MMTG	-1	3	no/PSTG
P63	31	ASMG	-1	3	no/VPoG
P117	3	MPoG	-0.5	2	sulcus
P117	33	PSMG	-0.5	2	sulcus
P117	32	PSMG	-1	3	no/PMTG
P164	25	MMTG	-0.5	2	sulcus
P170	26	MSTG	-0.5	2	sulcus

Table 11. Summary of errors unique to the SPM2 spatial normalization method

	SPM2				
ID	CSM #	Location	Score	Error	Correct Gyrus?
P54	24	VPrG	-1	3	no/VPoG
P54	16	VPoG	-1	3	no/VPrG
P55	37	AnG	-1	3	no/PMTG
P55	31	ASMG	-1	3	no/PSMG
P58	31	PSTG	-0.25	1	PMTG
P58	5	VPrG	-1	3	no/VP0G
P58	23	ASTG	-1	3	no/VPoG
P60	24	AMTG	-0.25	1	no/MMTG
P60	30	MITG	-1	3	no/MMTG
P60	35	ASTG	-1	3	no/VPoG
P61	27	MSTG	-1	3	no/PMTG
P62	25	AMTG	-0.25	1	MMTG
P62	5	VPrG	-0.25	1	OpIFG
P63	24	MITG	-0.25	1	MMTG
P63	27	MITG	-0.25	1	MMTG
P63	2	VPrG	-0.25	1	VPoG
P63	40	ASTG	-1	3	no/MMTG
P164	36	OpIFG	-0.25	1	TrIFG
P164	29	MSTG	-1	3	no/MMTG
P164	33	PMTG	-1	3	no/PITG
P164	7	VPRG	-1	3	no/VPoG
P170	24	AMTG	-0.25	1	MMTG
P176	25	OpIFG	-0.25	1	TrIFG

Seventeen errors were unique to the SPM2 spatial normalization method, representing over 27% of all SPM2 errors. Error analysis reveals that the most common region to be erroneously mapped was the ventral part of the precentral gyrus (VPrG), as more than 29% of unique errors should have been mapped to this parcel. There are four other parcels that each account for more than 10% of SPM2 unique errors: middle part of the inferior temporal gyrus (MITG), anterior part of the superior temporal gyrus (ASTG), middle part of the superior temporal gyrus (MSTG) and opercular part of the inferior frontal gyrus (OpIFG). Type 3 errors accounted for 59% of the unique errors with the remaining errors being type 1. There were no type 2 errors unique to the SPM2 method.

Language Site Localization

Localization accuracy for language sites mapped by Caret was 72.62% versus SPM2 accuracy of 84.52%. Caret incorrectly mapped 9 (42.9%) of the 21 language sites. SPM2 incorrectly mapped 6 (28.6%). Again, we observed that the superior temporal gyrus (STG) was the most problematic for both methods, with seven of the ten incorrectly mapped language sites being located on the superior temporal gyrus (STG). Five language sites were incorrectly mapped by both methods.

Table 12. Summary of mapping by both methods of 21 language sites in 11 subjects.

			CARET			SPM2		
ID	CSM #	Location	Score	Error	Correct Gyrus?	Score	Error	Correct Gyrus?
P54	20	PSTG	-0.5	2	sulcus	1		
P54	30	PSTG	-1	3	NO/PMTG	1		
P54	35	PSTG	1			1		
P54	36	PSMG	1			1		
P55	41	MSTG	-1	3	no/MMTG	-1	3	no/MMTG
P58	32	PMTG	1			1		
P60	29	MSTG	-1	3	no/MMTG	-1	3	no/MMTG
P60	31	PMTG	1			1		
P61	25	MSTG	-0.5	2	sulcus	-1	3	no/MMTG
P61	28	PMTG	1			1		
P61	29	PMTG	1			1		
P61	30	PSMG/AnG	-0.25	1	PSMG	-0.25	1	PSMG
P62	33	OpIFG	1			1		
P62	35	TrIFG	1			1		
P63	25	MSTG	-0.5	2	sulcus	1		
P117	21	ASMG	1			-.25	1	
P117	33	PSMG	-0.5	2	sulcus	1	1	
P164	35	VPRG	1			1		
P164	40	ASMG	1			1		
P170	26	MSTG	-0.5	2	sulcus	1		
P176	28	MSTG	1			1		

In order to refine the spread reduction analysis, we removed all incorrectly mapped language sites, resulting in a data set of 11 sites. We then ran the spread reduction calculation again with the revised data set (see table 14). The results are summarized in figures 28 and 29 and table 13.

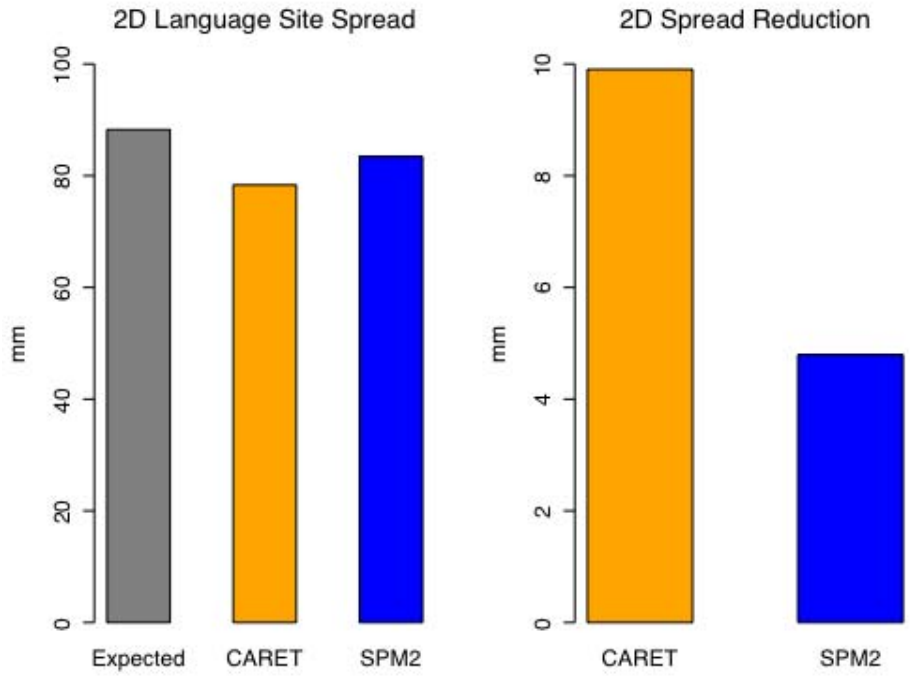

Figure 28. 2D analysis of mean distance between the 11 correctly mapped language sites

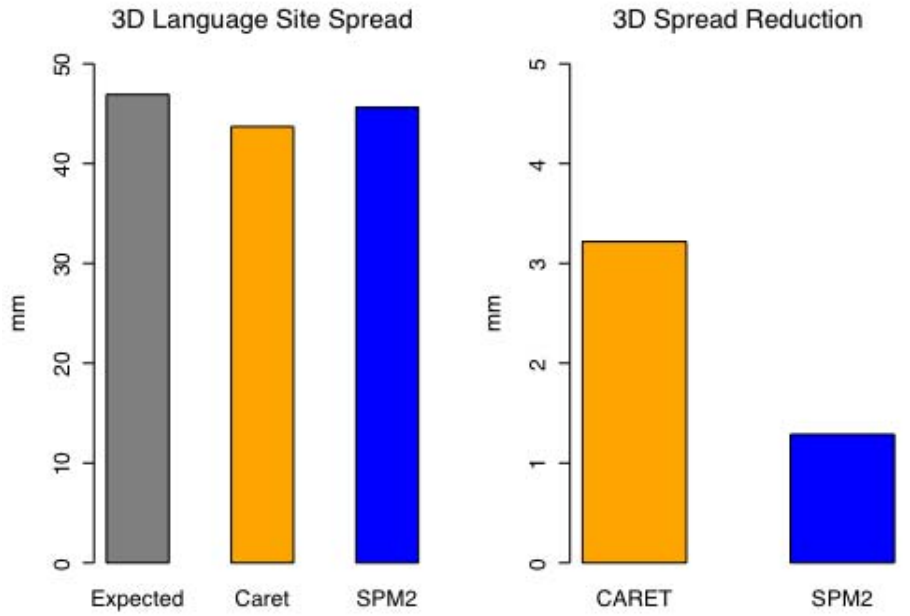

Figure 29. 3D analysis of mean distance between the 11 correctly mapped language sites

Table 13. Refined spread reduction results with the 11 correctly mapped language sites

n=11	2D Spread Reduction	3D Spread Reduction
Caret	9.9 mm	3.2 mm
SPM2	4.8 mm	1.3 mm

Table 14. Summary of 11 correctly mapped language sites

ID	CSM #	Location
P54	35	PSTG
P54	36	PSMG
P58	32	PMTG
P60	31	PMTG
P61	28	PMTG
P61	29	PMTG
P62	33	OpIFG
P62	35	TrIFG
P164	35	VPRG
P164	40	ASMG
P176	28	MSTG

The refined spread reduction analysis revealed an improvement for the Caret normalization results and a slight degradation of the SPM2 normalization results. Caret reduced the spread between sites by 5.1 mm more than SPM2 in 2D space. In 3d space, Caret reduced the spread by 1.9 mm more than SPM2. Using the jackknife estimate of variance method, we found that this difference remained statistically insignificant. However, the difference in the means show that a Caret mapping will, on average, be better than the SPM2 mapping by more than 5 mm in 2D space and almost 2 mm in 3D space. Also, the confidence interval revealed that a Caret mapping could be as much as 13 mm better than a SPM2 mapping in 2D space and more than 6 mm better than a SPM2 mapping in 3D space. A power t test calculation was used to estimate the number of subjects required to achieve a statistical significance of $p < .05$ and 80% power. We found that for 2D analysis we would need at least 55 subjects. For 3D analysis 120 or more subjects would be required.

Section 5: Discussion

Anatomical Variation between Source and Target

The common mapping errors support what visual inspection of the structural surfaces of both the source and target hemispheres revealed: locations of structural vagaries in both the colin27 and in our subjects' average surface reconstruction were where mapping error rates were 50% or greater (figure 31).

The colin27 atlas structural regions were observed by a neuroanatomist to be atypical in the ventral portion of the precentral gyrus (VPrG), supramarginal gyrus(SMG) and terminal ascending segment of the lateral fissure (figure 30). These uncommon localized folding patterns of the colin27 hemisphere help explain the average error rates of 50% or more in the VPrG and PSMG, circled in figure 30.

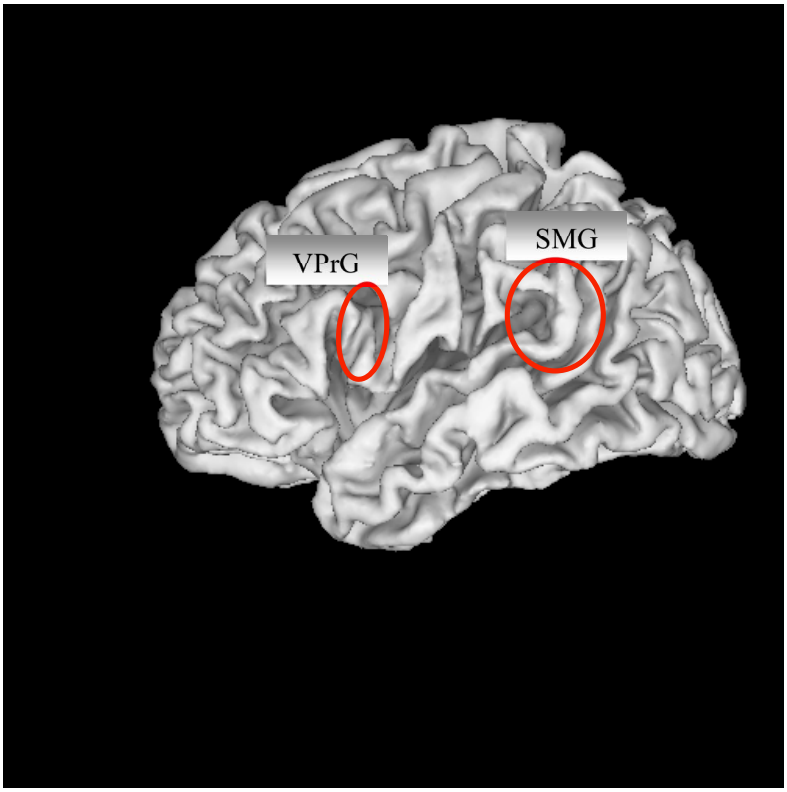

Figure 30. The colin27 atlas' lateral left hemisphere surface reconstruction with areas of uncommon cortical folding patterns circled in red.

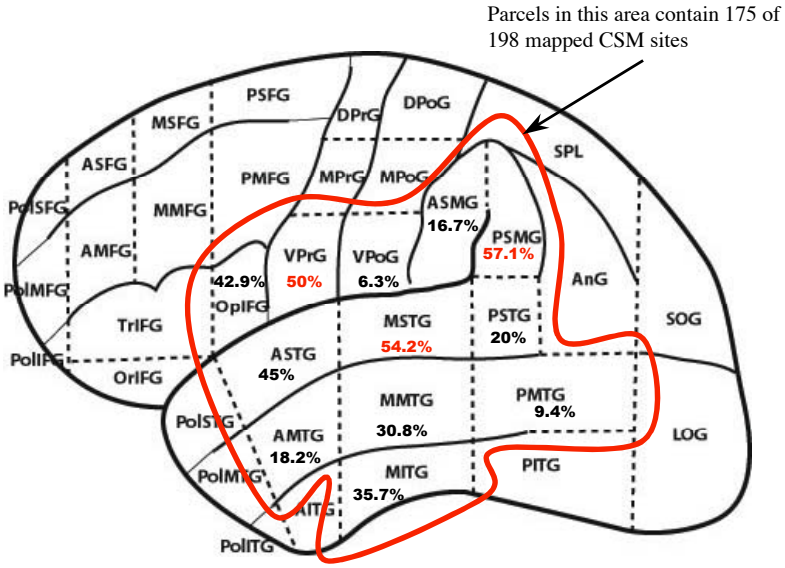

Figure 31. Most common parcels for mapped CSM sites are circled in red with the average error rate listed for each parcel.

Our analysis comparing a digital atlas of 12 normal subjects (PALS-B12) to 10 of our 11 epileptic subjects revealed that epileptic subjects have a broader superior temporal gyrus (STG) than the normal subjects (figure 32). Analysis of a sulcal depth difference flat map, revealed that the greatest difference between epileptic and normal subjects' left hemispheres is in the middle part of the superior temporal gyrus (MSTG) on the CPS scheme (figure 33).

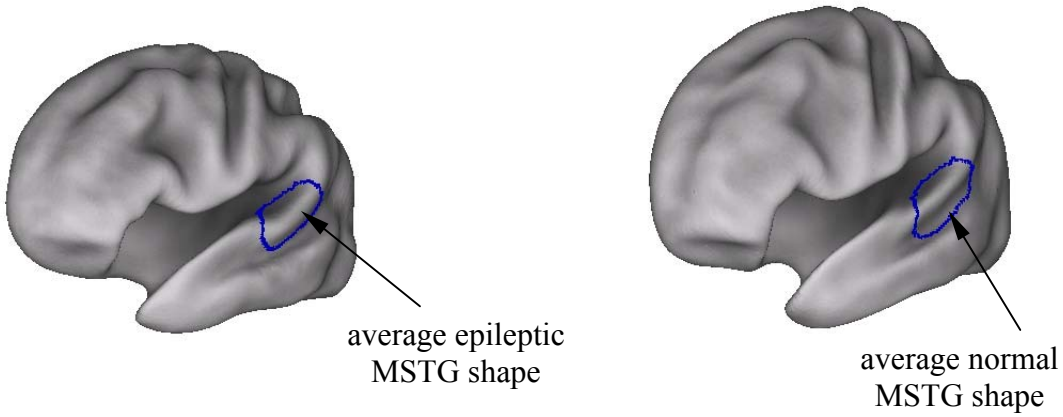

Figure 32. Comparison of inflated left hemisphere average surface reconstruction of 10 epileptic subjects in this study (left) to 12 young adult normal subjects included in the PALS-B12 atlas (right).

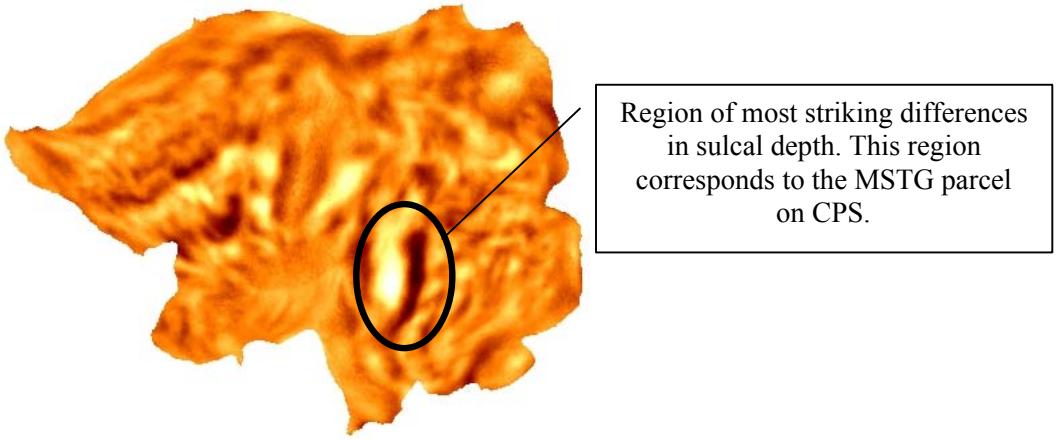

Figure 33. Sulcal difference map representing the differences between the average sulcal depth of 10 epileptic and 12 normal subjects. Dark areas represent where the epileptic subjects' gyri are deeper and the white areas represent where the epileptic gyri are shallower than the 12 normal subjects.

The colin27 atlas' uncommon folding patterns of the supramarginal gyrus and lateral fissure are documented by Ono in the ***Atlas of Cerebral Sulci***. Four left terminal ascending segment patterns were delineated. Upon inspection, the colin27 folding pattern most closely matched the pattern illustrated in figure 15.9D in the Ono text. It is described as follows: "a descending terminal portion which does not constitute the posterior transverse temporal sulcus." This pattern occurred in 4% of the 25 autopsy specimen brains examined for variations and consistencies in location, shape, size dimensions and relationships to parenchymal structures (Ono *et al.,* 1990). Two of the remaining three patterns represented 88% of the folding patterns found in this region with the final pattern representing 8% of the patterns found. This gyral pattern impacts the sulcal pattern of the supramarginal gyrus (SMG), as SMG surrounds the posterior tip of the lateral fissure, contributing to colin27 atlas' unusual folding pattern in this parcel.

It is well known that anatomical variation between source and target can prove problematic for accurate registration. This study supports previous findings that show we cannot expect to completely normalize folding patterns across individuals. It also highlights the bias introduced by a single brain atlas. In this study, we hypothesize that areas of important variability between source and target are a key cause of at least 20% of the total anatomical localization errors.

Possible solutions to the problem of important anatomical variation between source and target include creating a probabilistic atlas of epilepsy subjects, perhaps using the same 11 subjects. This atlas would incorporate the average sulcal shape of the subjects, presumably resulting in better anatomical alignment and more accurate normalization. Extrapolation of these findings to the normal brain would require a transform of the functional data to a normal subject atlas. An atlas of normal brains, like the PALS-B12 or ICBM atlases, would be a preferable target. What currently prevents this technique from being implemented is the limited functionality available to map CSM functional data to these atlases. There currently exists functionality to map fMRI data to these atlases as fMRI is the most commonly mapped functional data. However, CSM site data is relatively rare in the neuroscience community and therefore is not accommodated for as broadly as is fMRI. Additionally, using a probabilistic atlas introduces a problem in reliably measuring post-normalization surface distances that would need to be addressed and is discussed in Section 6.

Type 2 Errors

A paired t test of type 2 errors did reveal a statistically significant difference ($p < .01$) in the methods. SPM2 mappings resulted in only one type 2 error compared to 18 type 2 errors mapped using Caret. The average difference between methods was 1.55 errors per subject. We believe that this difference is attributable to the underlying differences in normalization approaches used by the different methods. The SPM2 algorithm maximizes a voxel intensity match between source and target. As a result, the volume-based method will very rarely end up with an alignment resulting in a pre-normalized gyral location (i.e. CSM sites are always on the gyrus) being relocated into a sulcus, where the voxel intensity is markedly less than the intensity found on a gyrus. The surface-based method, however, maximizes alignment of a set of landmarks based on cortical folding patterns without consideration for voxel intensity. If the selected landmarks vary enough between the source and target, then the normalized sulci and gyri will be deformed in ways that confound mapping of functional data to corresponding regions of the anatomical substrate. The Core6 landmark protocol was designed to minimize this problem by selecting the most stable landmarks and constraining the extent of each landmark to regions where it is reasonable to expect good correspondence across nearly all subjects (Van Essen, 2005). Since performing the spatial normalization for our 11 subjects (9/2004), there has been a clarification on the starting point of the lateral fissure landmark border that we believe will impact the normalization in the middle part of the superior temporal gyrus and sulcus (STS/STG), the region where there is important variation between the subjects' and colin27's cortical folding patterns and the region to which most errors were attributed. Specifically, redrawing the lateral fissure landmark border for each of the 11 subjects according to the clarified guidelines is expected to constrain the STS/STG more medial dorsally, which will tend to reduce differences summarized in Figures 32 and 33. Given this landmark revision, we would expect to see a marked decrease in type 2 errors as a result of Caret normalization.

Cost Benefit Analysis

Using SPM2 to normalize the CSM coordinates required notably less user input and time than using Caret, because SPM2 does not require a surface reconstruction for normalization to the target. To run SPM2 normalization, the only input required is a Minc file of the MRI and a text file including the original CSM coordinates. With this input, an experienced analyst can generate

the normalized cortical site coordinates in approximately 20 minutes or less. Using the surface-base method, the input required includes a surface reconstruction, which requires a total of 1 hour of interactive processing and 1-2 hours for segmentation. Once the surface reconstruction is complete, the input for the surface-based method is the surface reconstruction and the coordinate file. At this point, the automatic surface-based normalization takes about the same time as the volume-based method: 15-20 minutes. If a normalized set of deformed CSM coordinates is the only desired result from the anatomical normalization process, then the volume-based method is less expensive and will provide an overall accuracy of approximately 78%. If visualization of the results is desirable, then the surface-based method is superior to the volume-based method, which is not designed for visualization of cortical site data. (SPM2 is used to visualized fMRI, however) Without creating the surface reconstructions required for Caret, we would not have been able to localize the notable variation between the subjects' average surface and the target atlas in the superior temporal gyrus or assess the bias introduced by the colin27 atlas' atypical folding patterns in the supramarginal gyrus and ventral part of the central sulcus. Additionally, the visualization of the CSM mappings was critical to assessing method accuracy. Knowledge of the accuracy of a given method is key to researchers choosing the best spatial normalization method for their work.

The challenge of validating the volume-based method is discussed by Crum. He advocates for registration tools that monitor their own performance and estimate correspondence error with minimal intervention (Crum et al., 2003). We also support this type of functionality in spatial normalization tools like Caret and SPM2. We demonstrated that the surface-based method allows for more quantitative and qualitative assessment of tool performance than does the volume-based method. This evaluation led to a deeper understanding of the limitations and advantages of each method and provides a frame work that can be used, with modification, to determine spatial normalization accuracy.

Language Localization Patterns

Figure 34 illustrates the cortical parcellation of 16 language sites as mapped by Caret and SPM2. The five sites that were incorrectly mapped by both methods are excluded from this illustration.

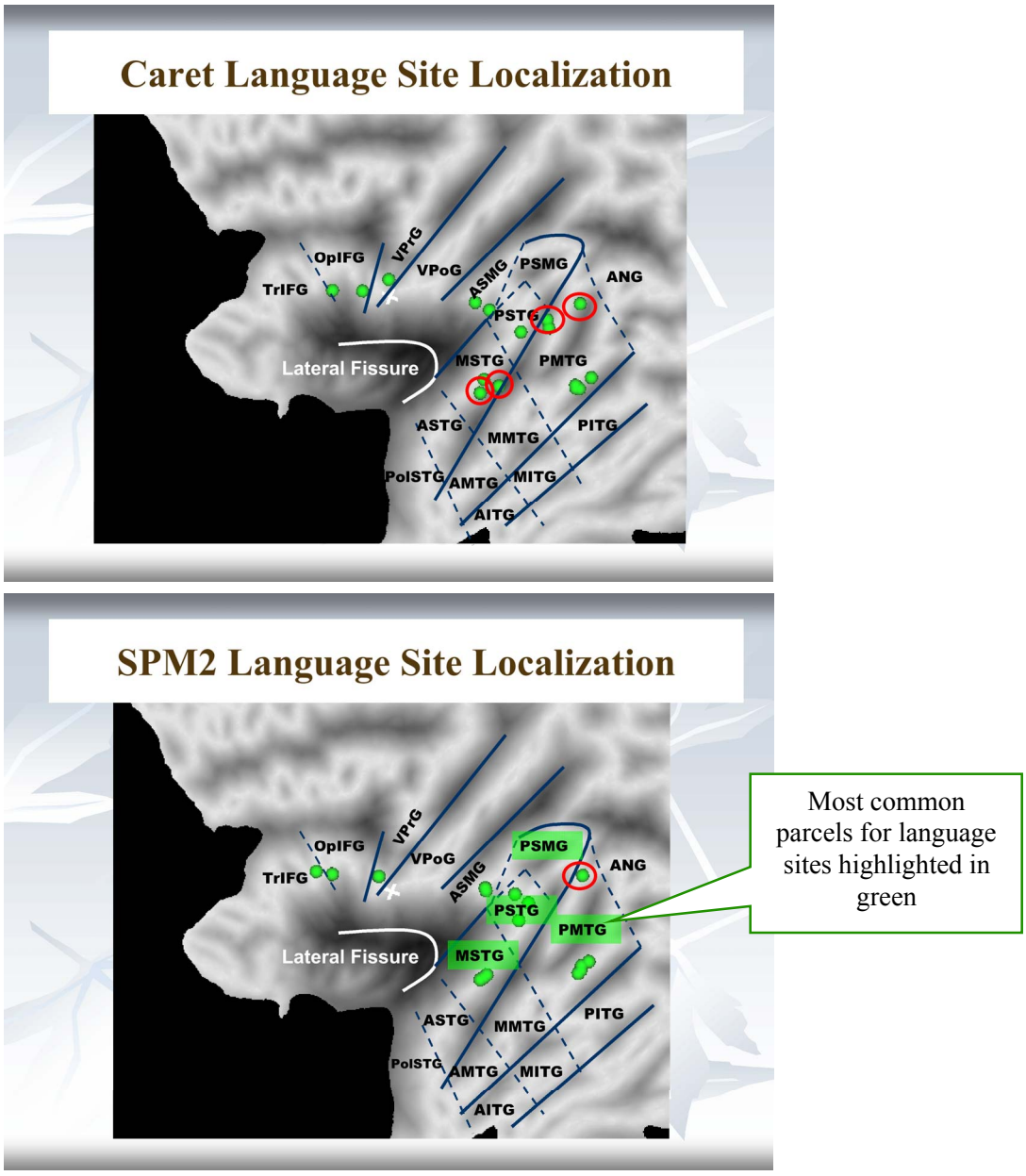

Figure 34. Mappings of 16 language sites on the colin27 atlas with incorrect mappings circled in red.

Section 6: Future Work

Possible future work includes repeating the study, with a larger sample, using a probabilistic atlas as the target, repeating the study using subject fMRI data instead of CSM site data, repeating the Caret normalization of the current data set using modified landmark guidelines, incorporating standard metrics into the evaluation protocol and repeating the study to compare Freesurfer, BrainVoyager, AFNI, a hybrid registration algorithm and a MMI registration algorithm.

As discussed in Section 2.3, we would have preferred a population atlas as our target, like PALS- 12B, because of the inherent structural bias introduced to normalization by any single brain atlas. We expect that using a probabilistic atlas would significantly increase the anatomical preservation accuracy of both methods. The problem of multi-fiducial mapping for CSM sites could be circumvented by using individual deformed files to assign nodes to the CSM sites that could then be viewed on a variety of substrates (e.g. colin27, PALS 12B, average subject surfaces, etc.) With this type of visualization, we would create a 'zone' for each site that would capture the average location of a given CSM site across subjects and likelihood as to where any given site would fall within this zone. This approach would require modification to the spread reduction calculation. To achieve statistical significance of $p < .05$and 80% power, we would want to increase the number of subjects to at least 60 and preferably 100 or more.

Functional MRI data has been collected on many of the subjects in the CSM database. It would be interesting to repeat this study, replacing the CSM data with the fMRI data, using multi-fiducial mapping to view results. This study could serve as validation of both methods and further contribute to an understanding of what accuracy can be expected when using each method.

We plan to repeat the surface-based method using the recently modified Core6 landmarks to analyze the impact this change will have on the mapping results. We expect that this modification will increase the accuracy of the surface-based method by 5-10%.

The metrics used in this study were designed based on the nature of the CSM functional data. It would be valuable to evaluate the methods using metrics used to validate other methods. For example dispersion metric of selected landmarks, overlap percentage and cross-comparison of maps would be interesting measures to use to further evaluate surface-based and volume-based methods.

Repeating the study using FreeSurfer, BrainVoyager and AFNI would provide more insight into how different surface-based and volume-based methods compare to each other and across categories. Evaluating hybrid spatial normalization methods like HAMMER and ROMEO, which employ feature-based and intensity matching techniques, would also be valuable. Additionally, a relatively recent development is the use of maximization of mutual information (MMI) registration. MMI is a strategy that has proved extremely successful at automatically computing the registration of 3-D multimodal medical images of various organs from the image content. Mutual Information (MI) is a basic concept from information theory, that is applied in the context of image registration to measure the amount of information that one image contains about the other. The MMI registration criterion postulates that the MI is maximal when the images are correctly aligned. The MMI criterion is volume based, uses a histogram instead of intensity matching and does not impose limiting assumptions on the nature of the relationship between corresponding voxel intensities. MMI has been shown to be a very general and powerful criterion, that can be applied automatically and reliably, without prior segmentation or preprocessing, on a variety of applications (Maes *et al.,* 2003). It would be interesting to compare the results of other surface-based and volume-based spatial normalization methods to a MMI method like that employed by Rueckert or D'Agostino.

List of References

Ashburner J, Csernansky JG, Davatzikos C et al. Computer-assisted imaging to assess brain structure in healthy and diseased brains. Lancet Neurol. 2003; 2(2):79-88.

Ashburner J, Friston KJ. Voxel-based morphometry: the methods. Neuroimage. 2000; 11:805-821.

Binder, JR, Frost JA, Hammeke TA, et al. Human Brain Language Areas Identified by Functional Magnetic Resonance Imaging. J of Neurosci. 1997; 17(1):353-362.

Brain Innovation. <http://www.brainvoyager.com>. Accessed December 2003.

Bransford JD, Brown AL, Cocking RR, Eds. **How People Learn: Brain, Mind, Experience, and School.** National Academies Press. 1999. <http://www.nap.edu/openbook/0309065577/html/>

Brett, M. The MNI brain and the Talairach atlas. MRC Cognition and Brain Sciences Unit. < http://www.mrc-cbu.cam.ac.uk/Imaging/mnispace.html>. Accessed Dec 2003.

Brinkley JF, Rosse C. Imaging and the Human Brain Project: A Review. Methods Inf Med. 2002; 41:245-60.

Brain and Anatomy Function. Traumatic Brain Injury Resource Guide. Centre for Neuro Skills. <http://www.neuroskills.com/edu/ceufunction7.shtml> Accessed Dec 2003.

Bookstein FL. Principal warps: thin-plate splines and the decomposition of deformations. IEEE Transactions on Pattern Analysis and Machine Intelligence. 1989; 11(6):567-585.

Burton H, Visual cortex activity in early and late blind people. J Neurosci 2003; 23:4005-4011.

Cachier P, Bardinet E, Dormont D, Pennec X, Ayache N. Iconic feature based nonrigid registration: the PASHA algorithm. Computer Vision and Understanding. 2003; 89:272-298.

Christensen GE, Rabbit RD, Miller MI. Deformable Template Using Large Deformation Kinetics. IEEE Transactions on Image Processing. 1996; 5(10):1435-1447.

Chui H, Win L, Schultz R, et al. A unified non-rigid feature registration method for brain mapping. Med Imag Anal. 2003 Jun; 7(2):113-130.

Collins DL, Evans AC. ANIMAL: Validation and Application of Nonlinear Registration-based Segmentation. International Journal of Pattern Recognition and Artificial Intelligence. 1997; 11(8):1271-1294.

Corina DP, Gibson EK, Martin R et al. Dissociation of action and object naming: evidence from cortical stimulation mapping. Hum Brain Mapping. 2005; 24:1-10.

Cox RW. AFNI: Software for analysis and visualization of functional magnetic resonance neuroimages. Computers and Biomedical Research. 1996; 29:162-173.

Crivello F, Schormann T, Tzourio-Mazoyer N, et al. Comparison of spatial normalization procedures and their impact on functional maps. Hum Brain Mapping. 2002 Aug; 16(4):228-50.

Crum WR, Griffin LD, Hill DLG et al. Zen and the art of medical image registration: correspondence, homology, and quality. NeuroImage. 2003 July; 20: 1425-1437.

D'Agostino E, Maes F, Vandermeulen D, Suetens P. A viscous fluid model for multimodal nonrigid image registration using mutual information. Lecture Notes in Computer Science. Proc. Medical Image Computing and Computer-Assisted Intervention. 2002, Sep; 2489:541-548.

Davatzikos C, Bryan RN. Using a deformable surface model. IEEE Transactions on Medical Imaging. 1996 Dec; 15(6):789-795.

Davatzikos C, Li HH, Herskovits E, et al. Accuracy and sensitivity of detection of activation foci in the brain via Statistical Parametric Mapping: a study using a PET simulator. NeuroImage. 2001; 13:176-184.

Davatzikos C, Bryan RN. Morphometric analysis of cortical sulci using parametric ribbons: a study of the central sulcus. J. Comput. Assist. Tomogr. 2002; 26(2):298-307.

Desai R, Liebenthal E, Possing ET, Binder JR. Volumetric vs. Surface-based Intersubject Alignment for Localization of Auditory Cortex Activation. CNS Poster, 2004.

Efron B, and Tibshirani RJ. Chapter 11. **An Introduction to the Bootstrap**. Chapman & Hall. 1993.

Fischl B, Sereno M, Dale A. Cortical surface-based analysis II: inflation, flattening, and surface-based coordinate system. NeuroImage. 1999; 9:195-207.

Fox PT, Mintun MA, Reiman EM, Raichle ME. Enhanced detection of focal brain responses using intersubject averaging and change-distribution analysis of subtracted PET images. J Cereb Blod Flow Metab. 1988 Oct; 8(5):642-653.

Gee JC, Reivich M, Bajcsy R. Elastically deforming 3D atlas to match anatomical brain images. J Comput Assist Tomogr. 1993 Mar-Apr; 17(2):225-236.

Gee JC, Barillot C, Le Briquer L, Haynor DR. Matching structural images of the human brain using statistical and geometrical image features. Proc. SPIE: Visualization in Biomedical Computing. 1995 Aug; 3573:278-289.

Hill DLG, Batchelor PG, Holden M, Hawks DJ. Medical Image Registration. Phys. Med. Biol. 2001; 46:R1-R45.

Joshi SC, Miller MI, Christensen GE, et al. Hierarchical brain mapping via a generalized Dirichlet solution for mapping brain manifolds. Proc. SPIE: Vision Geometry IV. 1995 Aug; 2573:278-289.

Joshi S. Brain Mapping. <http://cis.jhu.edu/~sarang/brain.html> Accessed Dec 2003.

Kikinis R, Jolesz FA, Lorensen WE, et al. 3D reconstruction of skull base tumors from MRI data for neurosurgical planning. Proceedings of the Society of Magnetic Resonance in Medicine Conference. 1991.

Kriegeskorte N, Goebel R. An efficient algorithm for topologically correct segmentation of the ortical sheet in anatomical MR volumes. NeuroImage. 2001; 14:329-346.

Kochunov PV, Lancaster JL, Fox PT. Accurate high speed spatial normalization using octree method. NeuroImage. 1999; 10:724-737.

Lancaster JL, Summerln JL, Rainey L, Freitas CS, Fox PT. The Talairach Daemon, a database server for Talairach Atlas Labels. Neuroimage. 1997; 5(4):S633.

Lee T-C, Kashyap R, Chu C-N. Building skeleton models via 3-D medial surface/axis thinning algorithms. Graph Models Image Processing. 1994; 56:462-78.

Le Goualher G, Prock E, Collins L, et al. Automated extraction and variability analysis of sulcal neuroanatomy. IEEE Trans. Med. Imag. 1999; 18:206-216.

Liu T, Shen D, Davatzikos C. Deformable registration of cortical structures via hybrid volumetric and surface warping. NeuroImage. 2004; 22:1790-1801

Lorenson W, Cine H. Marching cubes: a high-resolution 3-D surface reconstruction algorithm. Comput Graph. 1987; 21:163-9.

Mangin JF, Riviere D, Cachia A, et al. Object-Based Strategy for Morphometry of the Cerebral Cortex. IPMI, Ambleside, UK. 2003.

May A, Ashburner J, Buchel C, et al. Correlation between structural and functional changes in brain in an idiopathic headache syndrome. Nat. Med. 1999; 5(7):836-838.

Minoshima S, Koeppe RA, Frey KA, Kuhl DE. Anatomic standardization: linear scaling and nonlinear warping of functional brain images. J Nucl Med. 1994; 35:1528-1537.

Modayur B, Jakobovits R, Maravilla K, Ojemann G, Brinkley J. Evaluation of a visualization-based approach to functional brain mapping. Proc AMIA Annu Fall Symp. 1997; 429-433.

Ojemann G, Ojemann J, Lettich E et al. Cortical language localization in left, dominant hemisphere. J Neurosurg, 1989; 71:316-326.

Ono M, Kubik S, Abernathy CD. **Atlas of Cerebral Sulci.** New York. 1990.

Penny W. http://www.fil.ion.bpmf.ac.uk/spm/software/spm2/ Accessed Jan 2005.

Roland PE, Geyer S, Amunts K, et al. Cytoarchitectural maps of the human brain in standard anatomical space. Human Brain Mapping. 1997; 5:222-227.

Rueckert D, Frangi AF, Scnabel JA. Automatic construction of 3D statistical deformation models using nonrigid registration. Lecture Notes in Computer Science. Proc. Medical Image Computing and Computer-Assisted Intervention. 2001 Oct; 2208:77-94.

Salmond CH, Ashburner J, Vargha-Khadem F, et al. The precision of anatomical normalization in the medial temporal lobe using spatial basis functions. Neuroimage. 2002 Sep; 17(1):507-12.

Senda M, Ishi K, Oda K, et al. Influence of the ANOVA design and anatomical standardization on statistical mapping for PET activation. Neuorimage. 1998; 8:283-301.

Segmentation and Flattening Software. Wandell Lab. <http://white.stanford.edu/~brian/mri/segmentUnfold.htm>. Accessed Dec 2003.

Statistical Parametric Mapping. Wellcome Department of Imaging Neuroscience. < http://www.fil.ion.ucl.ac.uk/spm/>. Accessed Dec 2003.

Sugiura M, Kawashima R, Sadato N, et al. Anatomica validation of spatial normalization methods for PET. J Nucl Med. 1999; 40:317-322.

Prothero JS, Skandha4: An Slisp-based Interactive Raster Graphics Toolkit. <http://sig.biostr.washington.edu/projects/skandha4/tr/skandha4/>. 1995.

Thirion JP. Image matching as a diffusion process: an analogy with Maxwell demons. Med Image Anal. 1998; Sep; 2(3):243-260.

Thompson PM, Toga AW. A surface-based technique for warping three-dimensional images of the brain. IEEE Transactions on Medical Imaging. 1996; 15(4): 402-417.

Thompson PM, Cannon TD, Narr KL, et al. Genetic influences on brain structures. Nat. Neurosci. 2001b; 4(12): 1253-1258.

Toga AW, Mazziotta JC. **Brain Mapping: The Systems.** Academic Press. San Diego. 2000.

Toga AW, Thompson PM. Maps of the Brain. New Anat. 2001; 265:37-53.

Toga AW, Thompson PM. Temporal dynamics of brain anatomy. Annu. Rev. Biomed. Eng. 2003; 5:119-145.

Van Essen DC. Drury HA, Dickson J, Harwell J, et al. An Integrated Software Suite for Surface-based Analysis of Cerebral Cortex. JAMIA. 2001; 8:443-459.

Van Essen, DC. Windows on the brain. The emerging role of atlases and databases in neuroscience. Curr. Op. Neurobiol 2002; 12:574-579.

Van Essen DC. A population-average, landmark- and surface-based atlas of human cerebral cortex. Draft. 2005.

Wang Y, Staib LH. Boundary finding with prior shape and smoothness models. IEEE Transacations on Pattern Analysis and Machine Intelligence. 2000 July; 22(7):738-743.

Wernicke C (1874) Der aphasische Symptomenkomplex. Breslau: Cohn, Weigert.

Wesson KA. Brain Basics for the Teaching Professional. Science Master. <http://www.sciencemaster.com/columns/wesson/wesson_part_01.php> Accessed Dec 2003.

Woods RP, Grafton ST, Watson JDG, Sicotte NL, Mazziota JC. Automated Image Registration" II. Intersubject validation of linear and nonlinear models. Journal of Computer Assisted Tomography. 1999 Jan/Feb; 22(1): 153-165.

Appendix A: Evaluation Protocol

1. Patient MRI orientation and preparation

1.1. Create directory for Pxxx.

1.2. Download ExxxxxSx.mnc file from /usr/local/dataX/brainproject/patients/ directory into PXXX directory. Typically the directory will include 3 ExxxxxSx.mnc for any given patient. Sx assumes numerical values eg: S1, S2, S3. Typically, in this example, S1 will be the structural MR, S2 will include veins and S3 will include arteries. If not confident of the content of the 3 minc files, download all three and view in SureFit to confirm which is the MR file needed for normalization.

1.3. Resample volume to 1mm cubic voxels as follows:

1.3.1. Verify volume is in correct orientation (LPI) by calling mincheader Pxxx_Exxxxx_Sx.mnc at command line. Typically the volume will be oriented correctly but will not have cubic 1mm voxels.

1.3.2. Before resampling, call mincinfo Pxx_Exxxxx_Sx.mnc and get output like the following:

dimension name	length	step	start
zspace	256	0.892941	-107.6
yspace	256	0.892941	-114.5
xspace	256	0.892941	-117.7

1.3.3. This information is needed to calculate the nelements argument for the mincresample function. Calculate the nelements argument as follows:

dims_out=int(round(dim*pixdim_in/1.0))

dim=256

pixdim_in=0.892941

nelements <- int(round(256*0.892941/1.0)) = 229

This calculation has been built into the Excel spreadsheet:

Resample_PatientBrainData.xls seen in Appendix B.

1.3.4. Call the resample command and create a volume in 1 mm cubic voxels:

mincresample -clobber -nelements 229 229 229 -step 1.0 1.0 1.0 Pxxx_Exxxxx_Sx.mnc Pxxx_Exxxxx_Sx_111.mnc

1. Patient MRI orientation and preparation continued

1.4. If functional MRI (fMRI) images are available for a subject, it may be resampled as well and included in the normalization process.

1.5. Open SureFit in PXXX directory on the command line.

1.6. Read in the *_111.mnc volume by selecting Volume Operations: Read Volume 1 from the menu bar and selecting the desired .mnc file. If fMRI file is used, load that file in as Vol. 2. If the MR image is not centered in the Vol 1 window, left click on the image and drag to the desired location.

2. Volume preparation

2.1. To prepare the volume data for the segmentation process select SureFit: Volume Preparation from the menu bar. There are 7 tabs in the Volume Preparation window. Typically, we will use the first five tabs as follows:

2.2. Select Volume Information:

2.2.1. Subject Name: a unique identifier for each individual brain. Do not include the hemisphere in the subject name. Typically use the default name provided.

2.2.2. Investigator: Name of individual responsible for the study or segmentation

2.2.3. Group: UW SIG

2.2.4. Data Type: MRI

2.2.5. Resolution: 1.0 mm

2.2.6. Species: human

2.2.7. Comments: PXX identifier

2.2.8. Volume Extent: SureFit preserves information about the position of each cropped volume within the original image volume. This is useful when aligning structural and functional MR data from the same subject.

- Volume Already Cropped: Typically the original volume will be uncropped, thus select no
- Hemisphere: Typically select both=LR
- Region: Typically select entire cerebral hemisphere(one or both)
- Filename: select change and accept default file name

2.3. Select Volume Orientation:

2.3.1. SureFit's conventions are LPI, which means the left hemisphere is displayed on the left side. Typically volumes loaded from our files will be in the correct orientation. Follow the instructions in the Volume Oriention window to ensure that the volume is indeed correctly oriented. If the volume is correctly orientated, select yes.

2.3.2. If the volume is not correctly oriented, select no and follow the steps outlined to get the correct orientation and polarity. Once this has been achieved, select Save. This will create a volume in which Orient.mnc is appended to the initial volume name and use this as Vol1 for subsequent processing steps.

2. Volume Preparation continued

2.4. Select Anterior Commissure:

2.4.1. The view will automatically switch to coronal view. Move the parasagittal(red line) cursor to the midline.

2.4.2. Switch to the parasagittal view

2.4.3. Center the blue and green cross hairs on the anterior commissure (see reference photo in SureFit)

2.4.4. Switch back to coronal view and adjust parasagittal cursor to intersect the midline precisely at this coronal view

2.4.5. Press Set Anterior Commissure button

2.5. Select Define VOI and Identify Cut Faces:

Note: The SureFit segmentation algorithm currently works only on hemispheres and portions thereof; it does not work on entire brain volumes. You must crop to at most a left or right hemisphere before proceeding to segmentation. Typically we will crop the *left hemisphere.*

2.5.1. Select horizontal panel and scroll to the slice level where the hemisphere is widest and longest

2.5.2. Adjust the min and max X slider bars to choose the medio-lateral extent of the volume to be segmented. For the X axis, cropping several mm beyond midline, into the opposite hemisphere, is a good idea and prevents inadvertently clipping bits of VOI.

2.5.3. Adjust the min and max Y slider bars to choose the anterior-posterior extent of the volume to be segmented

2.5.4. Select the Crop button to apply the newly defined extent to the X and Y axes

2.5.5. Scroll through the volume to assure the entire VOI is visualized. Readjust the slider bars if needed and re-select the Crop button to restore the desired sub-volume.

2.5.6. Switch to the parasagittal panel and scroll to a slice where the partially cropped image volume is maximal in extent.

2.5.7. Adjust the min and max Z slider bars to the desired limits

2.5.8. Once satisfied with the defined VOI in all 3 planes, select Save.

2. Volume Preparation continued

2.5.9. Select the hemisphere and region for the newly cropped volume in the Enter Cropped Volume's Extent Settings window: Typically select Hemisphere: left and Region: entire cerebral hemisphere(one or both)

2.5.10. Select Save with default file name in the Save Volume As: window

2.5.11. Typically we will not deal with Identify Cut Faces

2.6. Select Set Peaks:

2.6.1. In the Hist window, use the left mouse button to move the red bar to the left-most peak of the histogram. If the histogram does not have a clear gray matter peak, select a value that results in roughly half the gray matter voxels being above threshold (appearing green in the volume window).

2.6.2. Select Set Gray Matter Peak button

2.6.3. In the Hist window, use the left mouse button to move the red bar to the right-most peak of the histogram. If the histogram does not have a clear white matter peak, select a value that results in roughly half of the white matter voxels being above threshold (appearing green in the volume window)

2.6.4. Select Set White Matter Peak button

2.7. We will not typically adjust the parameters using the List Parameters tab. Using the Resampling tab is not recommended for normal segmentation.

2.8. When complete with all volume preparation, select Save and Close.

3. Segmentation, surface generation and automated error correction

3.1. Make sure that the structural MRI volume to be segmented is loaded as Vol 1. If there is a functional MRI, it should be loaded as Vol 2.

3.2. An initial segmentation is run first to determine if bias correction or other pre-processing is needed. Select SureFit: Run SureFit. A notebook window appears with 3 tabs: Run SureFit, Interactive Error Correction and A La Cart. In the Run SureFit tab use the following selections:

- Segmentation Scope: Extract Cerebrum, Segment
- Fill Ventricles: Yes
- Leave Keep intermediate files unselected

3.3. Check for segmentation quality once initial segmentation is completed as follows:

3.3.1. Select the Interactive Error Correction tab.

3.3.2. In the window, press the Update Handle Count button to determine the number of topological errors (handles) for the volume loaded in Vol 2. Note: Occassionally, this method can yield a few (1-3) false positives (small handles in the volume that do not appear in the surface reconstruction). If Handle count number returned is greater than or equal to 15, then it is a good idea to consider some additional pre-processing to upgrade image quality before moving forward with the final segmentation. Those options include:

3.3.2.1. Some images may have **non-uniform intensity levels.** For example in three images we processed the occipital lobe intensities tended to be higher, so sulci fused over. The temporal lobe intensities, however, tended to be lower, so the anterior medial portions of it often fade out of the segmentation. Where bias correction was needed, we used FSL's best and fast applications as follows:

```
Minc2Analyze Pxxx_Exxxx_Sx_111.L.full.sMRI.mnc
bet Pxx_Exxxx_Sx_111.L.full.sMRI  Pxx_Exxxx_Sx_111.L.full.sMRI_bet -f 0.1 -g 0
fast -t1 -c 3 -n -v5 -l 500 -or Pxx_Exxxx_Sx_111.L.full.sMRI_bet.hdr
Analyze2Minc Pxx_Exxxx_Sx_111.L.full.sMRI_bet_restore.hdr
mv Pxx_Exxxx_Sx_111.L.full.sMRI_bet_restore.mnc  Pxx_Exxxx_Sx_111_bet_bc.L.full.sMRI.mnc
```

3.3.2.2. If this bias correction is performed, step 2: Volume Preparation needs to be re-done before moving onto final segmentation.

3. Segmentation, surface generation and automated error correction continued

3.3.3. Some images may result in **ventricle filling** problems.

3.3.3.1. Ventricle filling problems typically will require a customized work-around solution. For one of the instances of this problem type, we used a VElab utility called VolMorphOps that erodes or dilates the input volume and another utility, CombineVols to perform a logical "or" operation on two volumes. For this type of problem, it is best to consult with the analyst at the Van Essen lab (currently Donna Hanlon).

3.4. Secondary Segmentation: If there are less than 15 handles after initial segmentation, then once again select SureFit: Run SureFit. In the Run SureFit tab use the following selections:

- Segmentation Scope: Extract Cerebrum, Segment
- Fill Ventricles: Yes
- Generate Surface: select Correct Errors and Identify Sulci
- Leave Keep intermediate files unselected

3.5. Run SureFit button once desired options have been chosen

3.6. This process will generate a cortical segmentation and associated surfaces stored in the PXXX directory, including a SURFACES directory. The "fiducial" surface will automatically appear in a separate surface viewer window (VTK image) when the process is complete. The time to complete this process is currently approximately 2 hours on sulcus.

3.7. Select the L button (Lateral View) and save the VTK image as PXXVTK_Lateral_LHem.jpg using the Gimp (or comparable graphics software) in the PXXX directory.

4. Interactive error correction

4.1. Once the initial segmentation is run, the quality of the segmentation is checked to determine if interactive error correction is required

4.2. If the volumes are not yet loaded:

4.2.1. load the intensity volume as Vol 1:
Volume Operations: Read Volume 1: <patientIDs>_Sx_111.L.full.sMRI.mnc

4.2.2. Next, load the segmentation to be corrected as Vol 2:

Volume Operations: Read Volume 2:
PXXX/Segmentation/<patientIDs>_Sx_111.L.full.segment_vent_corr.mnc

4.3. Select SureFit: run SureFit: Ineractive Error Correction: Update Handle Count to determine the number of handles in the segmented volume

4.4. Select Surface Operations: Read Surface 1:
PXXX/SURFACES/<patientIDs>_Sx_111.L.full.segment_vent_corr.fiducial.<nodenum>.vtk

4.5. Read Surface 2:
PXXX/SURFACES//<patientIDs>_Sx_111.L.full.segment_vent_corr.inflated.<nodenum>.vtk

4.6. Select Surface Operations: Paint Surface and open
PXXX/SURFACES//<patientIDs>_Sx_111.L.full.segment_vent_corr.errors.<nodenum>.RGBpaint

4.7. Select SureFit: run SureFit: Interactive Error Correction tab. Click on Locate Objects button. You will be prompted for a minc file. If Vol 2 was run through error correction, then accept default *.errors.* file to bring up a list of object locations in the form: (xmin-xmax, ymin-ymax, zmin-zmax). These are the limits of objects that the error checking algorithm has flagged as problem areas.

4.8. In the slice window, scroll to the first set of specified limits for each dimension (x,y,z).

4.9. Press the keyboard letter “p” and rotate fiducial and inflated surfaces to find the red dot over the red surface patch representing the error.

4.10. Scroll through the volume in the slice window within the area of the error, toggling between Vol 2 and Vol 1 & 2 images to identify details and the nature of the residual error.

4. Interactive error correction continued

4.11. Most residual errors will require some type of surface patching. The tools for patching include the following:

4.11.1. **Toggle Voxels:** Press the Toggle Voxels button to switch the mouse buttons to the voxel editing mode. While in this mode, the left mouse button still positions the cursor, but the middle button makes the voxel white, and the right button makes it black. If multiple voxels need editing, the process can be expedited using the arrow keys to positions the cursor with one hand, while modifying voxels with the other hand on the mouse. Note that the voxel affected is determine by the position of the cross hairs and NOT the cursor. Zoom and pan are disabled until you press the Resume Normal Mouse Mode button, so be sure to exit the Toggle Voxels mode before resuming other operations. Also, you will want to check the box for apply to current slice only, so that your changes are limited to one slice at a time versus all slices at once.

4.11.2. **Masking:** The mask function allows you to toggle more than one voxel on and off at once. You can select the mask dimensions and place the mask using the cross hairs and select dilate or erode, depending on what is required for a given error correction.

4.11.3. **Flood-Filling:** This option is used for removing disconnected regions. If a "finger" has been disconnected by deleting voxels that link it to the main segmentation, press the Flood Fill Volume 2 button. The largest segmented object will remain, and smaller objects will disappear from Vol 2.

4.12. As you correct errors using these tools, you will want to perform two task periodically:

4.12.1. After making a correction, check whether or not you reduced the number of handles by selecting Update Handle Count.

4.12.2. If you have successfully corrected a handle, save the patched volume by selecting Save Edits. In the pop up file selection window, the default file name will have *.patch* appended to the current Vol 2 file name. Instead of using this file name, delete this appendage and revise the name to *.corr2.* to identify the second corrected volume and repeat this protocol until all errors are corrected.

4. Interactive error correction continued

4.13. In case of mistakes, the Undo button can be used to recover the most recent step taken. Changes made at earlier steps are recoverable if intermediate volumes have been saved, in which the partially patched volume can be reloaded.

4.14. To determine if the surface reconstruction is satisfactory after patching, generate a new surface as follows:

4.14.1. In the Run SureFit window select Use Segmentation Loaded in Vol 2 and Skip Error Correction. Unlike the Update Handle Count function, which operates on unsaved patches, generating a new surface uses the most recently saved version of the segmentation.

4.14.2. Check the fiducial and inflated surfaces for irregularities. If the surfaces look clean and the Update Handle Count results in 0-2 handles, Save Edits and note the final corrected version number. You are now ready to perform the final segmentation and prepare for flattening.

4.15. Final Segmentation:

- Use Segmentation in Vol 2
- Fill Ventricles: No
- Generate Surface: deselect Correct Errors and
  select Identify Sulci
- Leave Keep intermediate files unselected
- Prepare to flatten: Yes

4.16. When finished, exit SureFit.

5. Surface Flattening

5.1. Change to SURFACES and make a back up copy of the spec file:

cp Pxxx_Exxxxx_Sx_111.L.full.segment_vent_corrx.Surface.xxxxx.spec Pxxx_ *_corrx.Surface.xxxxxx.spec.bak

5.2. Open caret5 and select spec file

5.3. For species, select Human; leave Space field blank; for Category, select INDIVIDUAL.

5.4. select all and load

5.5. Surface: Flatten full or partial hemisphere

5.6. Flattening type: Full hemisphere (ellipsoid) and morph sphere

5.7. Accept Surfaces defaults (fiducial and ellipsoidal)

5.8. Accept AC position/offset defaults

5.9. Choose Human left standard cuts and make sure Smooth Fiducial Medial Wall is selected; select OK

5.10. Pull Continue Flattening full hemisphere dialog to the side.

5.11. Select Window: Viewing Window 2

5.12. Switch window 2 to the INFLATED view and resize the window larger.

5.13. Press M on window 2 to switch to a medial view.

5.14. Select XY on the drop-down menu to switch the rotation axis to XY.

5.15. Rotate the surface so the the ventral side is a bit more visible, and click on nodes along the calcarine sulcus and medial wall, as shown in the calc_medial.jpg.

5.16. Select Layers:Border:Draw Border

5.17. Select MEDIAL.WALL as the border name

5.18. Press Apply and draw a border in the main caret window on the compressed medial wall view of the spherical surface. Follow the route traced by the green ID nodes for the medial wall. Shift click to complete the border.

5.19. Select CalcarineCut as the border name

5.20. Press Apply and draw a border in the main caret window on the compressed medial wall view of the spherical surface. Follow the route traced by the green ID nodes for the calcarine sulcus. Make sure the calcarine border crosses the medial wall border. Shift click to complete the border.

5. Surface Flattening continued

5.21. Select Layers: Border: Delete border with mouse, and select the template borders for the medial wall and calcarine (not the ones you just drew, but the template borders the redrawn ones replace)

5.22. If necessary, delete existing Sylvian cut and redraw cut so that it does not cross Superior Temporal Gyrus, since this will be a registration landmark.

5.23. Click Continue Flattening on the dialog you pulled to the side.

5.24. After a while, an Initial Flattening dialog gives you the opportunity to make cuts, if there are no visible red patches of crossovers, click continue flattening and accept the default parameters on the following two dialogs. Flat and spherical morphing takes 20 minutes on a Dell Precision 450 (dual xeon processors) running RedHat 8 Linux.

5.25. When finished processing, an Align Surface to Standard Orientation dialog will appear, along with two bigger dialogs reporting the number of crossovers for the flat and spherical maps. More than 10-15 crossovers means there is some concern regarding the quality of the flattening.

5.26. If number of crossovers is acceptable, click OK to dismiss the statistics dialogs.

5.27. If necessary, use Viewing Window 2 L and D views to locate the ventral and dorsal ends of the central sulcus.

5.28. In the main caret window (flat map), click on the ventral tip of the central sulcus, and shift-click on the dorsal tip.

5.29. On the Align Surface to Standard Orientation dialog, check the Align Sphere box and click Apply.

5.30. File: Save Data File: Coord file: and replace FLAT_CYCLE5_OVERLAP_SMOOTH in the filename with FLAT_Cartesian. Change the coord fram to Cartesian Standard. Save the file.

5.31. File: Save Data File: Coord file: and select SPHERICAL ... CYCLE4 from the coord file drop-down menu. Replace CYCLE4 in the filename with Std. Change the Coord Frame to Spherical Standard. Change the orientation to Left Posterior Inferior.

5.32. File: Save Data File: Latitude-Longitude: and save the lat-lon coordinates generated during alignment to Pxxx_Exxxxx_Sx_111.L.xxxxx.latlon

5. Surface Flattening continued

5.33. Close the Align Surface to Standard Orientation dialog and switch the main caret window to the Fiducial surface. Select Toolbar: M for medial view.

5.34. Surface: Measurements: Generate Curvature to update the surface shape. Select Folding for the folding column and Gaussian for the gaussian column. Notice the medial wall looks smooth.

5.35. File: Save Data File : Surface Shape file: Pxxx_Exxxxx_Sx_111.L.full.segment_vent_corrx.xxxxx.surface_shape and overwrite the existing file.

5.36. Exit Caret

6. Translate cropped volume to magnet coordinate space

6.1. The current fiducial surface reflects the cropped volume (left hemisphere only): Pxxx_Exxxxx_Sx_111.L.full.sMRI.mnc. Thus, it must be translated by +Xmin,+Ymin,+Zmin to reflect the grid of the uncropped volume: Pxxx_Exxxxx_Sx_111.LR.full.sMRI.mnc (left and right hemispheres).

6.2. Get [XYZ]min from the params file:

grep min Pxxx_Exxxxx_Sx_111.L.full.sMRI.params

Look for these lines in the output:

Xmin=50
Ymin=23
Zmin=91

6.3. Get the magnet center from the uncropped volume:

mincinfo Pxxx_Exxxxx_Sx_111.LR.full.sMRI.mnc

dimension name	length	step	start
zspace	229	1	-107.6
yspace	229	1	-114.5
xspace	229	1	-117.7

6.4. Translate the fiducial surface +Xmin,+Ymin,+Zmin, then -117.7,-114.5,-107.6 like so:

6.4.1. Change to the Pxxx/SURFACES and open caret5

6.4.2. Select the REG-with-Colin_Core6 spec file.

6.4.3. Accept default spec file selections.

6.4.4. Make sure main window is set to the FIDUCIAL surface.

6.4.5. Surface: Transform: Translate and enter the Xmin,Ymin,Zmin values:

Translate X 50
Translate Y 23
Translate Z 91

6.4.6. Caution: mincinfo lists the origin in z, y, x order -- not x, y, z. So take care entering the parameters below. Surface: Transform: Translate

Translate X -117.7
Translate Y -114.5
Translate Z -107.6

6. Translate cropped volume to magnet coordinate space continued

6.4.7. File: Save Data File: Coord File: append "-magctr" after fiducial in the filename. In the comment field, enter, "Translated +50,23,91 (Xmin,Ymin,Zmin), then -117.7,-114.5,-107.6 (Minc start)." Leave the coord frame Native, but change the orientation to Left Posterior Inferior. Save.

6.4.8. Press Toolbar: Spec and locate the entry corresponding to the original fiducial coord file (i.e., without -magctr in the name); press X to remove this file from the spec file, so you don't select the wrong fiducial surface when mapping foci or registering the surface to colin.

6.4.9. Also click X to remove these .spec file entries:

RAW
all SPHERICAL except Std
ELLIPSOID
COMP MED WALL
all flat except Cartesian
all border files
TEMPLATE-CUTS bordercolor

6.5. Check to make sure the translated surface aligns with the volume as follows:

6.5.1. Use text editor to create this .spec file:

BeginHeader
Category INDIVIDUAL
Date Mon Mar 7 2005
Encoding ASCII
Hem-flag left
Species Human
EndHeader
CLOSEDtopo_file Pxxx_Exxxxx_Sx_111.L.full.segment_vent_corrx.xxxxx.topo
FIDUCIALcoord_file Pxxx_Exxxxx_Sx_111.L.full.segment_vent_corrx.fiducial-magctr.xxxxx.coord

6.5.2. Start Caret and load all files in the just-created .spec file

6.5.3. File:Import File: Minc: Pxxx.*.LR.full.SMRI.mnc

6.5.4. Switch to view: Volume; press D/C and select Overlay/Underlay: Volume

6.5.5. Toggle show surface box in lower right ON

6.5.6. Switch between Coronal, Horizontal and Parasagittal views. Scroll up and down to confirm alignment of surface outline with the volume.

6.5.7. If out of alignment, back track to determine cause of mis-alignment and redo until surface and volume alignment are confirmed.

7. Preparation for Caret normalization

7.1.1. In the terminal/shell, run the following commands in the Pxxx/SURFACES subdirectory:

cp
Pxxx_Exxxxx_Sx_111.L.full.segment_vent_corrx.Surface.xxxxxx.spec
Pxxx_Exxxxx_Sx_111.L.REG-with-Colin_Core6.xxxxx.spec

7.1.2. Note: Before running the next commands, make sure there are no spaces on either side of the * characters, or else you'll lose everything.

rm *CYCLE*coord Compression.HighSmooth.RGB_paint
coords_as_border.border debug* flat_morph_distortion.surface_shape
spherical_morph_distortion.surface_shape TEMPLATE-CUTS*
rm *.segment.*
rm *.segment_vent.*
rm *.segment_vent_corr.*

This is a good time to remove some of the intermediate patched segmentation volumes in Pxxx/SEGMENTATION. For example, if the final segmentation is Pxxx_Exxxxx_Sx_111.L.full.segment_vent_corrX.mnc, then don't delete that volume, but delete these:

Pxxx_Exxxxx_Sx_111.L.full.segment_vent_corr1.mnc

Pxxx_Exxxxx_Sx_111.L.full.segment_vent_corr2.mnc

We save these, too, although they're rarely needed once you get to this point:

Pxxx_Exxxxx_Sx_111.L.full.RadialPositionMap.mnc
Pxxx_Exxxxx_Sx_111.L.full.segment.mnc
Pxxx_Exxxxx_Sx_111.L.full.segment_vent_corr.mnc
Pxxx_Exxxxx_Sx_111.L.full.segment_vent.mnc

8. Drawings borders in Caret for surface normalization

Note: Also see the Spherical Registration section in **Caret5 User's Manual and Tutorial**, Version 5.1 April 9, 2004 (page 61). Some differences:

- colin SPM2 fiducial is used in lieu of 711-2B version
- "Core6" landmark set is used:
- adds superior temporal gyrus
- border extents avoid sulci margins
- uses parameters in deformation map provided in Appendix G

8. Drawings borders in Caret for surface normalization continued

8.1. You will need two caret sessions open side-by-side: One with the PXXX and one with the target atlas (in this case the target atlas is colin).

8.2. Each session will have the flat map in the main window, with the inflated surface in window 2. Make the windows as big as your screen will allow.

8.3. First, you'll click green "ID" nodes on the inflated surface to get an idea of where to start and stop drawing each border. We don't draw to the end of each sulcus, because near the margins, the correspondence becomes less clear between the individual's and colin's folding patterns. For example, colin has a branch at the dorsal tip of his central sulcus, whereas most subjects don't. By starting at the point where this branch merges, and beginning a similar distance from the medial wall in the individual, we can be confident that these landmarks correspond to one another.

8.4. For the atlas session: open Caret5 in COLIN.L.LANDMARKS_REG-with-INDIVIDUAL_CORE6 directory

8.5. Select caret_Pxxx_Exxxxx_Sx_111.L.REG-with-Colin_Core6.xxxxx.spec

8.5.1. Select Geom: atlas flat and inflated surfaces

8.5.2. Select Border:border color and Core6 border projection files

8.5.3. Select D/C : surface shape: Mean Curvature (Folding)

8.6. For the PXXX session: open Caret5 in PXXX/SURFACES directory

8.7. Select Geom: INFLATED, SPHERE_Std, and FLAT_Cartesian surfaces

8.8. Select Border: LANDMARKS.FromFlattening .borderproj file

8.9. Select Toolbar: Spec

8.10. Select LANDMARKS.FromFlattening borderproj; REPLACE existing borders

File: Open Data File: Border color file and navigate up and over to the colin directory

8.11. Select ForSPHERICAL.REGISTRATION_Human.Class3.bordercolor and copy the file to the existing directory.

8.12. Select Layers : borders: project borders: nearest tile. Border points on the origin may disappear.

8. Drawings borders in Caret for surface normalization continued

8.13. In both sessions do the following:

8.13.1. Switch to the flat map in the main window.

8.13.2. Window: Viewing Window 2 ; set to inflated surface

8.13.3. Toolbar: L in Window 2 for lateral view of inflated surface

8.13.4. Toolbar: D/C ; toggle on borders.

8.13.5. Select Borders from the D/C menu:

8.13.5.1.Toggle on Show first link red

8.13.5.2.Draw Borders as Points and Lines

8.14. Calcarine and Medial Wall borders: These were drawn at flattening, but generally some border points are nibbled off. Note that there are distinct gaps between the medial wall dorsal and ventral segments in the colin atlas borders that are used as the landmark reference. Replicating these gaps as closely as possible on the individual surfaces will reduce the probability of crossovers along the medial wall ventral segment during registration.

8.14.1. Touch up of these borders as needed is done using the Layers: Delete Border Point with Mouse feature in preparation for registration. For more detail, see *Spherical Registration to Atlas: "Core6" landmark set* link at http://pub:download@brainmap.wustl.edu/pub/donna/WASHINGTON/200503/p117.html

8.15. Identify Central Sulcus extent as follows:

8.15.1. If the individual's inflated surface doesn't align to the same coronal axis as the atlas, then select Z from the Toolbar's drop-down menu to switch the rotation axis to Z and rotate the surface until it is roughly AC-PC aligned (i.e., aligned along the atlas' coronal axis).

8.15.2. In PXXX, identify the central sulcus on the inflated lateral view, using the atlas as a guide. Click on a node in PXXX's central sulcus about where the ventral tip of the central sulcus border on colin -- about 15mm above the edge of the Sylvian fissure, where there is no ambiguity as to whether you are in the sulcus proper

8.15.3. Click on a node along the edge of the Sylvian fissure just below the node clicked above, so you can read out the distance measurement in the Identify window. If the distance is 12-18mm, then you're in the right ballpark.

8.15.4. Click on a node on the dorsal tip of the central sulcus.

8.15.5. Switch to dorsal view in both sessions.

8. Drawings borders in Caret for surface normalization continued

8.15.6. The node just clicked identifies which sulcus is the right one. Click on a node in that sulcus about 15mm from the edge of the medial wall -- again, where there is no ambiguity as to whether you are in the sulcus proper.

8.15.7. Click on a node along the medial wall just across from the last node clicked, to make sure the distance is about 15mm from the medial wall.

8.16. Identify Sylvian Fissure extent as follows:

8.16.1. The Sylvian fissure landmark border begins about 12mm along its primary fundus (SF) on the flat map posterior to its intersection with the main secondary fundus (SF2). On the inflated map this is just before the beginning of the dorsal (ascending) ramus of the Sylvian fissure and appears slightly posterior to the gyral inflation that is just posterior to the postcentral sulcus. Anteriorly, the landmark extends almost to the anterior and ventral limit of the primary fundus, 10 mm dorsal to the ventral margin of the frontal lobe. For more detail, see *Spherical Registration to Atlas: "Core6" landmark set* link at http://pub:download@brainmap.wustl.edu/pub/donna/WASHINGTON/200503/p117.html

8.17. Identify Superior Temporal Gyrus extent as follows:

8.17.1. Use Toolbar: L in the inflated view and again rotate about Z if needed to AC-PC align the individual's surface to match Colin's alignment.

8.17.2. Click on a node along the superior temporal gyrus (lower edge of the Sylvian fissure) directly below the node ID's for the ventral tip of the central sulcus.

8.17.3. Click on a node at the temporal pole, corresponding to the end point of the magenta-colored "SF_STSant" border.

8.18. With ID terminal points for each border on the inflated map, we can ***draw the borders*** on the flat map. Aim for the fundus (dark line) of the central sulcus and sylvian fissure, as it appears on the flat map's folding pattern, even if your ID marks miss the fundus. The SF_STSant landmark is a gyrus, so aim for the whitline. The green ID nodes show you where to start and stop drawing. Draw borders as follows:

8.18.1. Layers: Border : Draw Border.

8.18.2. Name: LANDMARK.CentralSulcus, Resampling: 4.0, Apply

8. Drawings borders in Caret for surface normalization continued

8.18.3. Click on a node at the temporal pole, corresponding to the end point of the magenta-colored "SF_STSant" border.

8.19. With ID terminal points for each border on the inflated map, we can ***draw the borders*** on the flat map. Aim for the fundus (dark line) of the central sulcus and sylvian fissure, as it appears on the flat map's folding pattern, even if your ID marks miss the fundus. The SF_STSant landmark is a gyrus, so aim for the whitline. The green ID nodes show you where to start and stop drawing. Draw borders as follows:

8.19.1. Layers: Border : Draw Border.

8.19.2. Name: LANDMARK.CentralSulcus, Resampling: 4.0, Apply

8.19.3. Starting at the ventral tip of the central sulcus, near the + origin/scale bar near the center of the surface, draw the central sulcus by dragging the mouse with the left mouse button depressed. When you get to the dorsal extent delimited by your green ID node, shift-click the left mouse button to terminate the border.

8.19.4. On the Draw Border dialog, select LANDMARK.SylvianFissure from the Name menu and click Apply.

8.19.5. Starting at the dorsal tip of the Sylvian fissure, just across from the + origin/scale bar near the center of the surface, draw the Sylvian fissure by dragging the mouse with the left mouse button depressed. When you get to the ventral extent delimited by your green ID node, shift-click the left mouse button to terminate the border.

8.19.6. On the Draw Border dialog, select LANDMARK.SF_STSant from the Name menu and click Apply.

8.19.7. Starting at the dorsal tip of the superior temporal gyrus (closer to the center of the surface), trace along the white line until you reach the end point, then shift-click.

8.19.8. If you're not happy with a border, select Layers: Border: Delete border with mouse as needed to delete a bad border and redraw.

8.19.9. Layers: Border: Project border: nearest tile

8.19.10. File: Save Data File: border projection file: PXXX_EXXXXX_SX_111.L.LANDMARKS.forReg-with-Colin_Core6.xxxxx.borderproj

8. Drawings borders in Caret for surface normalization continued

8.19.11. Switch to the SPHERICAL surface.

8.19.12. D/C : Surface Miscellaneous: Hide Surface

8.19.13. Toolbar View and rotate the invisible surface, making sure the landmarks look smooth and curvy, with no sharp turns or hooks (e.g., if a border point somehow got translated to the origin)

8.19.14. Toolbar: Spec ; and select Border from the spec selection menu.

Click X next to the PXXX_EXXXXX_SX_111.L.LANDMARKS.FromFlattening.xxxxx .borderproj entry to remove this entry from the spec file. Make sure PXXX_EXXXXX_SX_111.L.LANDMARKS.forReg-with-Colin_Core6.xxxxx.borderproj is the only borderproj entry, and there are no border entries. (keep ForSPHERICAL.REGISTRATION_Human.Class3.bordercolor as a bordercolor entry.)

8.19.15. Starting at the ventral tip of the central sulcus, near the + origin/scale bar near the center of the surface, draw the central sulcus by dragging the mouse with the left mouse button depressed. When you get to the dorsal extent delimited by your green ID node, shift-click the left mouse button to terminate the border.

8.19.16. On the Draw Border dialog, select LANDMARK.SylvianFissure from the Name menu and click Apply.

8.19.17. Starting at the dorsal tip of the Sylvian fissure, just across from the + origin/scale bar near the center of the surface, draw the Sylvian fissure by dragging the mouse with the left mouse button depressed. When you get to the ventral extent delimited by your green ID node, shift-click the left mouse button to terminate the border.

8.19.18. On the Draw Border dialog, select LANDMARK.SF_STSant from the Name menu and click Apply.

8.19.19. Starting at the dorsal tip of the superior temporal gyrus (closer to the center of the surface), trace along the white line until you reach the end point, then shift-click.

8.19.20. If you're not happy with a border, select Layers: Border: Delete border with mouse as needed to delete a bad border and redraw.

8. Drawings borders in Caret for surface normalization continued

8.19.21. Click on a node at the temporal pole, corresponding to the end point of the magenta-colored "SF_STSant" border.

8.20. With ID terminal points for each border on the inflated map, we can ***draw the borders*** on the flat map. Aim for the fundus (dark line) of the central sulcus and sylvian fissure, as it appears on the flat map's folding pattern, even if your ID marks miss the fundus. The SF_STSant landmark is a gyrus, so aim for the whitline. The green ID nodes show you where to start and stop drawing. Draw borders as follows:

8.20.1. Layers: Border : Draw Border.

8.20.2. Name: LANDMARK.CentralSulcus, Resampling: 4.0, Apply

8.20.3. Starting at the ventral tip of the central sulcus, near the + origin/scale bar near the center of the surface, draw the central sulcus by dragging the mouse with the left mouse button depressed. When you get to the dorsal extent delimited by your green ID node, shift-click the left mouse button to terminate the border.

8.20.4. On the Draw Border dialog, select LANDMARK.SylvianFissure from the Name menu and click Apply.

8.20.5. Starting at the dorsal tip of the Sylvian fissure, just across from the + origin/scale bar near the center of the surface, draw the Sylvian fissure by dragging the mouse with the left mouse button depressed. When you get to the ventral extent delimited by your green ID node, shift-click the left mouse button to terminate the border.

8.20.6. On the Draw Border dialog, select LANDMARK.SF_STSant from the Name menu and click Apply.

8.20.7. Starting at the dorsal tip of the superior temporal gyrus (closer to the center of the surface), trace along the white line until you reach the end point, then shift-click.

8.20.8. If you're not happy with a border, select Layers: Border: Delete border with mouse as needed to delete a bad border and redraw.

8.20.9. Layers: Border: Project border: nearest tile

8.20.10. File: Save Data File: border projection file: PXXX_EXXXXX_SX_111.L.LANDMARKS.forReg-with-Colin_Core6.xxxxx.borderproj

8. Drawings borders in Caret for surface normalization continued

8.20.11. Switch to the SPHERICAL surface.

8.20.12. D/C : Surface Miscellaneous: Hide Surface

8.20.13. Toolbar View and rotate the invisible surface, making sure the landmarks look smooth and curvy, with no sharp turns or hooks (e.g., if a border point somehow got translated to the origin)

8.20.14. Toolbar: Spec ; and select Border from the spec selection menu.

Click X next to the PXXX_EXXXXX_SX_111.L.LANDMARKS.FromFlattening.xxxxx .borderproj entry to remove this entry from the spec file. Make sure PXXX_EXXXXX_SX_111.L.LANDMARKS.forReg-with-Colin_Core6.xxxxx.borderproj is the only borderproj entry, and there are no border entries. (keep ForSPHERICAL.REGISTRATION_Human.Class3.bordercolor as a bordercolor entry.)

9. Caret normalization of individual surface to atlas

9.1. Now we are ready to run the normalization algorithm. Select

Surface: Deformation: Run Spherical Surface Deformation

9.1.1. Individual tab:

9.1.1.1. Spec: PXXX_EXXXXX_SX_111.L.REG-with-Colin_Core6.xxxxx.spec

9.1.1.2. Border: PXXX_EXXXXX_SX_111.L.LANDMARKS.forReg-with-Colin_Core6.xxxxx.borderproj

9.1.1.3. Closed Topo: PXXX_EXXXXX_SX_111.L.full.segment_vent_corrX.xxxxx.topo

9.1.1.4. Cut Topo: PXXX_EXXXXX_SX_111.L.full.segment_vent_corrX.CUT.xxxxx.topo

9.1.1.5. Fiducial Coord: PXXX_EXXXXX_SX_111.L.full.segment_vent_corrX.fiducial-magctr.xxxxx.coord

9.1.1.6. Spherical Coord: PXXX_EXXXXX_SX_111.L.full.segment_vent_corrX.SPHERE_Std.xxxxx.coord

9.1.1.7. Flat Coord: PXXX_EXXXXX_SX_111.L.full.segment_vent_corrX.FLAT_Cartesian.xxxxx.coord

9.1.2. Atlas tab:

9.1.2.1. Spec: ../../COLIN.L.LANDMARKS_REG-with-INDIVIDUAL_CORE6/Human.colin.L.REGISTER-with-INDIVIDUAL_CORE6.xxxxx.spec

9.1.2.2. Border: Human.colin.L.LANDMARKS_REG-with-INDIVIDUAL_CORE6.xxxxx.borderproj

9.1.2.3. Closed Topo: Human.colin.Cerebral.L.CLOSED.xxxxx.topo

9.1.2.4. Cut Topo: Human.colin.Cerebral.L.CUTS.xxxxx.topo

9.1.2.5. Fiducial Coord: Human.colin.Cerebral.L.FIDUCIAL.SPM2.03-12.xxxxx.coord

9.1.2.6. Spherical Coord: Human.colin.Cerebral.L.SPHERE.STD.xxxxx.coord

9.1.2.7. Flat Coord: Human.colin.Cerebral.L.FLAT.CartSTD.xxxxx.coord

9. Caret normalization of individual surface to atlas continued

9.1.3. Spherical Parameters tab:

9.1.3.1. Read Params from Deformation Map File:

../../COLIN.L.LANDMARKS_REG-with-INDIVIDUAL_CORE6/TEMPLATE_REG-with-POP-AVG_4K_NoFid.deform_map

9.2. Click OK to launch the deformation. This process takes 15-30 minutes, depending on the number of nodes and processing speed of your computer.

9.3. If you get a dialog reporting 12 or more crossovers, then something probably has gone wrong. Check your borders -- including their orientation.

9.4. View normalization results as described on page 62 of the **Caret5 User's Manual and Tutorial**, Version 5.1 April 9, 2004.

10. SPM2 normalization of individual volume to atlas

Note: This protocol assumes we are using a right-handed coordinate system: defaults.analyze.flip=0 in spm_defaults.m, neurological convention: right-on-right. The input volumes are Minc files whose X increases from patient left to right, and no flipping was done during normalization.

10.1. In SPM2 select fMRI Time Series

10.1.1. Change the following defaults:

Select Defaults: Spatial Normalisation:

Writing Normalised Template bounding box

Select Defaults: Spatial Normalisation: Writing Normalised : Voxel size 1 1 1.

10.2. Select Normalise: Determine parameters and write normalised.

10.3. Select Template image: T1.mnc

10.4. Select Source image: Pxxx_Exxxxx_Sx_111.mnc

10.5. Select Image to write: Pxxx_Exxxxx_Sx_111.mnc

10.6. At Select Source image, subj 2, select Done

10.6.1. Output will be generated after a few minutes and stored in directory as wPxxx_Exxxxx_Sx_111.hdr and wPxxx_Exxxxx_Sx_111.img files

10.7. Select Toolboxes: Deformations

10.8. Select Deformations: Deformations from sn.mat

10.9. Select sn.mat file: Pxxx_Exxxxx_Sx_111_sn.mat

10.9.1. Output will be generated a few minutes later and stored in directory as y_Pxxx_Exxxxx_Sx_111.hdr and y_Pxxx_Exxxxx_Sx_111.img files. The indicator for process completion is that the main SPM2 main menu becomes active again.

10.10. Select Deformations: Invert deformation

10.11. Select deformation field: y_Pxxx_Exxxxx_Sx_111.img

10.12. Select image to base inverse on: Change filter to read .mnc instead of .img and select Pxxx_Exxxxx_Sx_111.mnc

10.12.1. Output files will be generated a few minutes later when the SPM2 main menu become active again: iy_Pxxx_Exxxxx_Sx_111.hdr and iy_ Pxxx_Exxxxx_Sx_111.img and iy_ Pxxx_Exxxxx_Sx_111.mat

10.13. Quite SPM2

11. Create CSM coordinate files

11.1. Create coordinate file from CSM database

11.1.1. Import coordinates from CSM database by copying and pasting magnet coordinates into a text editor and adding header and assigning site types.

11.1.2. Coordinate file format:

```
BeginHeader
comment
date Fri Feb 04 2005
encoding ASCII
EndHeader
tag-version 1
tag-number-of-cells 4
tag-number-of-comments 0
tag-BEGIN-DATA
0 -62.83 11.99 45.9 Language.5420 0 Language
1 -64.12 -49.18 21.51 Stim.5430 1 Stim
2 -64.96 -42.48 28.76 Sensory.5435 2 Sensory
3 -56.38 -61.71 38.58 Motor.5436 3 Motor
4 -43.55 -22.55 32.12 Other.5439 4 Other
```

11.1.3. Save file as Pxxx_CSM.foci in Pxxx/SURFACES directory

11.2. Create coordinate color file

11.2.1. Use text editor to create color file (RGB) with following format:

```
BeginHeader
comment
date Fri Feb 04 2005
encoding ASCII
EndHeader
Language 0 255 0 Area 01 (green)
Motor 255 0 0 Area 02 (red)
Sensory 0 0 255 Area 03 (blue)
Other 255 255 255 Area 04 (white)
Stim 0 0 0 Area 05 (black)
```

11.2.2. Save as CSM.focicolor in Pxxx/SURFACES directory

11.3. View magnet space coordinates on individual surface

11.3.1. Open Caret in Pxxx/SURFACES directory

11.3.2. Select Pxxx_Exxxxx_Sx_111.L.REG-with-Colin_Core6.xxxxx.spec. Make sure there are no foci/focicolor files selected; select the inflated surface; and accept the remaining default selections. The fiducial should be the magctr version

11.3.3. Open Data File: Foci Color File: ../../COLIN.L.LANDMARKS_REG-with-INDIVIDUAL_CORE6/CSM.focicolor

11. Create CSM coordinate files continued

11.3.4. Open Data File: Foci File: Pxxx_CSM.foci

11.3.5. Press D/C and toggle on the Foci checkbox at the bottom.

11.3.6. Press L for a lateral view of the CSM sites. The CSM sites should appear centered around the root of the sylvian fissure.

11.3.7. Select Layers: Foci: Project Fiducial Foci, Hemisphere only, keep offset from surface setting

11.3.8. File: Save Data Files: Foci Projection Files: Pxxx_CSM.fociproj

11.3.9. Switch to the flat map view

11.3.10. Save flat coordinate file as follows:

11.3.10.1. File: Save Data File: Foci File

11.3.10.2. Foci Associated with Surface Type: Flat

11.3.10.3. Filename: Pxxx_CSM_flat.foci

11.3.11. Select D/C: Surface Shape: Depth to switch from viewing folding patterns to sulcal depth patterns

11.3.12. Select D/C: Foci menu: Draw Foci as Spheres; adjust foci size as desired

11.3.13. Select File: Save Window as Image: PXXX_CSM_flat.jpg

11.3.14. Switch to inflated and fiducial views and save those captures, if desired.

11.4. Align volume to AC-PC space

11.4.1. To create AFNI files (.HEAD and .BRIK) with the minc start variable, call '3dMINCtoAFNI Pxxx_Exxxxx_Sx_111.mnc' at the command line

11.4.2. Call 3drefit –markers Pxx_Exxxxx_Sx_111.HEAD before starting AFNI

11.4.3. Start AFNI

11.4.4. To view axial, sagittal and coronal views, click on image buttons

11.4.5. Select DEFINE MARKERS

11.4.6. Check allow edits box

11.4.7. Set AC superior edge by finding it in the slice windows. Once the cross hairs are aligned with the superior edge, select Set AC Superior Edge

11.4.8. Set AC posterior margin by moving 1 slice posterior and 1 slice inferior of the AC superior edge. Select Set AC Posterior Margin.

11.4.9. Set inferior edge of the PC by finding it in the axial slice window. Once the cross hairs are aligned with the inferior edge, select Set PC Inferior Edge

11. Create CSM coordinate files continued

11.4.10. Select 2 mid-sagittal points that are in the same sagittal plane. You want these points to contain CSF. After finding each of the two desired locations, select Set Sagittal Point.

11.4.11. Check that the sagittal points are acceptable by selecting the Quality button. If no warning, you can proceed. Otherwise, reselect the 2 sagittal points and recheck quality.

11.4.12. Select Transform Data button

11.4.13. Select AC-PC Aligned

11.4.14. Select Done

11.4.15. exit AFNI

11.4.16. The result of this process is two files: Pxxx_Exxxxx_Sx_111+acpc.HEAD and Pxx_Exxxxx_Sx_111+acpc.BRIK which will be used in the next steps.

11.5. Vecwarp preparation

11.5.1. Go to Pxxx/SURFACES directory

11.5.2. Copy Pxxx_xxxxx_Sx_111.L.full.segment_vent_corrx.fiducial-magctr.xxxxx.coord to Pxxx directory

11.5.3. Create in.vec file as follows:

11.5.3.1. At command line, mincinfo Pxxx_xxxxx_Sx_111.mnc, which will give you the (x,y,z) coordinates of the magnet center of this volume. Note that results of mincinfo list the coordinates (z,y,x).

11.5.3.2. In a text editor create the in.vec file with this data:

```
1 0 0 -x
0 1 0 -y
0 0 1 -z
```

11. Create CSM coordinate files continued

11.5.4. Create out.vec file as follows:

11.5.4.1.Call 3dinfo Pxxx_Exxxxx_Sx_111+acpc.HEAD. The output will provide three rows starting with:

R-to-L extent:

A-to-P extent:

I-to-S extent:

In the first row, we want the value associated with [L]. In the second row, we want the value associated with [P]. In the third row, we want the value associated with [I]

11.5.4.2.In a text editor create the out.vec file with this data:

```
1 0 0 -[L]
0 1 0 -[P]
0 0 1 [I]
```

11.6. The in.vec and out.vec files will be used to translate the .coord file to full brain grid for input to the ACPC warp. The out.vec file will be used to translated the ACPC warped .coord file to AC center. Run Vecwarp on the .coord file first at the command line in the Pxxx directory as follows:

11.6.1. Vecwarp –matvec in.vec –input Pxxx_xxxxx_Sx_111.L.full.segment_vent_corrx.fiducial-magctr.xxxxx.coord > pxxx.fbg.coord

11.6.2. Vecwarp –apar Pxxx_Exxxxx_Sx_111+acpc.HEAD –input pxxx.fbg.coord > pxxx.warp.coord

11.6.3. Vecwarp –matvec out.vec –input pxxx.warp.coord > pxxx.acpc.coord

11.7. Test that this process worked properly as follows:

11.7.1. Open AFNI

11.7.2. Switch to ACPC view

11.7.3. Select Define Datamode

11.7.4. Select Write Anat. This writes a Pxxx_Exxxxx_Sx_111+acpc.BRIK file

11.7.5. Quite AFNI

11. Create CSM coordinate files continued

11.7.6. Use text editor to create the following .spec file:

```
BeginHeader
Category INDIVIDUAL
Date Mon Mar 7 2005
Encoding ASCII
Hem-flag left
Species Human
EndHeader
volume_anatomy_file Pxxx_Exxxxx_Sx_111+acpc.HEAD
Pxxx_Exxxxx_Sx_111+acpc.BRIK
CLOSEDtopo_file
Pxxx_Exxxxx_Sx_111.L.full.segment_vent_corrx.xxxxx.topo
FIDUCIALcoord_file pxxx.acpc.coord
```

11.7.7. Start Caret and open the .spec file. Select all

11.7.8. Switch to volume vie and press D/C.

11.7.9. Switch to Overlay/Underlay-Volume from the menu at the top of the D/C menu

11.7.10. Toggle on the Show Surface Outline checkbox at the lower right

11.7.11. The contour should align perfectly with the volume display. If there is a translation or misalignment, something has gone wrong and you will need to back track, identify and solve the problem before moving forward.

11.8. Create AC-PC aligned coordinate file as follows:

11.8.1. Copy the Pxxx_CSM.foci to the Pxxx directory

11.8.2. In the Pxxx directory run the Vecwarp protocol on the .foci file as follows:

11.8.2.1. Vecwarp –matvec in.vec –input Pxxx_CSM.foci > pxxx.CSM_fbg.coord

11.8.2.2. Vecwarp –apar Pxxx_Exxxxx_Sx_111+acpc.HEAD –input pxxx.CSM_fbg.coord > pxxx.CSM_warp.coord

11.8.2.3. Vecwarp –matvec out.vec –input pxxx.CSM_warp.coord > pxxx.CSM_acpc.coord

11.8.3. The pxxx.CSM_acpc.coord is used for the pre-normalized coordinates input into to the algorithm for measuring spread reduction metric. See Appendix F for the source code and input .csv files.

12. Caret normalization of CSM coordinates to atlas coordinates

12.1. Open Caret5 in COLIN.L.LANDMARKS_REG-with-INDIVIDUAL_CORE6 directory

12.2. Select caret_P117_E10043_S4_111.L.REG-with-Colin_Core6.71785.spec, and make sure these files are selected, but don't Load files yet:

CLOSEDtopo_file Human.colin.Cerebral.L.CLOSED.71785.topo

CUTtopo_file Human.colin.Cerebral.L.CUTS.71785.topo

FIDUCIALcoord_file Human.colin.Cerebral.L.FIDUCIAL.SPM2.03-12.71785.coord

INFLATEDcoord_file Human.colin.Cerebral.L.INFLATED.71785.coord

FLATcoord_file Human.colin.Cerebral.L.FLAT.CartSTD.71785.coord

foci_file caret_P117_MAG.71785.foci (if not an option, see below to apply deformation)

foci_color_file CSM2.focicolor

surface_shape Human.colin.Cerebral.L.71785.surface_shape

12.3. Make sure these files are NOT selected:

CUTtopo_file caret_P117_E10043_S4_111.L.full.segment_vent_corr3.FLAT_Cartesian.71785.topo

FIDUCIALcoord_file caret_P117_E10043_S4_111.L.full.segment_vent_corr3.fiducial-magctr.71785.coord

FLATcoord_file caret_P117_E10043_S4_111.L.full.segment_vent_corr3.FLAT_Cartesian.71785.coord

surface_shape caret_P117_E10043_S4_111.L.full.segment_vent_corr3.71785.surface_shape

12.4. Load the selected files.

12.5. If the foci file was in the spec file when registration was performed, then it was deformed during registration. Otherwise, apply the deformation map as follows:

- 12.5.1. Surface: Deformation: Apply Deformation Map: caret_P117_E10043_S4_111.L.REG-with-Colin_Core6.2004_09_14_11_03.71785.deform_map
- 12.5.2. File Type: Foci
- 12.5.3. Data file: ../Pxxx/SURFACES/Pxxx_CSM.foci
- 12.5.4. Apply
- 12.5.5. Close the deformation dialog

12.6. Select File: Open Data File: type Foci: caret_Pxxx_CSM.foci

12.7. Replace any existing foci

12.8. If CSM.focicolor wasn't in the spec file, File: Open Data File: Foci Color: CSM.focicolor

12.9. Toolbar: L to switch to lateral view

12. Caret normalization of CSM coordinates to atlas coordinates continued

12.10. Toolbar: D/C and toggle on Foci

12.11. Layers: Foci: Project Fiducial Foci, Hemisphere only, keep offset from surface

12.12. File:Save Data File: Foci Projection: caret_Pxxx_CSM.fociproj

12.13. D/C: On the Shape drop-down menu, make sure Depth is the selected column; if this option isn't available, make sure you have Human.colin.Cerebral.L.xxxxx.surface_shape loaded -- not the deformed Pxxx surface shape file

12.14. D/C: Foci menu: Draw Foci as Spheres; adjust foci size as desired.

12.15. Switch to flat view.

12.16. File: Save Window as Image: caret_Pxxx_flat.jpg

12.17. Switch to inflated/fiducial views and save those captures, if desired.

12.18. Save flat foci coords as follows:

12.18.1. File: Save Data File: Foci File

12.18.2. Foci Associated with Surface Type: Flat

12.18.3. Filename: caret_Pxxx_CSM_flat.foci

12.19. caret_Pxxx_CSM.foci and caret_Pxxx_CSM_flat.foci files will be input into the PostNorm.csv and Flat_Postnorm.csv files for calcuation of spread reduction (see Appendix F)

13. SPM2 normalization of CSM coordinates to atlas

13.1. Create a coordinate file stripped of header and node numbers in Pxxx directory. Name file Pxxx_coord.stripped. See example of stripped coordinate file in Appendix C.

13.2. Move the ***norm_coord.m*** script (Appendix D) to the individual directory, Pxxx.

13.3. Start matlab in Pxxx directory

13.4. Run norm_coord('Pxxx_coord.stripped') which will call SPM2

13.5. Select iy_ Pxxx_Exxxxx_Sx_111.img file

13.6. Output should be spm_Pxxx_coord.stripped file in Pxxx directory. It will be a coordinate file stripped of any headers and comments

13.7. Once you have the SPM2-normalized CSM coordinates file, you can use the ***merge_spm_foci.sh*** script (Appendix E) at a Linux command line to generate a formatted coordinate file with the following command:
./merge_spm_foci.sh spm_Pxxx_coord.stripped Pxxx_CSM.foci >
spm_Pxxx_CSM.foci. Save this file in the Pxxx directory. This .foci file will serve as input into Caret for visualization of results.

13.8. Move spm_Pxxx_CSM.foci to the colin atlas directory (i.e., mv spm_P117.foci ../../COLIN.L.LANDMARKS_REG-with-INDIVIDUAL_CORE6)

13.9. cd ../../COLIN.L.LANDMARKS_REG-with-INDIVIDUAL_CORE6 ; caret5

13.10. Select caret_P117_E10043_S4_111.L.REG-with-Colin_Core6.71785.spec, and accept the default file selections with these exceptions:
toggle on INFLATED surface
toggle on CSM.focicolor
make sure any foci or fociproj files are deselected
select Human.colin.Cerebral.L.xxxxx.surface_shape—not the deformed Pxxx surface shape file

13.11. File: Open Data File: Foci: spm_Pxxx_CSM.foci

13.12. Toolbar: L to switch to lateral view

13.13. Toolbar: D/C and toggle on Foci

13.14. Layers: Foci: Project Fiducial Foci, Hemisphere only, keep offset from surface

13.15. File:Save Data File: Foci Projection: spm_Pxxx_CSM.fociproj

13. SPM2 normalization of CSM coordinates to atlas continued

13.16. D/C: On the Shape drop-down menu, make sure Depth is the selected column; if this option isn't available, make sure you have Human.colin.Cerebral.L.71785.surface_shape loaded -- not the deformed P117 surface shape file

13.17. D/C: Foci menu: Draw Foci as Spheres; adjust foci size as desired

13.18. Switch to flat view.

13.19. File: Save Window as Image: spm_Pxxx_flat.jpg

13.20. Switch to inflated/fiducial views and save those captures, if desired.

13.21. Save flat foci coords as follows:

13.21.1. File: Save Data File: Foci File

13.21.2. Foci Associated with Surface Type: Flat

13.21.3. Filename: spm_Pxxx_CSM_flat.foci

13.22. The spm_Pxxx_CSM.foci and spm_Pxxx_CSM_flat.foci files will be used for for input into PostNorm.csv and FlatPostNorm.csv files (see Appendix F)

Appendix B: Resampling MRI to 1mm Cubic Voxels

Excerpt from Resample_PatientBrainData.xls spreadsheet :

BrainID	dim name	length	step	start
P55	*xspace*	256	0.896471	-108.1
	yspace	256	0.896471	-101
	zspace	256	0.896471	-123.3
	dim in	256		
	voxdim in	0.896471		
	voxdim out	1		
	start	(-108.1, -101, -123.3)		
	dim out	**229**		
P58	*xspace*	256	0.86549	-106.1
	yspace	256	0.86549	-95
	zspace	256	0.86549	-110.2
	dim in	256		
	voxdim in	0.86549		
	voxdim out	1		
	start	(-106.1,-95.1,-110.2)		
	dim out	**222**		
P60	*xspace*	256	0.884706	-111.5
	yspace	256	0.884706	-113.5
	zspace	256	0.884706	-115.6
	dim in	256		
	voxdim in	0.884706		
	voxdim out	1		
	start	(-111.5,-113.5,-115.6)		
	dim out	**226**		

Appendix C: Creating a stripped coordinate file for use in SPM2

Use text editor to create file with coordinate data from the CSM database.

```
5420 -62.83 11.99 45.9
5430 -64.12 -49.18 21.51
5435 -64.96 -42.48 28.76
5436 -56.38 -61.71 38.58
5439 -43.55 -22.55 32.12
```

Save as Pxxx_CSM.stripped

Appendix D: norm_coord.m script

```
function norm_coord(infile)

P=spm_get(1,'iy_*.img','Select deformation');

P=[repmat(P,3,1) [',1';',2';',3']];
V=spm_vol(P);

file = spm_load(infile);
outfname = strcat('spm_',infile);
outfile = fopen(outfname,'w');
fprintf('Writing output file %s %d\n', outfname, length(file));

for i = 1:length(file),
x=file(i,2);
y=file(i,3);
z=file(i,4);
c = [x y z]';
vx = inv(V(1).mat)*[c ; 1];  % The voxel in the deformation to sample
normx = spm_sample_vol(V(1),vx(1),vx(2),vx(3),1);
normy = spm_sample_vol(V(2),vx(1),vx(2),vx(3),1);
normz = spm_sample_vol(V(3),vx(1),vx(2),vx(3),1);
fprintf('%d\n',i-1);
fprintf(outfile,'%d %.2f %.2f %.2f\n',i-1,normx,normy,normz);
end;
fclose(outfile);
```

Appendix E: merge_spm_foci.sh script

```
#!/bin/sh

if [ $# -ne 2 ]
then    echo "usage: merge_spm_foci.sh spm_foci_coords.txt mag.foci"
        exit 1
fi

SPMFOCI=$1
MAGFOCI=$2

HEADER=1
cat $MAGFOCI | while read line
do
if [ $HEADER -eq 1 ]
then
echo $line
else
FOCINUM=`echo "$line" |cut -f1 -d' '`
COORD=`grep "^$FOCINUM " $SPMFOCI| cut -f2-4 -d' '`
REST=`echo "$line" |cut -f5-8 -d' '`
echo "$FOCINUM $COORD $REST"
fi
hit=`echo $line |grep BEGIN-DATA`
if [ "$hit" ] ; then HEADER=0 ; fi
done
```

Appendix F: Spread reduction source code and input files

```
##############################################################################
## CALCULATING AVERAGE 2D EUCLIDIAN DISTANCE BETWEEN LANGUAGE SITES ACROSS 11
HUMAN BRAINS##
## DATE: 2-25-2005 ##
## AUTHOR: VERONICA SMITH        ##
##############################################################################

######################
##   PREP WORK##
######################

# CLEAN UP #
rm(list=ls(all=TRUE))

# IMPORTING DATA #
pre.dat <- read.csv("FlatPreNorm.csv")
post.dat <- read.csv("FlatPostNorm.csv")
pp.dat <- rbind(pre.dat, post.dat)

# SUMMARIZING DATA #
summary(pre.dat)
summary(post.dat)
summary(pp.dat)

# LOAD 3D PLOTTING PACKAGE #
library(scatterplot3d)
library(help=scatterplot3d)

################################
# PRENORM LANGUAGE SITE COORD  #
################################
langcoord.prenorm <-pre.dat[0,]
temp.matrix <- langcoord.prenorm
length <- dim(pre.dat)[1]
for(i in 1:length) {
if(pre.dat[i,"CSM.Region"] == 1) {
temprow <- pre.dat[i,]
temp.matrix <- rbind(temprow,langcoord.prenorm)}
langcoord.prenorm <- temp.matrix
} # END OF FOR LOOP #

############################
# CARET LANGUAGE SITE COORD #
############################
langcoord.caret <- post.dat[0,]
temp.matrix <- langcoord.caret
length <- dim(post.dat)[1]
for(i in 1:length) {
if((post.dat[i,"CSM.Region"] == 1) && (post.dat[i,"Algorithm"] == "Caret")) {
temprow <- post.dat[i,]
temp.matrix <- rbind(temprow,langcoord.caret)}

langcoord.caret <- temp.matrix
} # END OF FOR LOOP #
```

```
############################
# SPM2 LANGUAGE SITE COORD#
############################
langcoord.spm <- post.dat[0,]
temp.matrix <- langcoord.spm
length <- dim(post.dat)[1]
for(j in 1:length) {
if((post.dat[j,"CSM.Region"] == 1) && (post.dat[j,"Algorithm"] == "SPM2")) {
temprow <- post.dat[j,]
temp.matrix <- rbind(temprow,langcoord.spm)}
langcoord.spm <- temp.matrix
} # END OF FOR LOOP #

#########################################################
# CREATE LIST OF LANGUAGE SITES SEPARATED BY BRAIN ID #
#########################################################
lang.prenorm.list <- split(langcoord.prenorm, langcoord.prenorm$Brain.ID)


#######################################################
# ATTEMPT TO GET BRAIN LANG SITES IN CORRECT ORDER #
#######################################################

brainlist  <- langcoord.prenorm[c("Brain.ID","X", "Y", "Z")]
length <- dim(brainlist)[1]
brainID = 0
row = 0
tempNumRow = 0
brainlistlengths <- vector(length = 0)
for(m in 1:length) {
if (row==0) {
brainID <- brainlist[m,"Brain.ID"]
row = 1
}
else {

if(brainlist[m,"Brain.ID"] == brainID) {
row = row + 1
}
else {
brainlistlengths <- c(brainlistlengths, row)
row = 1
}
}
brainID <- brainlist[m,"Brain.ID"]
} # END OF FOR LOOP #

# brainlistlengths is a vector that lists the number of lang sites per brain in
the order the brains
# will be in calcdist.xx.matrices

brainlistlengths <- c(brainlistlengths,row)
```

```
##############################################################################
# CALCULATION OF NUMBER OF LANGUAGE SITES FOR EACH BRAIN AND TOTAL NUMBER OF
ROWS TO BE USED LATER #
##############################################################################
length <- length(lang.prenorm.list)
totalLength = 0
RowNum.vec <- vector(length =0)
for(k in 1:length) {
tempRowNum <- nrow(lang.prenorm.list [[k]])
tempLength = tempRowNum
if (length(RowNum.vec) >= 1) {
tempRowNum <- c(RowNum.vec,tempRowNum)
 }
RowNum.vec <- tempRowNum
totalLength <- totalLength + tempLength
} # END OF FOR LOOP #

#############################################################
# PRENORM DISTANCES BETWEEN LANGUAGE SITES W/IN EACH BRAIN #
#############################################################
prenorm.lang.list <- lapply(lang.prenorm.list,
function(cd){
dist.prenorm.matrix <- cbind(cd$X,cd$Y,cd$Z)
dist(dist.prenorm.matrix, method = "euclidean")
})

#############################################################
# CARET DISTANCES BETWEEN LANGUAGE SITES w/in EACH BRAIN #
#############################################################
lang.caret.list <-  split(langcoord.caret,langcoord.caret$Brain.ID)
postnorm.caret.list <- lapply(lang.caret.list,
function(cd){
dist.caret.matrix <- cbind(cd$X, cd$Y, cd$Z)
dist(dist.caret.matrix, method = "euclidean")
})

#############################################################
# SPM2 DISTANCES BETWEEN LANGUAGE SITES W/in EACH BRAIN #
#############################################################
lang.spm.list <- split(langcoord.spm, langcoord.spm$Brain.ID)
postnorm.spm.list <- lapply(lang.spm.list,
 function(cd){
 dist.spm.matrix <- cbind(cd$X, cd$Y, cd$Z)
 dist(dist.spm.matrix, method = "euclidean")
})
#############################################################
##DISTANCE ACROSS BRAINS FUNCTION (DAB) ##
#############################################################

DAB <- function(brainIDs, distmatrix) {
index <- outer(brainIDs, brainIDs, "<")
DAB.vec <- distmatrix[index]
DAB.vec<- as.vector(DAB.vec)
DAB.vec
}
```

```
#################################################################
# AVG PRENORM DISTANCES FOR LANGUAGE SITES ACROSS ALL BRAINS #
#################################################################
# PRENORM DATA SET OF LANGUAGE SITE COORD FOR ALL BRAINS #
coord.prenorm.matrix  <- langcoord.prenorm[c("X", "Y", "Z")]

# PRENORM DATA SET OF DISTANCES BETWEEN LANG SITES IN w/in and ACROSS BRAINS #
calcdist.prenorm <- dist(coord.prenorm.matrix, method = "euclidean")
calcdist.prenorm.matrix <- as.matrix(calcdist.prenorm)
prenorm.bIDs <- langcoord.prenorm$Brain.ID

prenorm.DAB.vec <- DAB(prenorm.bIDs, calcdist.prenorm.matrix)
prenorm.avgDAB <- mean(prenorm.DAB.vec)
expect.postnorm.avgDAB <- sqrt(1.3085)*prenorm.avgDAB


#################################################################
# AVG CARET DISTANCES FOR LANGUAGE SITES ACROSS ALL BRAINS #
#################################################################
coord.caret.matrix <- langcoord.caret[c("X", "Y", "Z")] # POSTNORM CARET DATA
SET OF LANG SITE COORD FOR BOTH BRAINS #
calcdist.caret <- dist(coord.caret.matrix, method = "euclidean") # POSTNORM
CARET DATA SET OF DISTANCES BETWEEN LANG SITES IN BOTH BRAINS #
calcdist.caret.matrix <- as.matrix(calcdist.caret)
caret.bIDs <- langcoord.caret$Brain.ID

caret.DAB.vec <- DAB(caret.bIDs, calcdist.caret.matrix)
caret.avgDAB <- mean(caret.DAB.vec)


#################################################
# AVG POSTNORM SPM2 DISTANCES ACROSS ALL BRAINS #
#################################################
coord.spm.matrix <- langcoord.spm[c("X", "Y", "Z")] # POSTNORM SPM DATA SET OF
LANGUAGE SITE COORD FOR BOTH BRAINS #
calcdist.spm <- dist(coord.spm.matrix, method = "euclidean") # POSTNORM SPM2
DATA SET OF DISTANCES BETWEEN LANG SITES IN BOTH BRAINS #
calcdist.spm.matrix <- as.matrix(calcdist.spm)
spm.bIDs <- langcoord.caret$Brain.ID

spm.DAB.vec <- DAB(spm.bIDs, calcdist.spm.matrix)
spm.avgDAB <- mean(spm.DAB.vec)


#################################################
#      PRESENTING RESULTS           #
#################################################

par(mfrow = c(1,2))

prelim.results <- matrix(c(expect.postnorm.avgDAB, caret.avgDAB, spm.avgDAB),
ncol=1)
rownames(prelim.results) <- c("Expected","CARET", "SPM2")
barplot(t(prelim.results), beside = T, main ="2D Language Site Spread", ylim =
c(0,100), ylab = "mm", col=c("grey50","orange","blue"))
```

```
##############################################
#DELTA BETWEEN PRENORM AND POSTNORM DISTANCES#
##############################################

normdelta.caret <- expect.postnorm.avgDAB-caret.avgDAB
normdelta.spm <- expect.postnorm.avgDAB-spm.avgDAB

delta.results <- matrix(c(normdelta.caret, normdelta.spm), ncol =1)
rownames(delta.results) <- c("CARET", "SPM2")
barplot(t(delta.results), beside = T, main = "2D Spread Reduction", ylim =
c(0,10), ylab = "mm" , col=c("orange", "blue"))

make.id.pairs<-function(brainIDs) {
  index <- outer(brainIDs, brainIDs, "<")
  id1<-outer(brainIDs, brainIDs, function(i,j) i)
  id2<-outer(brainIDs, brainIDs, function(i,j) j)

  data.frame(id1=id1[index], id2=id2[index])
}

##############################################
# CREATING DATA FRAME FOR STATISTICAL ANALYSIS #
##############################################

# jackknife estimate of  variance #

ids<-make.id.pairs(brainlist$Brain.ID)

uniqueids<-unique(brainlist$Brain.ID)

differences.DAB.vec<-caret.DAB.vec-spm.DAB.vec

jackknife.diffs<-sapply(uniqueids,
                        function(i) mean(differences.DAB.vec[ids$id1!=i &
ids$id2!=i]))

mean.differences<-mean(differences.DAB.vec)
se.differences<-sqrt(var(jackknife.diffs)*10)

ci.mean<-mean.differences+c(-1.96,1.96)*se.differences
p.value<- 2*pnorm(abs(mean.differences)/se.differences,lower.tail=FALSE)
```

```
    ##############################################################################
#
## CALCULATING AVERAGE EUCLIDIAN DISTANCE BETWEEN LANGUAGE SITES ACROSS 11
HUMAN BRAINS##
## DATE: 02-25-05##
## AUTHOR: VERONICA SMITH  ##
##############################################################################

######################
##   PREP WORK##
######################

# CLEAN UP #
rm(list=ls(all=TRUE))

# IMPORTING DATA #
pre.dat <- read.csv("PreNorm_acpc.csv")
post.dat <- read.csv("PostNorm.csv")
#pp.dat <- rbind(pre.dat, post.dat)

# SUMMARIZING DATA #
summary(pre.dat)
summary(post.dat)
#summary(pp.dat)

# LOAD 3D PLOTTING PACKAGE #
library(scatterplot3d)
library(help=scatterplot3d)

################################
# PRENORM LANGUAGE SITE COORD  #
################################
langcoord.prenorm <-pre.dat[0,]
temp.matrix <- langcoord.prenorm
length <- dim(pre.dat)[1]
for(i in 1:length) {
if(pre.dat[i,"CSM.Region"] == 1) {
temprow <- pre.dat[i,]
temp.matrix <- rbind(temprow,langcoord.prenorm)}
langcoord.prenorm <- temp.matrix
} # END OF FOR LOOP #

############################
# CARET LANGUAGE SITE COORD #
############################
langcoord.caret <- post.dat[0,]
temp.matrix <- langcoord.caret
length <- dim(post.dat)[1]
for(i in 1:length) {
if((post.dat[i,"CSM.Region"] == 1) && (post.dat[i,"Algorithm"] == "Caret")) {
temprow <- post.dat[i,]
temp.matrix <- rbind(temprow,langcoord.caret)}

langcoord.caret <- temp.matrix
} # END OF FOR LOOP #
```

```
##########################
# SPM2 LANGUAGE SITE COORD#
##########################
langcoord.spm <- post.dat[0,]
temp.matrix <- langcoord.spm
length <- dim(post.dat)[1]
for(j in 1:length) {
if((post.dat[j,"CSM.Region"] == 1) && (post.dat[j,"Algorithm"] == "SPM2")) {
temprow <- post.dat[j,]
temp.matrix <- rbind(temprow,langcoord.spm)}
langcoord.spm <- temp.matrix
} # END OF FOR LOOP #

#########################################################
# CREATE LIST OF LANGUAGE SITES SEPARATED BY BRAIN ID #
#########################################################
lang.prenorm.list <- split(langcoord.prenorm, langcoord.prenorm$Brain.ID)


#####################################################
# ATTEMPT TO GET BRAIN LANG SITES IN CORRECT ORDER #
#####################################################

brainlist  <- langcoord.prenorm[c("Brain.ID","X", "Y", "Z")]
length <- dim(brainlist)[1]
brainID = 0
row = 0
tempNumRow = 0
brainlistlengths <- vector(length = 0)
for(m in 1:length) {
if (row==0) {
brainID <- brainlist[m,"Brain.ID"]
row = 1
}
else {

if(brainlist[m,"Brain.ID"] == brainID) {
row = row + 1
}
else {
brainlistlengths <- c(brainlistlengths, row)
row = 1
}
}
brainID <- brainlist[m,"Brain.ID"]
} # END OF FOR LOOP #

# brainlistlengths is a vector that lists the number of lang sites per brain in
the order the brains
# will be in calcdist.xx.matrices

brainlistlengths <- c(brainlistlengths,row)
```

```
#############################################################################
CALCULATION OF NUMBER OF LANGUAGE SITES FOR EACH BRAIN AND TOTAL NUMBER OF ROWS
TO BE USED LATER #
#############################################################################
length <- length(lang.prenorm.list)
totalLength = 0
RowNum.vec <- vector(length =0)
for(k in 1:length) {
tempRowNum <- nrow(lang.prenorm.list [[k]])
tempLength = tempRowNum
if (length(RowNum.vec) >= 1) {
tempRowNum <- c(RowNum.vec,tempRowNum)
 }
RowNum.vec <- tempRowNum
totalLength <- totalLength + tempLength
} # END OF FOR LOOP #

#############################################################
# PRENORM DISTANCES BETWEEN LANGUAGE SITES W/IN EACH BRAIN #
#############################################################
prenorm.lang.list <- lapply(lang.prenorm.list,
function(cd){
dist.prenorm.matrix <- cbind(cd$X,cd$Y,cd$Z)
dist(dist.prenorm.matrix, method = "euclidean")
})

#############################################################
# CARET DISTANCES BETWEEN LANGUAGE SITES w/in EACH BRAIN #
#############################################################
lang.caret.list <-  split(langcoord.caret,langcoord.caret$Brain.ID)
postnorm.caret.list <- lapply(lang.caret.list,
function(cd){
dist.caret.matrix <- cbind(cd$X, cd$Y, cd$Z)
dist(dist.caret.matrix, method = "euclidean")
})

#############################################################
# SPM2 DISTANCES BETWEEN LANGUAGE SITES W/in EACH BRAIN #
#############################################################
lang.spm.list <- split(langcoord.spm, langcoord.spm$Brain.ID)
postnorm.spm.list <- lapply(lang.spm.list,
 function(cd){
 dist.spm.matrix <- cbind(cd$X, cd$Y, cd$Z)
 dist(dist.spm.matrix, method = "euclidean")
})
#############################################################
##DISTANCE ACROSS BRAINS FUNCTION (DAB) ##
#############################################################
DAB <- function(brainIDs, distmatrix) {
index <- outer(brainIDs, brainIDs, "<")
DAB.vec <- distmatrix[index]
DAB.vec<- as.vector(DAB.vec)
DAB.vec
}
```

```
#################################################################
# AVG PRENORM DISTANCES FOR LANGUAGE SITES ACROSS ALL BRAINS #
#################################################################
# PRENORM DATA SET OF LANGUAGE SITE COORD FOR ALL BRAINS #
coord.prenorm.matrix  <- langcoord.prenorm[c("X", "Y", "Z")]

# PRENORM DATA SET OF DISTANCES BETWEEN LANG SITES IN w/in and ACROSS BRAINS #
calcdist.prenorm <- dist(coord.prenorm.matrix, method = "euclidean")
calcdist.prenorm.matrix <- as.matrix(calcdist.prenorm)
prenorm.bIDs <- langcoord.prenorm$Brain.ID

prenorm.DAB <- DAB(prenorm.bIDs, calcdist.prenorm.matrix)
prenorm.avgDAB <- mean(prenorm.DAB)
expect.postnorm.avgDAB <- ((1.440741874)^.3333) * prenorm.avgDAB

#################################################################
# AVG CARET DISTANCES FOR LANGUAGE SITES ACROSS ALL BRAINS #
#################################################################

coord.caret.matrix <- langcoord.caret[c("X", "Y", "Z")] # POSTNORM CARET DATA
SET OF LANG SITE COORD FOR BOTH BRAINS #
calcdist.caret <- dist(coord.caret.matrix, method = "euclidean") # POSTNORM
CARET DATA SET OF DISTANCES BETWEEN LANG SITES IN BOTH BRAINS #
calcdist.caret.matrix <- as.matrix(calcdist.caret)
caret.bIDs <- langcoord.caret$Brain.ID

caret.DAB.vec <- DAB(caret.bIDs, calcdist.caret.matrix)
caret.avgDAB <- mean(caret.DAB.vec)

#################################################
# AVG POSTNORM SPM2 DISTANCES ACROSS ALL BRAINS #
#################################################
coord.spm.matrix <- langcoord.spm[c("X", "Y", "Z")] # POSTNORM SPM DATA SET OF
LANGUAGE SITE COORD FOR BOTH BRAINS #
calcdist.spm <- dist(coord.spm.matrix, method = "euclidean") # POSTNORM SPM2
DATA SET OF DISTANCES BETWEEN LANG SITES IN BOTH BRAINS #
calcdist.spm.matrix <- as.matrix(calcdist.spm)
spm.bIDs <- langcoord.caret$Brain.ID

spm.DAB.vec <- DAB(spm.bIDs, calcdist.spm.matrix)
spm.avgDAB <- mean(spm.DAB.vec)
```

```
#####################################################
#      PRESENTING RESULTS           #
#####################################################

par(mfrow = c(1,2))

final.results <- matrix(c(expect.postnorm.avgDAB, caret.avgDAB, spm.avgDAB),
ncol=1)
#colnames(final.results) <- c("Expected","CARET", "SPM2")
rownames(final.results) <- c("Expected", "Caret", "SPM2")
barplot(t(final.results), beside = T, main ="3D Language Site Spread", ylim =
c(0,50), ylab = "mm", col=c("grey50","orange","blue"))

#############################################
#DELTA BETWEEN PRENORM AND POSTNORM DISTANCES#
#############################################

normdelta.caret <- expect.postnorm.avgDAB-caret.avgDAB
normdelta.spm <- expect.postnorm.avgDAB-spm.avgDAB

delta.results <- matrix(c(normdelta.caret, normdelta.spm), ncol =1)
rownames(delta.results) <- c("CARET", "SPM2")
barplot(t(delta.results), beside = T, main = "3D Spread Reduction", ylim =
c(0,5), ylab = "mm" , col=c("orange", "blue"))

################################################
# CREATING DATA FRAME FOR STATISTICAL ANALYSIS #
################################################

make.id.pairs<-function(brainIDs) {
  index <- outer(brainIDs, brainIDs, "<")
  id1<-outer(brainIDs, brainIDs, function(i,j) i)
  id2<-outer(brainIDs, brainIDs, function(i,j) j)

  data.frame(id1=id1[index], id2=id2[index])
}

# jackknife estimate of  variance #

ids<-make.id.pairs(brainlist$Brain.ID)

uniqueids<-unique(brainlist$Brain.ID)

differences.DAB.vec<-caret.DAB.vec-spm.DAB.vec

jackknife.diffs<-sapply(uniqueids,
                        function(i) mean(differences.DAB.vec[ids$id1!=i &
ids$id2!=i]))

mean.differences<-mean(differences.DAB.vec)
se.differences<-sqrt(var(jackknife.diffs)*10)

ci.mean<-mean.differences+c(-1.96,1.96)*se.differences
p.value<- 2*pnorm(abs(mean.differences)/se.differences,lower.tail=FALSE)
```

Input Files:
Excerpt from FlatPostNorm.csv

Brain ID	CSM Region	Site Number	X	Y	Z	Algorithm
54	3	10	11.18795	8.862825	0	Caret
54	3	12	-6.763459	45.548531	0	Caret
54	3	13	35.895584	43.534492	0	Caret
54	3	14	35.293655	57.411488	0	Caret
54	3	15	5.266497	82.270172	0	Caret
54	3	16	38.877956	78.978302	0	Caret
54	4	18	82.049553	-11.708981	0	Caret
54	4	19	46.575829	64.932083	0	Caret
54	4	2	-38.191551	33.86076	0	Caret
54	1	20	90.022171	23.418528	0	Caret
54	5	21	85.187706	-6.319094	0	Caret
54	4	22	-10.156957	2.844942	0	Caret
54	4	23	-12.421206	-0.884871	0	Caret
54	2	24	-7.401104	-1.123019	0	Caret
54	4	25	-41.34903	47.406235	0	Caret
54	4	26	-39.649734	31.792488	0	Caret
54	2	3	-10.001882	61.294136	0	Caret
54	1	30	92.752426	19.398674	0	Caret
54	5	31	83.236671	19.405651	0	Caret
54	1	35	78.551491	10.833484	0	Caret
54	1	36	104.180176	39.605854	0	Caret
54	4	37	-22.400347	4.385891	0	Caret
54	5	42	116.294731	-10.695324	0	Caret
54	5	43	75.691322	-36.96801	0	Caret
54	3	10	17.78986	13.352521	0	SPM2
54	3	12	-2.366655	55.623337	0	SPM2
54	3	13	25.799614	47.554543	0	SPM2
54	3	14	27.175005	59.168766	0	SPM2
54	3	15	2.620024	85.125488	0	SPM2
54	3	16	6.860496	91.754105	0	SPM2
54	4	18	45.04126	18.850975	0	SPM2
54	4	19	43.134949	68.490898	0	SPM2
54	4	2	-40.237881	41.196213	0	SPM2
54	1	20	75.08091	23.137539	0	SPM2
54	5	21	70.536285	-7.097998	0	SPM2
54	4	22	-12.022094	9.477371	0	SPM2
54	4	23	-8.731981	3.458286	0	SPM2
54	2	24	3.425389	8.311852	0	SPM2
54	4	25	-40.967079	48.751202	0	SPM2
54	4	26	-44.068794	37.846371	0	SPM2

Input Files:

Excerpt from PostNorm.csv

Brain ID	CSM Region	Site Number	X	Y	Z	Algorithm
54	3	10	-63.82	-7.532	12.588	Caret
54	3	12	-56.92	5.503	41.632	Caret
54	3	13	-50.01	-17.85	33.39	Caret
54	3	14	-49.45	-19.31	44.795	Caret
54	3	15	-42.86	-17.11	59.118	Caret
54	3	16	-52.8	-30.78	57.216	Caret
54	4	18	-49.31	-36.85	8.4897	Caret
54	4	19	-38.97	-26.66	43.719	Caret
54	4	2	-40.43	14.97	36.867	Caret
54	1	20	-52.87	-52.62	20.228	Caret
54	5	21	-47.73	-40.58	10.555	Caret
54	4	22	-60.39	9.072	9.5786	Caret
54	4	23	-56.46	12.82	8.5118	Caret
54	2	24	-57.29	10.37	3.5565	Caret
54	4	25	-46.61	14.55	48.95	Caret
54	4	26	-39.67	16.87	36.897	Caret
54	2	3	-47.06	-3.755	47.295	Caret
54	1	30	-56.81	-55.13	16.654	Caret
54	5	31	-56.41	-50.59	21.538	Caret
54	1	35	-62.86	-53.79	16.159	Caret
54	1	36	-47.97	-60.92	27.693	Caret
54	4	37	-57.95	11.69	19.075	Caret
54	5	42	-63.43	-53.08	-11.23	Caret
54	5	43	-52.09	-24.79	-1.809	Caret
54	3	10	-65.18	-12.26	17.62	SPM2
54	3	12	-56.62	-5.31	44.33	SPM2
54	3	13	-59.22	-16.7	47.51	SPM2
54	3	14	-51.74	-15.27	55.97	SPM2
54	3	15	-41.48	-16.66	63.53	SPM2
54	3	16	-44.69	-24.2	65.59	SPM2
54	4	18	-65.57	-29.98	19.77	SPM2
54	4	19	-44.42	-25.27	49.78	SPM2
54	4	2	-53.19	11.6	45.47	SPM2
54	1	20	-63.22	-56.81	28.92	SPM2
54	5	21	-65.78	-37.77	21.85	SPM2
54	4	22	-59.66	2.94	14.9	SPM2
54	4	23	-60.49	7.31	8.19	SPM2
54	2	24	-59.46	0.5	8.86	SPM2
54	4	25	-47.49	15.57	52.16	SPM2
54	4	26	-55.67	13.5	41.02	SPM2
54	2	3	-46.96	-1.48	55.01	SPM2

Appendix G: Deformation Map File

BeginHeader
comment Deformed with CARET v5.11
date Sun Jun 6 15:26:44 2004
encoding ASCII
EndHeader
deform-map-file-version 2
flat-or-sphere DEFORM_SPHERE
deformed-file-name-prefix caret_
source-directory
source-spec Human.colin.L.REGISTER-with-POP-ATLAS.xxxxx.spec
source-landmark-border Human.colin.L.LANDMARKS_REG-with-INDIVIDUAL_CORE6.xxxxx.borderproj
source-closed-topo Human.colin.Cerebral.L.CLOSED.xxxxx.topo
source-cut-topo Human.colin.Cerebral.L.CUTS.xxxxx.topo
source-fiducial-coord Human.colin.Cerebral.L.FIDUCIAL.TLRC.711-2B.xxxxx.coord
source-sphere-coord Human.colin.Cerebral.L.SPHERE.STD.xxxxx.coord
source-deform-sphere-coord
deformed_4K_NoFidHuman.colin.Cerebral.L.SPHERE.STD.xxxxx.coord
source-deform-flat-coord
source-flat-coord Human.colin.Cerebral.L.FLAT.CartSTD.xxxxx.coord
source-resampled-flat-coord
source-resampled-deformed-flat-coord
source-resampled-cut-topo
sphere-resolution 4610
border-resampling 2 8.000000
spherical-number-of-cycles 3
smoothing-parameters 0 1.000000 100 20 10 30
morphing-parameters 0 1 0.300000 0.600000 0.500000 0.500000 300 20
smoothing-parameters 1 1.000000 100 20 10 5
morphing-parameters 1 1 0.300000 0.600000 0.500000 0.500000 300 5
smoothing-parameters 2 1.000000 50 20 10 1
morphing-parameters 2 1 0.300000 0.600000 0.500000 0.500000 300 2
flat-parameters 900 0.000010 1.000000 20
target-directory
target-spec Human.POP_AVG.L.REGISTER_Normal_B6-with-INDIVIDUAL.73730.spec
target-landmark-border Human.POP_AVG_Normal_B6_Projected.L.SPHERE.border
target-closed-topo ../POP_AVERAGE.L/Human.sphere_6.73730.topo
target-cut-topo ../POP_AVERAGE.L/Human.sphere_6.73730.topo
target-sphere-coord ../POP_AVERAGE.L/Human.sphere_6.73730.coord
target-fiducial-coord ../POP_AVERAGE.L/Human.sphere_6_forFIDUCIAL.73730.coord
target-flat-coord
output-spec-file deformed_4K_NoFidHuman.colin.L.REGISTER-with-POP-ATLAS.73730.spec
sphere-fiducial-sphere-ratio false 0.500000
inverse-deformation false
DATA-START